

End Depth Ratio of Free Over-Fall for Different Channel Cross-Sections in Sub-Critical and Super Critical Flow Regimes

Ehsan Abrari

Submitted to the
Institute of Graduate Studies and Research
in partial fulfillment of the requirements for the degree of

Doctor of Philosophy
in
Civil Engineering

Eastern Mediterranean University
February 2018
Gazimağusa, North Cyprus

Approval of the Institute of Graduate Studies and Research

Assoc. Prof. Dr. Ali Hakan Ulusoy
Director

I certify that this thesis satisfies the requirements as a thesis for the degree of Doctor of Philosophy in Civil Engineering.

Assoc. Prof. Dr. Serhan Şensoy
Chair, Department of Civil Engineering

We certify that we have read this thesis and that in our opinion it is fully adequate in scope and quality as a thesis for the degree of Doctor of Philosophy in Civil Engineering.

Assoc. Prof. Dr. Mustafa Ergil
Supervisor

Examining Committee

1. Prof. Dr. Cevza Melek Kazezyılmaz Alhan
2. Prof. Dr. Mehmet Emin Birpınar
3. Prof. Dr. Zalihe Nalbantoğlu Sezai
4. Assoc. Prof. Dr. Mustafa Ergil
5. Assoc. Prof. Dr. Umut Türker

ABSTRACT

In this study, the ratio between the end depth and the upstream depth which is known as the end depth ratio (EDR), is computed for the exponential (rectangular, triangular, and parabolic), the generalized trapezoidal (rectangular, triangular, semi-triangular, trapezoidal, semi-trapezoidal, inverted triangular and semi-inverted triangular) and the generalized circular (without horizontal base, with horizontal base at 4 different heights) channel cross-sections using different analytical methods for both sub- and super critical flow regimes, since these selected cross-sections are widely used in practice and also having experimental data sets for the comparison. Apart from that, based on the previously suggested theories for both sub- and super critical flow regimes the EDR and the end depth discharge (EDD) relationships for the above-mentioned cross-sections are as well obtained.

As a novelty, two new approaches as well suggested as a part of this study that were only requiring the continuity and the energy equations; the three velocity point approach and the infinite number velocity points approach. These suggested approaches eliminate the need of the end pressure coefficient that was expected to be determined experimentally. These computed EDR and EDD values of the different theoretical approaches and the experimental data set of relevant cross-sections were statistically compared. Subsequently, using the brink depth, the direct discharge simple empirical relationships are generated for both flow regimes being a part of the main aim of this study, based on 4 different approaches that would be a toolkit for the engineers in practice in the relevant field. These proposed relationships are as

well compared with their theoretically obtained results through the proper statistical measuring indices for their accuracies.

Keywords: Brink, Circular, EDD, EDR, End depth, Exponential, Trapezoidal

ÖZ

Bu çalışmada, farklı analitik yaklaşımlar kullanılarak, hem nehir hem sel rejimi akımlar için pratikte çokca kullanılan ve deneysel verileri de mukayese için mevcut olan üssel (dikdörtgen, üçgen ve parabolik), genel ikizkenar trapez (dikdörtgen, üçgen, trapez, yarı-trapez, ters üçgen ve yarı-ters üçgen) ve genel dairesel (tabansız ve 4 farklı seviyede düz tabanı olan) geometrik enkesitler seçilmiş ve uç derinlik ile menba derinlik oranları (EDR) hesaplanmıştır. Ayrıca, nehir rejimi ve sel rejimi akımlar için önceki yaklaşım yöntemleri de kullanılarak yukarıda belirtilen enkesitler için EDR ve uç derinliğe bağlı debi (EDD) bağıntıları da elde edilmiştir. Yenilik olarak, ayrıca, bu çalışmanın bir parçası olarak sadece süreklilik ve enerji denklemleri kullanılarak iki yeni çözüm yöntemi önerilmiştir; üç hız noktası ile sonsuz sayıda hız noktası yaklaşımları. Önerilen yaklaşımlar için uç derinlikteki basınç katsayısının deneysel olarak belirlenmesi gereksinimine ihtiyaç duyulmamaktadır. Hesaplanmış EDR ve EDD bağıntıları, benzer enkesitler için, mevcut teorik ve deneysel verilerle istatistiksel olarak karşılaştırılmıştır. Daha sonra, sahada ilgili konularda uygulama yapan mühendislere yönelik, her iki akış rejimi için, uç derinliğe bağlı olarak debiyi doğrudan hesaplayabilecek basit amprik bağıntılar, 4 farklı yaklaşım yöntemi ile bu çalışmanın esas hedefi olarak türetilmiştir. Bu bağıntıların doğrulukları, teorik olarak üretilen değerlerle uygun istatistiksel endeksler yardımıyla karşılaştırılmıştır.

Anahtar kelimeler: Dairesel, EDD, EDR, Trapez, Uç derinlik, Üssel

TO MY FAMILY ESPECIALLY MY PARENTS

ACKNOWLEDGMENT

First and foremost, I would like to express my profound appreciation and sincere thanks to my supervisors, Assoc. Prof. Dr. Mustafa Ergil for his invaluable instruction and inspiration. I am grateful to him not only for his supervision, but for his major contribution in the formation of my character and skills as a young researcher. I eagerly hope to have another chance to work under his supervision.

I must give my special thanks to Assoc. Prof. Dr. Mohammad Karim Beirami. He was indeed a “private tutor” providing me with invaluable advice, direction and new viewpoints while I was carrying this research.

I want to thank the jury members in the committee, Prof. Dr. Cevza Melek Kazezyılmaz Alhan, Prof. Dr. Mehmet Emin Birpınar, Prof. Dr. Zalihe Nalbantoğlu Sezai, and Assoc. Prof. Dr. Umut Türker for taking the time to read and comment on my work.

Special thanks goes to Dr. Mark Streling for being kind enough to provide me with experimental data sets without which this research would have been remained incomplete.

I would like to offer my sincere thanks to all those who assisted me during my PhD study in particular the staff of Civil Engineering Department.

I would also like to thank my dear friend Dr. Nima Tazehzadeh due to helping me for the thesis format. I only hope that one day I will be able to do something equally valuable for him.

I want to say many thanks to all of my friends in the North Cyprus and abroad for helping me to enjoy my life besides work on this thesis. In no particular order, thank you to Dr. Alireza Rezaei, Dr. Hamid Mir Mohammad Sadeghi, Dr. Mehdi Hosseinpour, Dr. Ahmad Haseeb Payab, and Mir Mohammad Ali Malakoutian.

Finally I have to say I am richly blessed to have my parents who are always there for me. I would not be who and where I am now without the love, support, inspiration and advice of them. I would also like to express my deep gratitude to my brother “Dr. Ashkan Abrari” and my sister “Dr. Aida Abrari” for their encouragement and support. Undoubtedly, the completion of this research would not have been possible without my family support.

LIST OF SYMBOLS AND ABBREVIATIONS

A_c	The cross-sectional area of the flow at that fictitious section
A_e	The flow area at the end section
A_n	The flow area at the normal section
$A_{(1)to(2)}$	The sub-sectional flow area between the top and the second points of the end section
$A_{(2)to(3)}$	The sub-sectional flow area between the second and third points of the end section
$A_{(np-1)to (np)}$	The sub-sectional flow area between the $np-1^{\text{th}}$ point and the bottom of the end section
a_y	The normal acceleration
B	The bottom width
C_p	The pressure coefficient
C_v	The velocity head correction coefficient
D	The diameter
dA	The elemental infinitesimal flow area
d_e	The hydrostatic pressure head at the brink
d_i	The pressure head of the streamtube i
dh_E	The elemental infinitesimal depth
dQ	The elemental infinitesimal discharge
dx	The infinitesimal distance along x -direction
F_e	The pressure force at the end section
F_n	The pressure force at the normal section

Fr_c	The critical Froude number
Fr_n	The upstream normal Froude number
g	The acceleration due to gravity
H_n	The total energy head at the upstream normal section
h	The coordinate normal to channel bottom
h_E	The vertical distance measured from the total energy head
h_l	The local energy head loss
$I = y + Z$	
$\hat{I} = \frac{I}{D}$	
K_e	The pressure coefficient at the end section
k	The local energy loss coefficient due to the streamline curvature at the vicinity of the brink
m	The side slope ($m:1$; horizontal : vertical)
P_e	The mean pressure value at the end section
P_c	The channels wetted perimeter at the fictitious critical depth section
P_n	The channels wetted perimeter at the normal depth section
p	The general pressure distribution
Q	The flow rate (discharge)
r_{eb}	The radius of streamline curvature at the channel bottom of the end section
r_i	The radius of curvature of the streamtube i
r_s	The radius of curvature of the streamline
S	The longitudinal bed slope
S_c	The critical bed slope

S/S_c	The relative bed slope
T	The top width of water in contact with atmospheric pressure (the free surface flow width)
T_c	The top width of the flow at the fictitious critical water depth section
T_e	The top width of the flow at the end section
T_n	The top width of the flow at the normal section
u_{eb}	The flow velocity at the bottom of the channels of the end section
u_{et}	The flow velocity at the top of the channels of the end section
u_i	The flow velocity of the streamtube i
V	The mean flow velocity at any distance x within the control volume
V_e	The mean flow velocity at the end section
V_n	The mean flow velocity at the normal section
v_{eb}	The average velocity at the bottom of the end section
v_{ec}	The average velocity at the centroidal depth of the end section
v_{et}	The average velocity at the top of the end section
v_{np}	The velocity at the bottom of the end section for the infinite number velocity points method
v_l	The velocity at the top of the end section
W	The gravity force of water within the control volume
y	The flow depth at any distance x within the control volume measured from the brink towards upstream
\bar{y}	The centroidal depth at the end section, measured from the channel bottom to the centroid of that relevant cross-section
$\hat{y} = \frac{y}{D}$	

y_c	The critical water depth
y_e	The end (brink) depth
y_n	The flow depth at the normal section
y_{ep}	The effective piezometric head at the end section
y_i	The flow depth of the streamtube i
z	The elevation measured above the datum
$\hat{Z} = \frac{Z}{D}$	
α_e	The velocity correlation coefficient at the end section
α_n	The velocity correlation coefficient at the normal section
β_e	Boussinesq coefficient at the end section
β_n	Boussinesq coefficient at the normal section
γ	The specific weight of water
ρ	The mass density of water
τ	The wall and the bed shear stresses
$\zeta_{cir} = \frac{SD^{1/3}}{n^2 g}$	
EDD	The end depth discharge
EDR	The end depth ratio
EGL	The energy grade line

TABLE OF CONTENTS

ABSTRACT	iii
ÖZ	v
DEDICATION	vi
ACKNOWLEDGMENT	vii
LIST OF SYMBOLS AND ABBREVIATIONS	ix
LIST OF TABLES	xviii
LIST OF FIGURES.....	xix
1 INTRODUCTION.....	1
1.1 General.....	1
1.2 Hydraulic Characteristics of Free Over-fall	2
1.3 Aim of the Study.....	6
2 LITERATURE REVIEW.....	9
2.1 General.....	9
2.1.1 Exponential Channel Cross-sections	10
2.1.2 Generalized Trapezoidal Channel Cross-sections	16
2.1.3 Generalized Circular Channel Cross-sections	19
3 USE OF DIFFERENT ANALYTICAL METHODS FOR DEFINING THE FLOW AROUND THE BRINK DEPTH.....	24
3.1 General.....	24
3.2 Existing Methodologies	24
3.2.1 The Momentum Approach.....	24
3.2.2 The Boussinesq Approximation Theory	27
3.2.3 The Conservation of Energy Approach	29

3.2.4 The Free Vortex Theory	31
3.2.5 Sharp-Crested Weir Approach.....	34
3.3 Suggested Solution Methodologies	37
3.3.1 The Three Velocity Points Method.....	37
3.3.2 The Infinite Number Velocity Points Method (n-Velocity Points Method)	39
4 DIFFERENT ANALYTICAL SOLUTIONS OF THE END DEPTH RATIO (EDR) FOR VARIOUS CHANNEL CROSS-SECTIONS	43
4.1 General.....	43
4.2 The Channel Cross-sections	44
4.2.1 Exponential Channel Cross-sections	44
4.2.2 Generalized Trapezoidal Channel Cross-sections	45
4.2.3 Generalized Circular Channel Cross-sections	48
4.3 End Depth Ratio (EDR) for Various Channel Cross-sections.....	49
4.3.1 Previously Applied Theories	49
4.3.1.1 The Energy Method.....	49
4.3.1.2 Momentum Equation Coupled with the Free Vortex Theory	51
4.3.1.3 The Sharp Crested Weir Theory.....	53
4.3.1.3.1 The Continuity Equation.....	53
4.3.1.3.2 The Energy Equation.....	56
4.3.2 The Suggested Approaches.....	58
4.3.2.1 Three Velocity Points Method	58
4.3.2.2 Infinite Number (n-) Velocity Points Method	60
5 RESULTS AND DISCUSSION	62
5.1 Introduction	62

5.2 Exponential Channel Cross-sections	63
5.2.1 EDR for Sub-critical Flow Regimes	63
5.2.2 EDD for Sub-critical Flow Regimes.....	63
5.2.3 EDR for Super Critical Flow Regimes	66
5.2.3.1 EDR of Rectangular Channel Cross-sections.....	68
5.2.3.2 EDR of Parabolic Channel Cross-sections.....	71
5.2.3.3 EDR of Triangular Channel Cross-sections.....	74
5.2.4 EDD of Super Critical Flow Regimes	77
5.2.4.1 EDD of Rectangular Channel Cross-sections	78
5.2.4.2 EDD of Parabolic Channel Cross-sections.....	78
5.2.4.3 EDD of Triangular Channel Cross-sections.....	78
5.3 Generalized Trapezoidal Channel Cross-sections	80
5.3.1 EDR for Sub-critical Flow Regimes	80
5.3.1.1 EDR of Trapezoidal Channel Cross-sections.....	80
5.3.1.2 EDR of Inverted Triangular Channel Cross-sections.....	85
5.3.1.3 EDR of Semi-trapezoidal and Semi-inverted Triangular Channel Cross-sections	87
5.3.2 EDD for Sub-critical Flow Regimes.....	87
5.3.2.1 EDD of Trapezoidal Channel Cross-sections.....	88
5.3.2.2 EDD of Inverted Triangular Channel Cross-sections	91
5.3.2.3 EDD of Semi-trapezoidal and Semi-inverted Triangular Channel Cross-sections	93
5.3.3 EDR for Super Critical Flow Regimes	93
5.3.3.1 EDR of Trapezoidal Channel Cross-sections.....	94
5.3.3.2 EDR of Inverted Triangular Channel Cross-sections.....	99

5.3.3.3 EDR of Semi-trapezoidal and Semi-inverted Triangular Channel Cross-sections	100
5.3.4 EDD for Super Critical Flow Regime.....	100
5.3.4.1 EDD of Trapezoidal Channel Cross-sections.....	101
5.3.4.2 EDD of Inverted Triangular, Semi-trapezoidal and Semi-inverted Triangular Channel Cross-sections	105
5.4 Generalized Circular Channel Cross-sections with Flat-base	105
5.4.1 EDR for Sub-critical Flow Regimes	105
5.4.2 EDD for Sub-critical Flow Regimes.....	110
5.4.3 EDR for Super Critical Flow Regimes	113
5.4.4 EDD for Super Critical Flow Regimes	121
5.5 Direct Discharge Prediction.....	129
5.5.1 Sub-critical Flow Regimes.....	129
5.5.1.1 Generalized Trapezoidal Channel Cross-sections.....	129
5.5.1.2 Generalized Circular Channel Cross-sections.....	130
5.5.2 Super Critical Flow Regimes	132
5.5.2.1 Exponential Channel Cross-section	134
5.5.2.1.1 Rectangular Channel Cross-sections.....	134
5.5.2.1.2 Parabolic Channel Cross-sections	134
5.5.2.1.3 Triangular Channel Cross-sections	135
5.5.2.2 Generalized Trapezoidal Channel Cross-section	135
5.5.2.2.1 Trapezoidal and Inverted Triangular Channel Cross-sections ..	135
5.5.2.2.2 Semi-trapezoidal and Semi-inverted Triangular Channel Cross-sections	136
5.5.2.3 Generalized Circular Channel Cross-section	137

6 CONCLUSION AND RECOMMENDATIONS	139
6.1 Conclusion.....	139
6.2 Recommendations for Future Studies.....	142
REFERENCES.....	144
APPENDICES.....	153
Appendix A: The velocity head correction coefficient (C_v).....	154
Appendix B: Solution of three velocity points method for the exponential channel cross-sections.....	155
Appendix C: Solution of three velocity points method for the generalized trapezoidal channel cross-sections.....	157
Appendix D: Solution of three velocity points method for the generalized circular channel cross-sections	160
Appendix E: Solution of infinite number velocity points method for the exponential channel cross-sections.....	163
Appendix F: Solution of infinite number velocity points method for the generalized trapezoidal channel cross-sections	165
Appendix G: Solution of infinite number velocity points method for the generalized circular channel cross-sections.....	167

LIST OF TABLES

Table 4.1: The coefficient η_1 and the exponent η_2 constants that are used for generating the relevant cross-sections.....	45
Table 5.1: Computed EDR values and EDD relationships based on the two suggested methods of this study for the exponential channel cross-section.....	65
Table 5.2: Comparison between the computed EDR values of the different suggested methods of this study with the observed data of Dey and Ravi Kumar (2002) and the theoretical study by Beirami et al. (2006).....	86
Table 5.3: Comparison of observed data of \hat{Q} by Sterling and Knight (2001) with the computed data of \hat{Q} of the energy method.....	123
Table 5.4: Comparison of observed data of \hat{Q} by Sterling and Knight (2001) with the computed data of \hat{Q} of the free vortex theory.....	124
Table 5.5: Comparison of observed data of \hat{Q} by Sterling and Knight (2001) with the computed data of \hat{Q} of the three velocity points method.....	125
Table 5.6: Comparison of observed data of \hat{Q} by Sterling and Knight (2001) with the computed data of \hat{Q} of the infinite number velocity points method.....	126
Table 5.7: Equation of discharge (Q) based on the end depth (y_e) at sub-critical flow regime for different channel cross-sections using different theoretical methods.....	131
Table 5.8: Equation of discharge (Q) based on the end depth (y_e) at super critical flow regime for different channel cross-sections using different theoretical methods with the range of applicability of the effective parameters.....	138

LIST OF FIGURES

Figure 1.1: (a) Sketch of a free over-fall along the longitudinally mild slope; (b) the longitudinally steep slope, for general channel cross-section with the proposed pressure distribution over the control volume between the upstream section ($u-u$) and the end section ($e-e$) with the transversal cross-section..... 4

Figure 1.2: A typical sketch of the velocity (v) and the pressure (p) profiles deviations along the non-uniform flow zone that is occurring between the cross-sections $n-n$ ($x=-l$) and $e-e$ ($x=0$)..... 5

Figure 3.1: (a) Sketch of a typical channel cross-section (transversal) of the free over-fall at sub- and supercritical flow regime where the region between $n-n$ and $e-e$ are representing the suggested control volume; (b) the streamline patterns of a free over-fall..... 25

Figure 3.2: Sketch of a typical channel cross-section (transversal) of the free over-fall on a mild or steep (longitudinal) slope..... 32

Figure 3.3: (a) Sketch of a free over-fall at sub- and supercritical flow regime; (b) flow over a sharp-crested weir with a sill ‘ w ’ 36

Figure 3.4: Sketch of a typical channel cross-section (transversal) of the free over-fall on a mild or steep (longitudinal) slope with the proposed three velocity locations for the velocity distribution profile at the brink ‘ y_e ’ 39

Figure 3.5: Sketch of a typical channel cross-section (transversal) of the free over-fall on a mild or steep (longitudinal) slope showing the representative sub-section ($np-1$) and how the velocity locations are established to form the velocity distribution profile at the brink ‘ y_e ’ 40

Figure 4.1: Sketch of the exponential channel cross-section (transversal) of the free over-fall on a mild or a steep (longitudinal) slope	44
Figure 4.2: Sketch of the free over-fall at (a) the trapezoidal cross-section with symmetric sides; (b) the inverted-triangular (Δ -shaped) cross-section with symmetric sides (transversal) on mild or steep (longitudinal) slope.....	46
Figure 4.3: Sketch of free over-fall on the generalized circular channel cross-section (transversal) having flat base of the free over-fall on a mild or a steep (longitudinal) slope	49
Figure 4.4: Sketch of a free over-fall along the longitudinal symmetric sides trapezoidal channel cross-section with the proposed brink pressure distribution and its transversal (cross-sectional) details.....	54
Figure 5.1: Comparison between the variation of ε_e on \tilde{S} for $0.08 \text{ (m)} \leq y_c \leq 0.2 \text{ (m)}$ (m) and $B = 0.2 \text{ (m)}$ of the two suggested theoretical approaches and the theoretical solution of the free vortex theory with the study of (a) Anderson (1967); (b) Murty Bhallamudi (1994); and (c) Ferro (1999) in rectangular channel cross-sections.....	70
Figure 5.2: Comparison between the computed EDR values of the two suggested theoretical approaches and the free vortex theory with the experimental data set of the EDR of Jagannadha Rao (1961) in rectangular channels.....	71
Figure 5.3: Comparison between the variation of ε_e on \tilde{S} for $0.08 \text{ (m)} \leq y_c \leq 0.2 \text{ (m)}$ and $T_c = 0.2 \text{ (m)}$ of the two suggested theoretical approaches and the theoretical solution of free vortex theory with the study of (a) Anderson (1967); (b) Murty Bhallamudi (1994); and (c) the theoretical solution of the sharp-crested weir theory in parabolic channel cross-sections	73

Figure 5.4: Comparison between the variation of ε_e versus \tilde{S} for any value of m and $y_c=0.2$ and the theoretical study of (a) Anderson, (1967); (b) Murty Bhallamudi (1994); and (c) Ferro (1999) in triangular channel cross-sections..... 76

Figure 5.5: Comparison of the computational EDR values of the two suggested theoretical approaches and the free vortex theory of this study with the experimental data set of the EDR value by Rajaratnam and Muralidhar, (1964) in triangular channel cross-sections 77

Figure 5.6: Comparison between the experimentally determined non-dimensional discharge values with the computed non-dimensional discharge values of the two suggested approaches and the free vortex theory for (a) rectangular; and (b) triangular channel cross-sections 80

Figure 5.7: Comparison between the relevant theoretical and experimental EDR results of the previous studies and the computed EDR results of the energy method of the trapezoidal channel cross-section with symmetric sides at sub-critical flow regime..... 84

Figure 5.8: Comparison between the relevant theoretical and experimental EDR results of the previous studies and the computed EDR results of the (a) three velocity points method; and (b) infinite number velocity points method of the trapezoidal channel cross-section with symmetric sides at sub-critical flow regime 85

Figure 5.9: Comparison between the non-dimensional discharge (Q^*) values obtained from the energy method and the other relevant theoretical and experimental results for the trapezoidal channel cross-section with symmetric sides at sub-critical flow regimes..... 89

Figure 5.10: Comparison between the non-dimensional discharge (Q^*) values obtained based on the (a) three velocity points method; and (b) infinite number

velocity points method and the other relevant theoretical and experimental results for the trapezoidal channel cross-sections with symmetric sides at sub-critical flow regimes	90
Figure 5.11: Comparison between the non-dimensional discharge (Q^*) values with (a) the energy method; (b) the three velocity points method; and (c) the infinite number velocity points and the other relevant theoretical and experimental results for the inverted-triangular channel cross-sections at sub-critical flow regimes	92
Figure 5.12: Comparison between the ε_e values obtained based on four theoretical methods and the ε_e values of the (a) Boussinesq approach by Murty Bhallamudi (1994); and (b) sharp-crested weir theory for the trapezoidal channel cross-sections at supercritical regimes	96
Figure 5.13: Comparison between ε_e values based on four suggested methods and ε_e values based on the experimental data sets of Pagliara and Viti (1995) in trapezoidal channel cross-sections at super critical flow regimes	97
Figure 5.14: Comparison between ε_e values based on four suggested methods and ε_e values obtained based on the theoretical study (a) of Murty Bhallamudi (1994); and (b) the sharp-crested weir theory in trapezoidal channel cross-sections in super critical regimes	98
Figure 5.15: Comparison between ε_e and \tilde{S} values based on the suggested four methods for the range of $0.1 \leq N_c \leq 0.45$ and $m = 1$ with the (a) Boussinesq approach by Dey and Ravi Kumar (2002); and (b) sharp-crested weir theory by Dey and Ravi Kumar (2002) for inverted triangular channel cross-sections in super critical flow regimes	100

Figure 5.16: Comparison between the computed non-dimensional discharges (Q^*) of the proposed four methods and the experimental data sets of Q^* by Pagliara and Viti (1995) for the trapezoidal channel cross-sections at super critical flow regime..... 102

Figure 5.17: Comparison between the computed non-dimensional discharges (Q^*) of the suggested four methods and the theoretical Q^* results of the (a) Boussinesq approach of Murty Bhallamudi (1994); and (b) sharp-crested weir theory for the trapezoidal channel cross-sections at super critical flow regimes..... 104

Figure 5.18: EDR values based on the proposed methods of circular channel cross-section with flat-base for (a) $\hat{Z} = 0$; (b) $\hat{Z} = 0.25$; (c) $\hat{Z} = 0.33$; (d) $\hat{Z} = 0.5$; and (e) $\hat{Z} = 0.66$ at sub-critical flow regimes..... 109

Figure 5.19: Comparison between the non-dimensional discharges (\hat{Q}) values of the suggested methods for the circular channel cross-section with flat-base and the experimental data set of Sterling (1998) for (a) $\hat{Z} = 0$; (b) $\hat{Z} = 0.25$; (c) $\hat{Z} = 0.33$; (d) $\hat{Z} = 0.5$; and (e) $\hat{Z} = 0.66$ at sub-critical flow regimes..... 113

Figure 5.20: Comparison between ε_e versus \tilde{S} values based on the proposed four methods and (a) Dey (2002) by the Boussinesq approach; and (b) Dey (2002) by the sharp-crested weir theory of the circular channel cross-section for $\hat{Z} = 0$, $D =$ any value, and $0.3 \leq \hat{y}_c \leq 0.8$ 116

Figure 5.21: Comparison between ε_e versus \tilde{S} values based on the proposed four methods and (a) Dey (2002) by the Boussinesq approach; (b) Dey (2002) by the sharp-crested weir approach of the circular channel cross-section for $\hat{Z} = 0.25$, $D =$ any value, and $0.1 \leq \hat{y}_c \leq 0.6$ 117

Figure 5.22: Comparison between ε_e versus \tilde{S} values based on the proposed four methods and (a) Dey (2002) by the Boussinesq approach; (b) Dey (2002) by the sharp-crested weir approach of the circular channel cross-section for $\hat{Z} = 0.5$, $D =$ any value, and $0.1 \leq \hat{y}_c \leq 0.4$ 118

Figure 5.23: ε_e values based on the suggested methods of this study versus (a) ε_e values based on the theoretical study of Dey (1998) using Boussinesq approach; and (b) ε_e values based on the theoretical study of Ahmad (2012) using sharp-crested weir theory in circular channel with $\hat{Z} = 0$ 119

Figure 5.24: ε_e values based on the suggested methods of this study versus (a) ε_e values based on the theoretical study of Dey (2003) using Boussinesq approach; and (b) ε_e values based on the theoretical study of Ahmed (2005) using sharp-crested weir theory in circular channel with $\hat{Z} = 0.5$ 120

Figure 5.25: Comparison between the computed non-dimensional discharges (\hat{Q}) of the suggested methods of this study with (a) the theoretical \hat{Q} results of Dey (1998); and (b) the theoretical \hat{Q} results of Ahmad (2012) for the circular channel cross-section at super critical flow regime with $\hat{Z} = 0$ 127

Figure 5.26: Comparison between the computed non-dimensional discharges (\hat{Q}) of the suggested methods of this study with (a) the theoretical \hat{Q} results of Dey (2003); and (b) the theoretical \hat{Q} results of Ahmad (2005) for the circular channel cross-section at super critical flow regime with $\hat{Z} = 0.5$ 128

Chapter 1

INTRODUCTION

1.1 General

In open channels flow, a free over-fall as one type of the drop structures is a phenomenon where the flow separates at the sharp edge and forms a free nappe due to an abrupt end (drop) in the channel bottom. This occurrence offers the use of the free over fall as a flow measuring structure that eliminates the need of any calibration. The depth of flow at the location where the sudden drop occurs is known as the brink depth section or the end-depth section. This brink depth value depends on the shape of the channel cross-section, the longitudinal slope of the channel bed and the characteristics of the free nappe. The critical flow depth (y_c) being a driving parameter as a control section in open channels so as to determine the flow discharge amount, since there exists a unique relationship between the critical flow depth (y_c) and the discharge (Q). Therefore, it can be used to estimate the discharge through the rivers, streams, flumes and irrigation channels as well. Knowing that, the exact location of the critical flow depth along the longitudinal channel cross-section is depending on the discharge amount and the channels transversal cross-section characteristics, it is not easy to determine it. To overcome this problem, the pivotal experimental work by Rouse (1936) for rectangular channel cross-section in sub-critical flow regime enlightens the researchers to relate the end depth to the critical depth since the end depth (brink) location never changes. Since then, this feature attracted the interest of the researchers where they apply the concept of free over-fall

in their theoretical studies and experimental observations to measure the discharge values for both sub- and super critical flow regimes.

1.2 Hydraulic Characteristics of Free Over-fall

Measuring the flow discharge (Q) in open channels is crucial, but adequate instruments are needed, usually making the measurement costly and time-consuming. In open channel flow, a free over-fall is followed by an abrupt channel end where the flow separates at the sharp edge and forms a free nappe. The free surface profile in the immediate vicinity of a free over-fall is schematically illustrated in Figs. 1.1(a) and 1.1(b) for general channel cross-sections along longitudinally mild and steep slopes, respectively. Line ($e-e$) refers to the transversal cross-section at the end of the channel (called the brink) where the free over-fall occurs. The depth of water at the brink depends on the shape of the channel cross-section, the slope of the channel and the characteristics of the free nappe. The rapidly varied flow (RVF) zone that occurs within the region between the brink/end section ($e-e$) and the upstream cross-section ($u-u$) is called the brink zone. As shown in Fig. 1.1(a), the critical flow depth (y_c) occurs at the upstream flow section ($u-u$) along the mildly sloping channel and forms a gradually varied flow (GVF) zone since the flow regime is sub-critical. Further upstream from this GVF zone, uniform flow characteristics prevail. Fig. 1.1(b) shows the location of the RVF zone along the steeply sloping channel where the flow regime is super critical, as GVF never occurs. As this figure implies, normal depth (y_n) forms at the upstream flow section ($u-u$) provided that the longitudinal length of the channel is sufficiently long.

From the upstream section to the brink where the RVF zone occurs, the water surface curvature gradually decreases forming a control section. At the upstream section

where the RVF starts, the vertical component of the acceleration is weak, and the pressure distribution can safely be assumed to be hydrostatic. However, at the end section (brink), the pressure at the upper and the lower points of the free nappe is zero, ensuring a strong departure from the hydrostatic pressure distribution that prevails in open channel. Previous theoretical and experimental studies at the RVF zone have found a relationship between the depth of the water at the end section (y_e) and the upstream water depth (y_c or y_n) and defined this relationship as the end depth ratio (EDR). The gravity affects the curvature of the free nappe that extends a short distance upstream of the end section, leading to flow acceleration that causes the water depth at the brink to be the minimum, hence causing the EDR always to be less than unity.

A typical free over-fall with free nappe at sub- and super critical flow regime for uniform and non-uniform zones are detailed in Fig. 1.2 where $n-n$ ($x=-l$) is representing the end of the uniform zone (i.e. the beginning of the non-uniform zone) and $e-e$ ($x=0$) representing the end of the non-uniform flow zone (i.e. the brink). Once the non-uniform flow zone starts, the pressure distribution differs from the hydrostatic one and transforms gradually within this zone along the flow direction and at the brink a pattern of a non-symmetric parabola with a maximum occurring not at the middle but closer to the channel bottom is assumed to be formed as shown in Fig. 1.2. This figure also details how the uniform velocity (v) and the pressure (p) distribution along the flow direction within the non-uniform flow zone deviates.

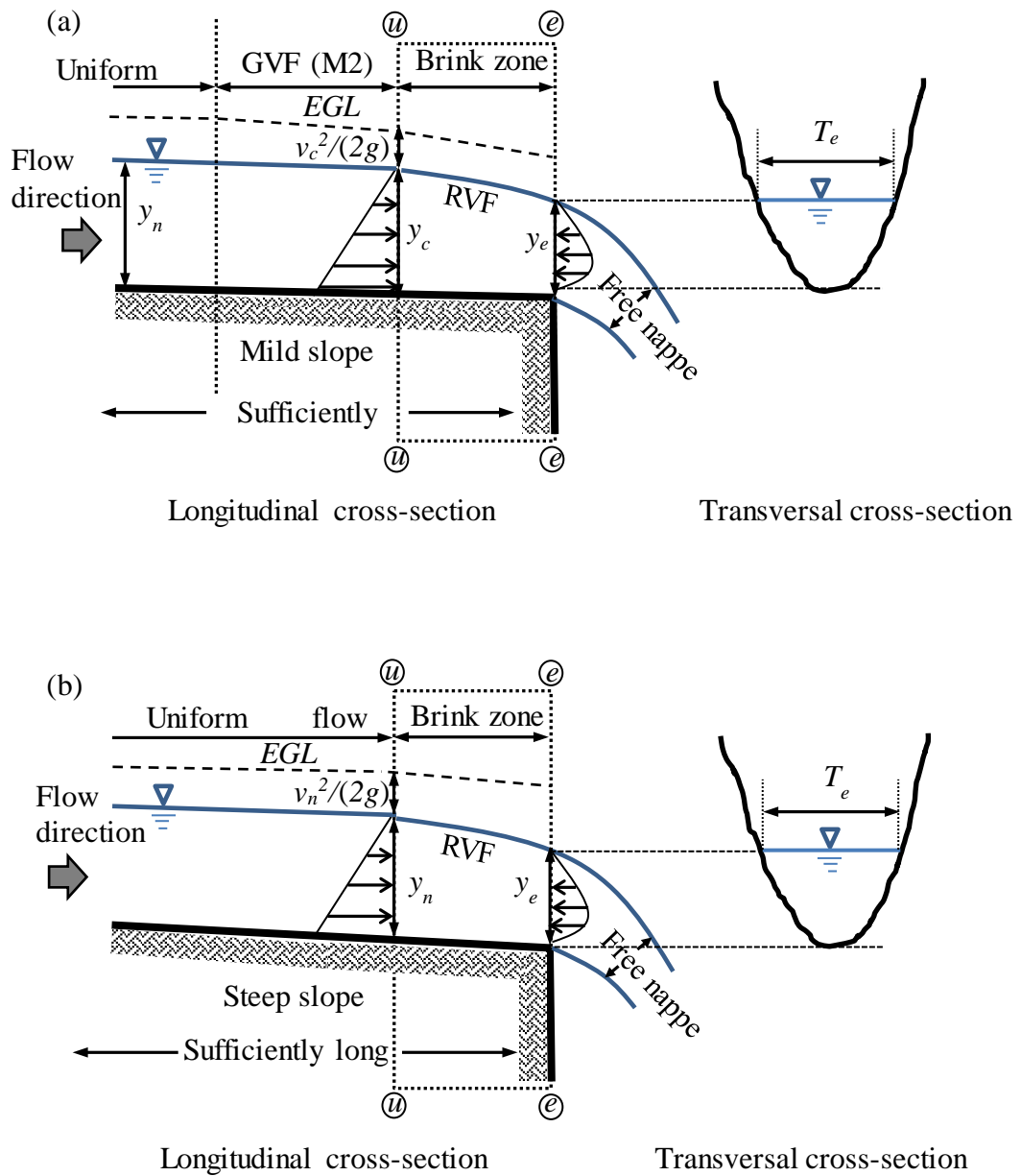


Figure 1.1: (a) Sketch of a free over-fall along the longitudinally mild slope; (b) the longitudinally steep slope, for general channel cross-section with the proposed pressure distribution over the control volume between the upstream section ($u-u$) and the end section ($e-e$) with the transversal cross-section

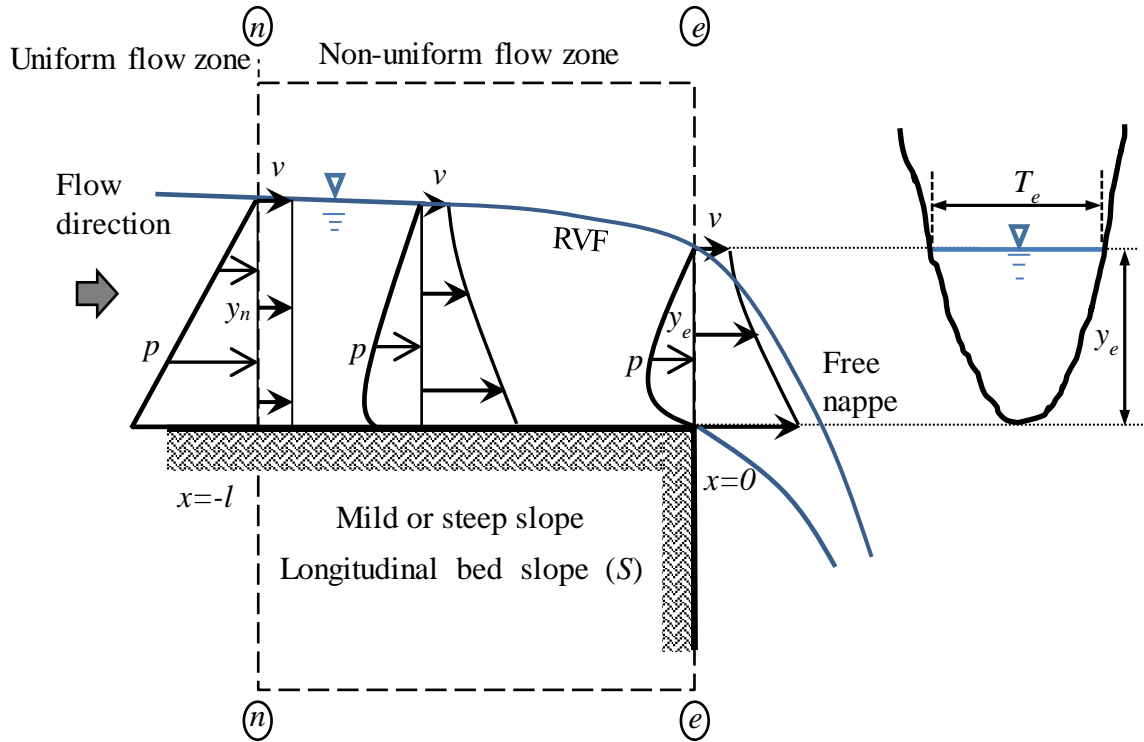


Figure 1.2: A typical sketch of the velocity (v) and the pressure (p) profiles deviations along the non-uniform flow zone that is occurring between the cross-sections $n-n$ ($x=-l$) and $e-e$ ($x=0$)

By coupling the EDR with the upstream Froude number, another relationship between the depth of water at the end section and the flow discharge (Q) can be obtained and is referred to as the end depth discharge (EDD). This enables the free over-fall to be used as a flow metering device in open channels (laboratory flumes, irrigation channels, etc.). Since the critical depth (y_c) bears a unique relationship with the discharge (Q) through a critical Froude number ($Fr_c=1$), a relationship between the end depth (y_e) and the critical depth (y_c), the discharge (Q) can eventually be related to the end depth (y_e) in a free over-fall in a sub-critical flow regime. However, in super critical flow regimes, since the normal depth (y_n) is less than the critical depth (y_c), the discharge (Q) can be given by a relationship between the end depth (y_e) and the channel bed slope (S).

Due to that, various practically in use cross-sectional shapes were studied theoretically and experimentally to predict the EDR from which the end depth discharge (EDD) relationships can be computed without applying the critical Froude number approach. Most of the analytical methods are based on the application of either the momentum equation and/or the continuity equation with different assumptions, especially regarding the velocity and the pressure distributions at the end section. In momentum approach, the accuracy of the prediction of the EDR and the EDD values depends upon the precision of the measurement of the end pressure coefficient that should be determined experimentally or assumed theoretically.

The situation of the free over-fall is analogous to the flow over a sharp-crested weir without sill. Therefore, the continuity equation based on the sharp-crested weir theory can be used to determine the EDR and the EDD relationships of the same section with zero brink pressure effect. Many experimental works on free over-falls with various cross-sectional shapes by different researchers with different assumptions as discussed above have been performed to enlighten the characteristics of this phenomenon and show the degree of accuracy of different analytical methods as well. Even rare, there are some theoretical studies attempting to apply the energy equation coupled with the streamline curvature for the determination of the EDR and the EDD values.

1.3 Aim of the Study

Due to the difficulties faced while performing experiments at super critical flow regimes and complexity of the theoretical mathematical expressions, most of the studies dealt mainly with the theoretical application of the governing equations in sub-critical flow regimes (i.e. inserting Froude number as unity). However, this is not

a normal condition in practice. In addition, measuring the flow depth at the critical section is not an easy task since its occurring location is not known exactly. Yet, there are limited numbers of free over-fall studies on steep slopes. Therefore in this study, the ratio between the end depth and the upstream depth which is known as the end depth ratio (EDR) is computed for those cross-sections that are widely used in practice. To ease the derivation calculations, the selected cross-sections are grouped into three broad categories. The exponential channel cross-section category represents the rectangular, the triangular and the parabolic cross-sectional shapes. The generalized trapezoidal channel cross-section category represents other than the rectangular and the triangular, the trapezoidal, the semi-trapezoidal, the inverted triangular and the semi-inverted triangular cross-sectional shapes. The generalized circular channel cross-section category represents circular channel cross-sections with no flat base and with flat base at four different heights (Z). For the above mentioned cross-sections, different analytical methods for both sub- and super critical flow regimes were studied. These selected cross-sections are widely used in practice and most of them are having experimental data sets (obtained by previous relevant studies) hence used for the comparison. This study not only solves the free over-fall based on the previously suggested theories for both sub- and super critical flow regimes; the energy method, the sharp-crested weir theory and the free vortex theory in order to generate the EDR and the EDD relationships for the above-mentioned cross-sections, but also offers two new approaches; the three velocity points method and the infinite number velocity points method (n -velocity points) that are only utilizing the continuity and the energy equations. These two suggested approaches eliminate the need of the end pressure coefficient that was expected to be determined experimentally. Subsequently, the direct discharge simple empirical

relationships being a part of the main aim of this study are computed by four different approaches (the energy method, the free vortex theory, the three velocity points method and the infinite number velocity points method) that would be a toolkit for the engineers in practice in the relevant field. The results of this study are compared with the relevant existing experimental data sets and the other relevant theoretical results available in the literature so as to check their accuracies through the statistical measuring indices namely the linear regression ' R^2 ' and the percentage mean absolute relative error 'MARE'.

Chapter 2

LITERATURE REVIEW

2.1 General

This chapter presents an overview of flow characteristics of the free over-fall problems in open channel for the generalized prismatic channel cross-sections. These generalized prismatic cross-sections not only represent the different cross-sectional shapes, but are also representative of the geometries that are often approximated for the modeling of the natural rivers and/or directly used in flumes. The details provided in this chapter intentionally kept as brief as possible, since all of the relevant topics discussed here can be found in different textbooks and/or relevant review papers like Chow, 1959; Henderson, 1966; Subramanya, 1997; Dey, 2002. This chapter is not only reviewing the computation of the end depth ratio (EDR) and the end depth discharge (EDD) relationships, but also discusses the application of the different theoretical methods and experimental works of the various researchers for different channel cross-sections in mildly and steeply sloping longitudinal channel beds. The chapter is sub-sectioned into three broad categories based on prismatic channel cross-sectional shapes where different theoretical methods and experimental works of various researchers are detailed briefly for the determination of the EDR and EDD values.

In the first sub-section, the review of the generalized exponential channel cross-section for both sub- and super critical flow regimes (flowing over mild or steep

slopes) are discussed based on the previous theoretical and experimental studies. The successive sub-section details the review of the generalized trapezoidal channel cross-section whereas, the last sub-section reviews the generalized circular channels cross-section for both sub- and super critical flow regimes based on the previous relevant theoretical and experimental studies.

2.1.1 Exponential Channel Cross-sections

The free surface profile depends upon the discharge (Q) amount and the critical depth (y_c), but the exact location of the critical flow depth is not known for the free over-falls. In order to overcome this difficulty, the pivotal experimental work by Rouse (1936) for rectangular channel cross-section in sub-critical flow regime, enlightens the researchers to create the relationship between the end depth and the critical depth from which the discharge can be estimated, since the end depth (brink) location never changes and being easy to measure. He related the critical flow depths of certain discharges to their end depths that were occurring within the mildly sloping rectangular channel cross-sections and referred to it as an end depth ratio (EDR) which is the ratio of the water depth at the brink (y_e) to the critical water depth (y_c). For sub-critical flow regimes in rectangular channel cross-sections, he found EDR to be 0.715. Since then, this feature attracted the interest of the researchers where they apply the concept of free over-fall in their theoretical studies and experimental observations in order to determine the end depth ratio and the end depth discharge (EDD) of the free over-fall in different channel cross-sections for both sub- and super critical flow regimes.

Jaeger (1948) coupled the momentum and the energy equations using the Boussinesq approximation to compute the EDR in horizontal rectangular channels and obtained a value of 0.725 for sub-critical flows. Delleur et al. (1956) solved the momentum

equation in order to compute the EDR of the rectangular free over-falls by assuming the pressure over the brink is a dependent variable of hydrostatic pressure. They also carried out the experimental work to investigate the effects of slope and channel wetted perimeter roughness on the free over-fall. They observed that, the EDR value is influenced by the relative slope which is the ratio of the channels longitudinal bed slope (S) to the fictitious critical slope (S_c) but it is independent on the wetted perimeter roughness in super critical flow regimes. In sub-critical flows, the value of the EDR was found to be 0.706 for the rectangular channel cross-sections. Diskin (1961) used the momentum equation by assuming the zero brink pressure effect and obtained the EDR values of 0.667, 0.731 and 0.775 for rectangular, parabolic and triangular channel cross-sections at sub-critical flow regime, respectively. Rajaratnam and Muralidhar (1964a) studied the flow over mildly sloping channel beds where, they applied the momentum equation to the exponential (power-law) channel cross-sections and derived a theoretical equation for the EDR. They conducted various experiments in order to verify their theoretical approach and they found the EDR values to be 0.795 and 0.772 for triangular and parabolic channels, respectively. They also studied the exponential cross-sections of the free over-fall on steep slope channel beds and they expressed the EDR as a function of relative slope (S/S_c) where the variation of the end pressure coefficients to the relative slopes was as well presented graphically. Then on, Rajaratnam and Muralidhar (1968) performed experimental studies on smooth rectangular cross-sections of the free over-falls in more detail. They measured the bed pressures and the bed shear stresses of the brink (end section) for different channel bed slopes (zero, adverse, mild and steep).

Ali and Sykes (1972) applied the free vortex theory to compute the EDR of free over-fall in sub-critical flow regime for exponential channel cross-section. The computed values of the EDR were found to be 0.678, 0.798 and 0.747 for rectangular, triangular and parabolic channel cross-sections, respectively. Rajaratnam et al. (1976) presented the results of an experimental study in order to assess the effect of slope and roughness on EDR for rectangular channel cross-sections. In sub-critical flow regimes, the EDR values decrease with the increase in relative roughness (the ratio of the Nikuradse equivalent sand roughness (k_s) to the critical depth (y_c)). However, in super critical flow regimes, the magnitude of the EDR decreases with the increase in relative slope (S/S_c). Kraijenhoff and Dommerholt (1977) experimentally study the effect of the longitudinal bed slope (mild) and the wall roughness of the rectangular cross-sections of the free over-fall. Their result yielded that, the EDR value was not effective on the slope and the roughness, since the average value of the EDR was found to be 0.714.

Hager (1983) for the computation of the EDR in rectangular channel cross-sections utilized the momentum and the extended energy equations and also took into account the curvature of the streamlines. He obtained an equation for the ratio of the end depth (y_e) to the critical depth (y_c) with respect to the upstream Froude number (Fr_n) for super critical flow regimes as:

$$\frac{y_e}{y_c} = \frac{Fr_n}{Fr_n + \frac{4}{9}} \quad (2.1)$$

The above-mentioned equation yields the value of EDR to be 0.696 in sub-critical flow regimes with unconfined nappe. The free surface profile was analyzed on the

control volume between the upstream and downstream of the end section as well within this work.

Montes (1992) numerically computed the pressure distribution at the end (brink) section of the rectangular channels, based on the potential flow solution. He found that, the pressure is zero at the channel bed and the free surface with a maximum value of pressure $p = 0.18\gamma y_e$ at $y = 0.16y_e$. His computed curve was in good agreement with the experimental data sets of Rouse (1932), Veronese (1948), Replogle (1962) and Rajaratnam and Muralidhar (1968).

Ferro (1992) experimentally presented that, the value of the EDR is not influenced due to the width changes of the rectangular channel cross-sections of the free over-fall at sub-critical flow regimes. He reported the EDR value of 0.760 for five different widths. Based on the computed EDR values, around 90% of the calculated discharge values were within 5% of his experimental obtained data set. Subramanya (1997) extended Anderson's (1967) work based on the theoretical application of the energy equation to compute the EDR value for exponential channel cross-section in both sub- and super critical flow regimes. The computed EDR values were found to be 0.694, 0.734 and 0.762 for rectangular, parabolic and triangular channel cross-sections respectively. Also the variation of the EDR with the upstream normal Froude number (Fr_n) was presented graphically for super critical flow regimes. Davis et al. (1998) have performed several experiments in order to investigate the effect of the longitudinal channel bed slope (S) and the Manning-Strickler roughness coefficient (n) for the rectangular channel cross-section of the free over-fall. They found out that, the EDR value is dependent on the above mentioned channel

characteristics. They were in fact the first researchers whom obtained the EDR equations as a function of S and n .

$$\frac{y_e}{y_c} = 134.84S^2 - 12.66S + 0.778 \quad (2.2)$$

$$\frac{y_e}{y_c} = 0.846 - 0.219\sqrt{\frac{S}{n}} \quad (2.3)$$

For the zero slopes, by substituting $S = 0$ into Eq. (2.3), gives the EDR value of 0.846 which is well above the experimental and theoretically obtained values of the other researchers.

Dey (2000) used the momentum equation based on the Boussinesq approximation and theoretically obtained the EDR relationship in steeply sloping rough rectangular channels cross-sections. The effect of the streamline curvature at the free surface was also used to calculate the flow profile of the upstream of the end section. The computed results obtained by Dey (2000) were within the acceptable range of the experimental data of Rajaratnam et al. (1976). Ahmad (2002) also carried out an experimental study of the free over-fall in sub-critical flow regimes for the triangular channel cross-sections and obtained the value of the EDR to be 0.802. Ahmad (2003) applied the sharp-crested weir theory by inserting a brink pressure coefficient in order to establish higher accuracy for the discharges in both sub- and super critical flow regimes for the rectangular channels. The EDR values found by him to be 0.780 and 0.758 in sub-critical flow regime for confined and unconfined nappes, respectively. In super critical flow regimes, the relationship between the end depth (

y_e) and the critical depth (y_c), determined from the continuity equation and was given as:

$$\frac{y_e}{y_c} = \frac{3Fr_n^{\frac{1}{3}}}{\left(2(1-Cp) + Fr_n^2\right)^{\frac{3}{2}} - \left(Fr_n^2 - 2Cp\right)^{\frac{3}{2}}} \quad (2.4)$$

where C_p represents the end pressure distribution coefficient that should be evaluated through experiments. He also found that, y_e/y_c value decreases with the increase in relative slope (S/S_c). The predicted results obtained by Ahmad (2003) in fact agreed well with the experimental datasets in the literature.

Tigrek et al. (2008) experimentally studied the rectangular free over-fall at sub- and super critical flow regimes, both in smooth and rough surface channels. The effect of the longitudinal channel bed slope and the channel bed roughness on the ratio of y_e/y_c was investigated for both flow regimes. They concluded that, the slope and the roughness did not change the average value of y_e/y_c being 0.683 in sub-critical flow regime. However, unlike the sub-critical flow regimes, for super critical flow regimes, they found that, the longitudinal channel bed slope (S) and the roughness coefficient (n) do affect the ratio of y_e/y_c similar to the earlier researchers. Using the curve fitting technique, they suggested the following equation:

$$\frac{y_e}{y_c} = 0.773 - 0.018 \sqrt{\frac{S}{n}} \quad (2.5)$$

Vatankhah (2015) applied the sharp-crested weir theory for the exponential (power-law) channel cross-sections for sub-critical flow regimes and obtained the EDR values to be 0.715, 0.777 and 0.817 for rectangular, parabolic and triangular channel

cross-sections, respectively. He also obtained a generalized EDD relationship of the free over-fall in sub-critical flow regimes only.

2.1.2 Generalized Trapezoidal Channel Cross-sections

Diskin (1961) performed the earliest theoretical research and derived a general equation for the end depth (y_e) of the free over-fall for trapezoidal cross-sections in sub- and super critical flow regimes. He applied a theoretical approach based on the momentum equation and derived a general equation for the end depth of free over-fall by assuming zero pressure at the brink section. He also carried out series of experiments in trapezoidal channel cross-section and concluded that, the theoretical results based on this approach were not sufficiently accurate so as to be used for the flow discharge measurements.

Rajaratnam and Muralidhar (1970) used momentum equation to obtain the EDR relationship of the trapezoidal free over-fall in mildly and steeply sloping channels. The pressure coefficient was measured experimentally and incorporated in this theoretical analysis. They performed some experiments as well for a wide range of the longitudinal bed slopes, in order to validate their theoretical approach for both flow regimes. In sub-critical flow regimes, they obtained the EDR value ranging from 0.705 to 0.758. Whereas, in super critical flow regimes, their EDR values were expressed as a function of the relative slope (S/S_c). Furthermore, within their studies, the free surface profiles, the bed shear stresses, the velocity and the pressure distributions in the vicinity of the end section were investigated.

Keller and Fong (1989) theoretically studied the trapezoidal free over-fall for sub-critical flow regime and they were the first that comprised the contribution of the

brink depth pressure effect in the momentum equation based on Replogle (1962) measurements, where they super impose the effect of the pressure to the rectangular and the triangular channel cross-sections. They also conducted experiments on horizontal slopes for trapezoidal channel cross-sections so as to validate their computed equation of the EDR based on the theoretical approach.

Murty Bhallamudi (1994) theoretically investigated the EDR in the trapezoidal and the exponential channel cross-sections of free over-falls based on the momentum equation and the Boussinesq approach for sub- and super critical flow regimes and presented a methodology for estimating the discharge (Q) from the given value of the end depth. Water surface profiles were also computed based on the momentum equation for different channel cross-sections that were carrying flows in sub- and super critical regimes.

Anastasiadou-Partheniou and Hatzigiannakis (1995) studied the free over-fall in symmetric sided trapezoidal channel cross-sections using the sharp crested weir without crest and demonstrated a general equation of the EDR where the curvature of the streamline at the brink was considered for both sub- and super critical flow regimes. The predicted discharges were also presented graphically and compared with the experimental data sets of Keller and Fong (1989) for flows in the sub-critical regime and also experimental data sets of Diskin (1961) for flows in super critical regime. They also suggested an approach for computing the free surface profile between the upstream section and the brink section using the energy equation.

Ferro (1999) assumed that, the flow over a free over-fall simulates the flow over a sharp-crested weir without a crest and deduced the end depth discharge (EDD)

relationships for rectangular, triangular channel cross-sections for both sub- and super critical flow regimes. Furthermore, by super imposing the flow discharge of the rectangular and the triangular channel cross-sections, the EDD relationship of the trapezoidal channel cross-section was obtained by him. Ahmad (2001) applied the sharp-crested weir theory and obtained the discharge values in sub-critical flow regimes for trapezoidal channel cross-sections with symmetric sides by considering the quadratic pressure distribution at the brink. The computed values of the EDD were compared with various experimental data sets of previous studies. Dey and Ravi Kumar (2002) applied the continuity equation based on the sharp-crested weir theory and also the momentum equation coupled with the Boussinesq approximation so as to determine the EDR values for the inverted symmetric sided triangular (Δ) cross-sections in sub-critical regime. The estimation of the discharges from the known end depth was presented for both methods and were verified through the relevant experiments.

Ramamurthy et al. (2004) formulated a precise relationship between the end depth (y_b) and the discharge (Q) for the trapezoidal channel cross-sections in a sub-critical flow regime only. Ramamurthy et al. (2006) also developed a VOF (Volume of Fluid) model for the free over-fall to predict the pressure distribution, the velocity distribution and the water surface profile in the horizontal bed slope of the trapezoidal channel cross-sections.

Beirami et al. (2006) solved the momentum equation based on the free vortex theory and determined the EDR relationships for the flows in different channel cross-sections at sub-critical flow regimes only. They constructed various monograms to facilitate the prediction of the flow discharges from the given values of the end

depths for those different channel cross-sections. They also found the pressure coefficients at the end section using the free vortex theory.

Ahmad and Azamathulla (2012) extended the theoretical method based on the sharp-crested weir theory for sub-critical flow regimes of the trapezoidal free over-falls to compute the EDR and the EDD relationships for the super critical flow regimes. The experimental data sets of Diskin (1961) were used in order to verify their theoretical study. Furthermore, direct solution for discharge was provided graphically for different values of side slopes. Vatankhah (2013) as well presumed that, the flow over a free over-fall simulates the flow over sharp-crested weir (with zero crest height), so using the continuity equation obtained the EDD relationship only for the trapezoidal and the inverted triangular channel cross-sections in sub-critical regimes only. He also proposed direct discharge equations in terms of the end depth for these two cross-sections, separately.

2.1.3 Generalized Circular Channel Cross-sections

Rohwer (1943) carried out some experiments in horizontal slopes for circular channel cross-sections in order to obtain a direct discharge relationship for the known values of the end depth (y_e) and the channel cross-sections diameter (D) where he obtained an empirical relationship as:

$$Q = 8.58 D^{0.62} y_e^{1.82} \quad (2.6)$$

In this equation, y_e and D are in inches, and Q is in gallon per minute. He limited the validity of this equation to be up to $0.5 D$, since he reported that the flow depth became unstable when it was more than the half of the channel cross-section diameter. Using momentum equation by assuming the zero pressure at the end

section, Smith (1962) generated an equation for the EDR in circular channel for sub-critical flow regimes. He conducted the experiments in order to validate his generated theoretical equation. Rajaratnam and Muralidhar (1964b) used momentum equation to get the EDR relationship for the circular channel cross-section in both sub- and super critical flow regimes. In sub-critical flow regimes, the value of EDR was found to be 0.725. However, in super critical flow regimes, they reported the value of the EDR as a function of the relative slope (S/S_c). They also carried out a large number of experiments in order to verify their theoretical approach.

Ali and Ridgway (1977) applied the free vortex theory to get the relationship of the EDR for horizontal slope for circular channel of the free over-fall. Also Subramanya and Kumar (1993) applied the energy approach in order to compute the EDR and the EDD relationships of the circular channel cross-section of the free over-fall for sub-critical flow regimes. Clausnitzer and Hager (1997) used momentum equation for the circular channel cross-sections at super critical flow regimes and obtained the following dimensionless equation for the ratio of the end depth to the critical depth as:

$$\frac{y_e}{y_c} = \left(\frac{2F_1^2}{1 + 2F_1^2} \right)^{\frac{2}{3}} \quad (2.7)$$

where $F_1 = Q / (gDy_n^4)^{0.5}$.

Dey (1998) analyzed the free over fall for circular channel cross-sections in order to compute EDR relationship, by applying the momentum equation based on Boussinesq approximation for both sub- and super critical flow regimes. In sub-critical flow regime, the value of the EDR was found to be around 0.750 for a critical

flow depth to diameter ratio (y_c/D) up to 0.82. However, in super critical flow regimes, the EDR was expressed as a function of the longitudinal bed slope (S). The prediction of the discharge was presented for both flow regimes. Furthermore, the streamline curvature of the free surface was utilized to compute the flow profile upstream of the end section of the free over fall.

Sterling and Knight (2001) experimentally studied the circular channel cross-sections with and without a horizontal bed (flat bed) in order to obtain the EDR and the EDD values for both sub- and super critical flow regimes. Their experiments were carried out in PVC channel of having a length of 21.26 m. In order to investigate the influence of the flat bed with different heights of Z with a range of $0 \leq Z < D$, upon the EDR, five different values of flat base (bed) were examined ($Z/D = 0.00, 0.25, 0.33, 0.50, 0.66$) for both flow regimes. They found that, the EDR for a given cross-section geometry is 0.743 for sub-critical flow regimes. However, in super critical flow regimes, the EDR value was expressed as a function of the relative slope (S/S_c) and the flat bed height (Z) of the channel cross sections.

Dey (2001) used sharp-crested weir theory by assuming zero pressure at the end section to calculate the EDR and the EDD relationships of the circular channel cross-sections only for sub-critical flow regimes. The computed EDR varies linearly from 0.72 to 0.74 for a critical depth diameter ratio (y_c/D) up to 0.82. Dey (2002b) also presented a comprehensive review of the important experimental and theoretical studies of the free over-falls in various channel cross-sections of different researchers. Dey (2003) used the momentum equation based on Boussinesq approach in order to calculate the end depth ratio (EDR) and the end depth discharge (EDD)

relationships of the inverted semi-circular channel cross-section for sub- and super critical flow regimes. He conducted some experiments on mild and steep longitudinal slopes in order to validate his proposed theoretical attempt. According to the Anderson's (1967) work, Dey et al. (2003) applied the energy equation based on the Boussinesq assumption to compute the end depth ratio and the discharge for the inverted semi-circular channel at sub-critical flow regimes. They also conducted experiments in order to verify their theoretical approach.

Raikar et al. (2004) applied the artificial neural network (ANN) to determine the EDR value for smooth inverted semi-circular channels in both sub- and super critical flow regimes. The experimental data sets of Dey (2003) were used for training and validating their work.

Ahmad (2005) applied the theoretical procedure to get the EDD relationships for the inverted semi-circular channel in both sub- and super critical flow regimes using sharp-crested weir theory. Direct prediction for discharge in super critical flow regimes was provided graphically as a part of his study.

Pal and Goel (2006) applied a support vector machine based modeling technique to determine the end depth ratio and discharge of a free over-fall for inverted semi-circular and circular channels with flat bases at different heights for both sub- and super critical flow conditions. Their computed results were verified using the relevant previous studies.

Nabavi et al. (2011) applied the free vortex theory to predict the end pressure distribution of the free over-fall. This method was then coupled with the momentum

equation to determine the EDR relationship from which the EDD relationship for the flat-based circular and the U-shaped channel cross-sections in sub-critical flow regimes were estimated only.

Ahmad (2012) used sharp-crested weir theory with zero height to get the EDD relationship for circular channel in both sub- and super critical flow regimes. The computed discharges agreed well with the experimental data sets in sub-critical flow regime.

Chapter 3

USE OF DIFFERENT ANALYTICAL METHODS FOR DEFINING THE FLOW AROUND THE BRINK DEPTH

3.1 General

To establish a theoretical relationship between the flow depth and the brink depth, in literature for different channel cross-sections, fundamental theories (the conservation of mass, the conservation of momentum and the conservation of energy) are either applied separately or coupled with the secondary (auxiliary) theories like the streamline equations, the sharp crested weir approach, the free vortex theory, the pressure distribution equation of the flow, etc. The brief details of these approaches that are available in literature are given below. Furthermore, two new approaches (three velocity points and infinite number velocity points), as a novelty, are as well introduced and detailed.

3.2 Existing Methodologies

3.2.1 The Momentum Approach

Referring to Fig. 3.1 (a), the control volume; which is occurring between the normal section ($n-n$) and the end section ($e-e$) where the free nappe forms, the water surface elevation rapidly decreases in a very short longitudinal distance. The detailed investigations of this flow profile suggested that, in the vicinity of the end section, the streamline curvature is considerable at the free water surface due to the strong vertical component of the flow acceleration, though it is zero at the channel bed. At

the downstream (end) section, the pressure above and below the dropping free nappe is atmospheric. Hence, the pressure distribution in fact differs from the hydrostatic one and is generally assumed to have a shape resembling a non-symmetric parabola with a maximum occurring not at the middle but closer to the channels bottom part (Replogle 1962).

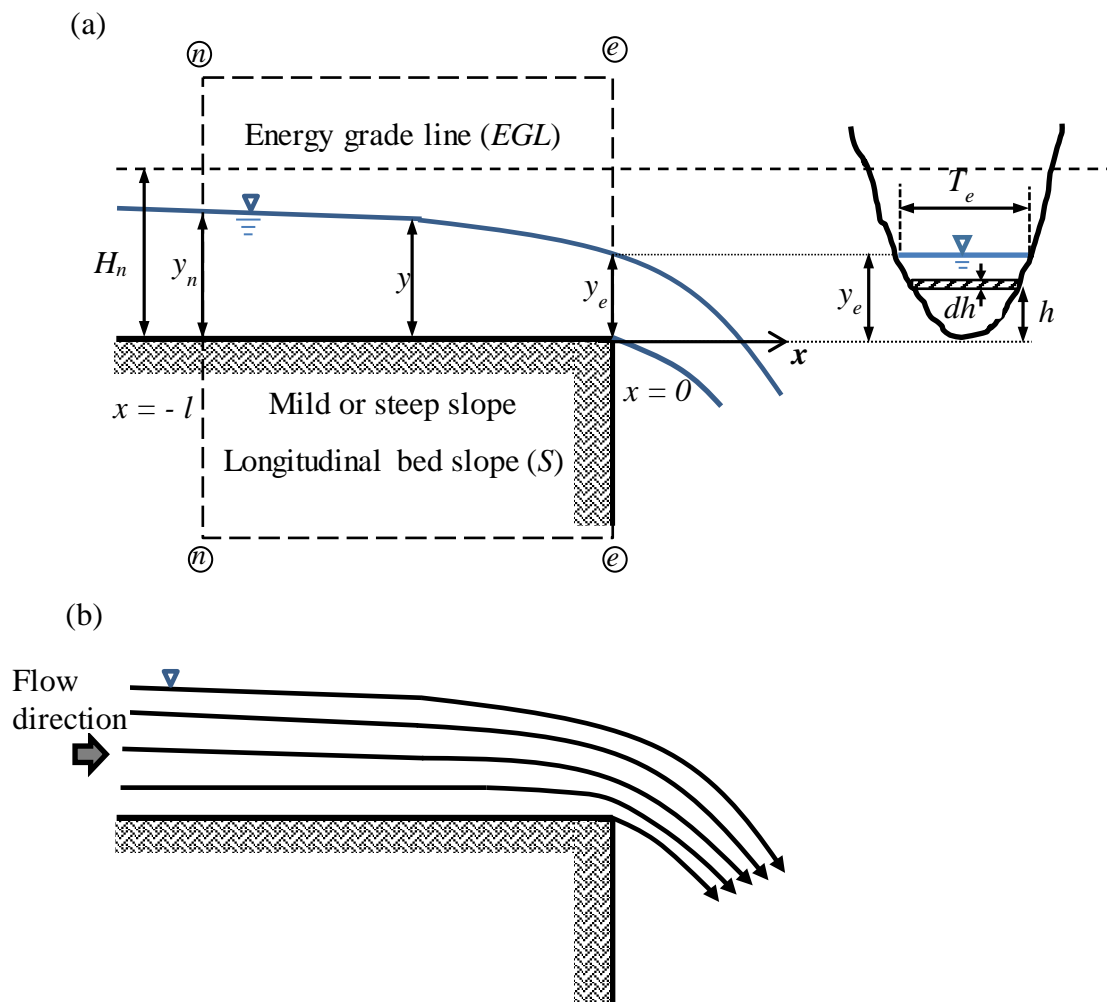


Figure 3.1: (a) Sketch of a typical channel cross-section (transversal) of the free over-fall at sub- and supercritical flow regime where the region between $n-n$ and $e-e$ are representing the suggested control volume; (b) the streamline patterns of a free over-fall

Applying one-dimensional momentum equation over the control volume between the normal and the end sections of the free over-fall for different channel cross-sections having a longitudinal bed slope S (Fig. 3.1 (a)), yields:

$$F_n - F_e - \int \tau dx + W \sin(\arctan S) = \rho Q(\beta_e V_e - \beta_n V_n) \quad (3.1)$$

where F_n = the pressure force at the normal section; F_e = the pressure force at the end section; τ = the wall and the bed shear stresses; dx = the infinitesimal distance along x -direction; W = the gravity force of water within the control volume; ρ = the mass density of water; Q = the flow rate (discharge); β_n = Boussinesq coefficient at the normal section; β_e = Boussinesq coefficient at the end section; V_n = the mean flow velocity at the normal section; and V_e = the mean flow velocity at the end section.

The subscripts ‘ n ’ and ‘ e ’ denoting the flow conditions at the upstream normal section where $x=-l$ and the downstream end section where $x=0$, respectively. For simplicity, β_e and β_n are assumed to be unity (Dey 2003; Nabavi et al. 2011).

To simplify the theoretical analysis, a state of pseudo-uniform flow is assumed within the control volume where, by definition, the wall and the bed shear stresses are compensated by the stream-wise component of the gravity force of water. Hence, the pressure force difference becomes equal to the rate of change of momentum within the control volume. In sub-critical flow regimes, an error of around 1% in estimation of the EDR is obtained due to exclusion of the wall and bed shear stresses (Henderson 1966). Since in super critical flow regimes, the stream-wise component of the gravity force is considerable, the accuracy of the theoretical results depending on, how the wall and the bed shear stresses were balanced by the longitudinal component of the gravity force of water. Nevertheless, the assumption of pseudo-

uniform flow for super critical flow regimes are yielding acceptable results (Dey 1998; and Murty Bhallamudi 1994). Hence, the simplified form of Eq. (3.1) is:

$$F_n - F_e = \rho Q(V_e - V_n) \quad (3.2)$$

Introducing $F_n = \gamma \bar{y}_n A_n$, $F_e = \gamma K_e \bar{y}_e A_e$, $V_e = Q/A_e$, $V_n = Q/A_n$ into Eq. (3.2), yields:

$$\gamma \bar{y}_n A_n - \gamma K_e \bar{y}_e A_e = \rho Q^2 \left(\frac{1}{A_e} - \frac{1}{A_n} \right) \quad (3.3)$$

where γ = the specific weight of water; A_n = the flow area at the normal section; A_e = the flow area at the end section; Q = the flow rate (discharge); K_e = the pressure coefficient at the end section. While generating the equation, a pressure coefficient (K_e) at the end section has to be introduced. This pressure coefficient should be determined either by experimental data sets or by application of the Boussinesq approach or by applying the free vortex theory (as detailed below), since there exists a relationship between the pressure coefficient with these approaches.

3.2.2 The Boussinesq Approximation Theory

Fig. 3.1 (a) details a free surface flow with a convex upward water surface over a free over-fall, where the radius of curvature of the free surface (r_s) is given by:

$$\frac{1}{r_s} = \frac{\frac{d^2 y}{dx^2}}{\left[1 + \left(\frac{dy}{dx} \right)^2 \right]^{3/2}} \quad (3.4)$$

The free surface curvature at the vicinity of the brink varies from a finite value at the free surface to zero at the channel bed as given in Fig. 3.1 (b) (Dey 2003; Dey et al. 2003; Murty Bhallamudi 1994; Subramanya 1997). So, for the infinitesimal length of

the free surface, the radius of this streamline curvature (r_s) can be simplified and approximated as:

$$\frac{1}{r_s} = \frac{d^2y}{dx^2} \quad (3.5)$$

where r_s = the radius of curvature of the streamline and y = the flow depth at any distance x within the control volume measured from the brink.

Noting that, the convex upward water surface $\frac{d^2y}{dx^2}$ yielding negative values.

According to Boussinesq approximation (Dey 2002b; Dey 2003; Jaeger 1957), a linear variation of the streamline curvature with depth is assumed. Hence, the radius of curvature of the streamline at any point at a height y above the channel bottom is given by:

$$\frac{1}{r} = \frac{d^2y}{dx^2} \cdot \frac{h}{y} \quad (3.6)$$

where h = the coordinate normal to channel bottom.

The normal acceleration (a_y) based on this assumption is given as:

$$a_y = \frac{V^2}{r} = ky \quad (3.7)$$

where:

$$k = \frac{V^2}{h} \cdot \frac{d^2h}{dx^2} \quad (3.8)$$

and V = the mean flow velocity at the distance x within the control volume.

On curvilinear flows with the normal acceleration (a_y), the general pressure distribution (p) using the integration of the Euler equation, can be expressed as:

$$\frac{p}{\gamma} + z = \int \frac{V^2}{rg} dr + \text{constant} \quad (3.9)$$

where Z = the elevation measured above the datum; and g = the acceleration due to gravity.

Using Eqs. (3.7) and (3.8), Eq. (3.9) is integrated so as to determine the effective piezometric head (y_{ep}) at the end section:

$$y_{ep} = y_e + \frac{1}{3} \frac{V_e^2 y_e}{g} \cdot \frac{d^2 y}{dx^2} \quad (3.10)$$

3.2.3 The Conservation of Energy Approach

Referring to Fig. 3.1 (a), the specific energy (E) at section $x=0$ (denoted by suffix ‘ e ’) is obtained as:

$$E_e = y_{ep} + \alpha_e \frac{V_e^2}{2g} \quad (3.11)$$

where α_e = the velocity correlation coefficient at the end section; and V_e = the mean flow velocity at the end section ($x = 0$).

Inserting Eq. (3.10) and substituting $V_e = Q/A_e$ into Eq. (3.11), the following equation for the specific energy at the end section is generated:

$$E_e = y_e + \frac{1}{3} \frac{Q^2 y_e}{g A_e^2} \cdot \frac{d^2 y}{dx^2} + \alpha_e \frac{Q^2}{2g A_e^2} \quad (3.12)$$

where y_e = the flow depth at the end section.

According to Subramanya (1997), the water surface is a continuously failing curve along the flow direction that starts within the channel somewhere upstream of the brink (end), passes through the brink and ends up as a trajectory of a gravity fall. Therefore, the rate of change of slope of the free surface at the end section is expressed as:

$$\left. \frac{d^2 y}{dx^2} \right|_{x=0} = -\frac{g}{V_e^2} = -\frac{g A_e^2}{Q^2} \quad (3.13)$$

The upstream Froude number (Fr_n) is defined as:

$$Fr_n = \frac{Q T_n^{1/2}}{g^{1/2} A_n^{3/2}} \quad (3.14)$$

where T_n = the top width of the flow at the normal section.

Substituting Eqs. (3.13) and (3.14) into Eq. (3.12) and normalizing this computed equation with respect to the upstream normal depth (y_n), yields:

$$\frac{E_e}{y_n} = \frac{2}{3} \frac{y_e}{y_n} + \alpha_e \frac{A_n^3 Fr_n^2}{2 T_n y_n A_e^2} \quad (3.15)$$

where y_n = the flow depth at the normal section.

In a similar way, referring to Fig. 3.1 (a), the specific energy at the normal section ($x=-l$) is obtained and then, by substituting Eq. (3.14) into this computed equation and normalizing it with the upstream normal depth (y_n), gives:

$$\frac{E_n}{y_n} = 1 + \alpha_n \frac{A_n Fr_n^2}{2T_n y_n} \quad (3.16)$$

where α_n = the velocity correlation coefficient at the normal section.

In accordance with Anderson (1967) and Subramanya (1997), since the frictional head losses along the short distance on the control volume of the free over-fall are negligible, the specific energy between the upstream normal section and the downstream end section can be safely assumed to be equal. Therefore, by equating Eqs. 3.16 and 3.17, gives:

$$\frac{2}{3} \frac{y_e}{y_n} + \frac{A_n^3 Fr_n^2}{2T_n A_e^2 y_n} - \frac{A_n Fr_n^2}{2T_n y_n} - 1 = 0 \quad (3.17)$$

Noting that, both α_e and α_n are assumed to be unity.

3.2.4 The Free Vortex Theory

As previously pointed out and detailed in Fig. 3.1 (b), the streamline curvature is substantial at the vicinity of the end section of the free over-fall. In order to insert the effect of the streamline curvature into the above mentioned fundamental equations, the substantial streamline curvature has been considered by utilizing the free vortex theory. According to this theory, the approximate centrifugal pressure head at any streamtube was obtained through the Newton's law of acceleration as $h_i u_i^2 / (r_i g)$ (Chow 1959). Therefore, at the end section, the pressure head corresponding to any streamtube i can be given as:

$$d_i = y_i \left(1 - \frac{u_i^2}{r_i g} \right) \quad (3.18)$$

where d_i = the pressure head of the streamtube i ; y_i = the flow depth of the streamtube i ; u_i = the flow velocity of the streamtube i ; r_i = the radius of curvature of the streamtube i ; and g = the acceleration due to gravity. Since the pressure head at the bottom of the end section is zero, the radius of streamline curvature at the channel bottom of the end section (r_{eb}) can be expressed as:

$$r_{eb} = \frac{u_{eb}^2}{g} \quad (3.19)$$

where u_{eb} = the flow velocity at the channel bottom of the end section.

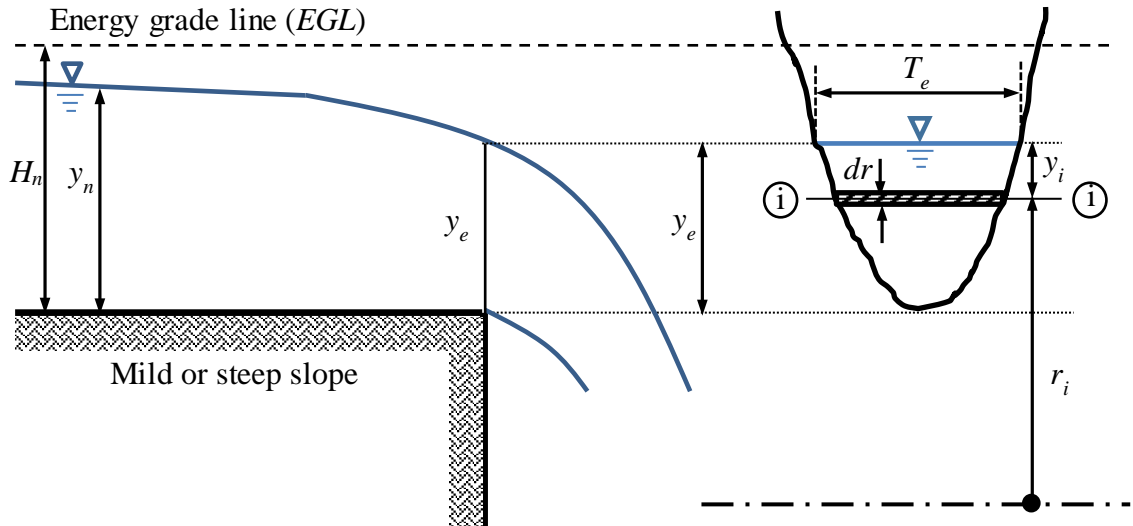


Figure 3.2: Sketch of a typical channel cross-section (transversal) of the free overfall on a mild or steep (longitudinal) slope

According to Ali and Sykes (1972), the velocity head at the upper and the lower nappe can be obtained by applying the Bernoulli's theorem:

$$\frac{u_{et}^2}{2g} = H_n - y_n \quad (3.20)$$

$$\frac{u_{eb}^2}{2g} = H_n \quad (3.21)$$

where u_{et} = the flow velocity at the top of the channels end section, u_{eb} = the flow velocity at the bottom of the channels end section. Note that, the subscripts 'et' and 'eb' denote the flow conditions at the channel top of the end section and the channel bottom of the end section, respectively. Therefore, the general velocity head at any flow depth of the end section y_i can be expressed as:

$$\frac{u_i^2}{2g} = H_n - y_n + \left(\frac{y_i}{y_e}\right)y_n \quad (3.22)$$

where y_n = the flow depth at the normal section. Noting that $H_n = y_n + V_n^2/(2g)$ is the total energy head at the upstream normal section.

Solving Eqs. (3.19) and (3.21) simultaneously, yields $r_{eb} = 2H_n$. Then, by applying Bernoulli's equation between the upstream and the downstream sections and using the Free Vortex theory as $u_i r_i = u_{eb} r_{eb} = \text{constant}$, the radius of the curvature of the streamtube i at the end section is computed as:

$$r_i = \frac{2H_n \sqrt{2gH_n}}{\sqrt{2g \left[H_n - y_n + \left(\frac{y_i}{y_e}\right)y_n \right]}} \quad (3.23)$$

If y_e is divided into 'n' number of parallel streamlines, by substituting Eqs. (3.22) and (3.23) into Eq. (3.18), the pressure head (d_i) for each streamline is obtained:

$$d_i = y_i - \frac{y_i \left[H_n - y_n + \left(\frac{y_i}{y_e} \right) y_n \right]^{3/2}}{H_n^{3/2}} \quad (3.24)$$

For general case, when $y = y_i$, the pressure force at the end section is:

$$F_e = \gamma \int_0^{h_e} \left\{ y - \frac{y \left[H_n - y_n + \left(\frac{y}{y_e} \right) y_n \right]^{3/2}}{H_n^{3/2}} \right\} dy \quad (3.25)$$

A coefficient of pressure force K_e at the end section is given as:

$$K_e = \frac{F_e}{0.5 \gamma h_e^2} \quad (3.26)$$

3.2.5 Sharp-Crested Weir Approach

The flow over a free over-fall in different channel cross-sections can be assumed to be similar to the flow over a sharp-crested weir of the same section with zero height (Anastasiadou-Partheniou and Hatzigiannakis 1995; Ferro 1999; Ahmad 2003; Vatankhah 2013; Vatankhah 2015) as detailed in Figs. 3.3 (a) and (b). Therefore, the theoretical procedure applied for computing the discharge over a sharp-crested weir without sill can also be used for free over-falls so as to obtain the end depth ratio (EDR). It should be noted that, the discharge coefficient of the weir ($C_d = C_f \cdot C_c \cdot C_v$) depends on the longitudinal head loss correction coefficient (C_f), the contraction coefficient (C_c) and the velocity head correction coefficient (C_v) (Vatankhah 2015). As discussed in the previous section, the pressure distribution at the brink section

resembles slightly skewed parabolic shape with its mean value considerably less than the hydrostatic one (Replogle 1962); so, the curve for the actual pressure distribution profile is expected to lie under the linearly hydrostatic pressure profile. In order to apply the fundamental equations (the conservation of mass, momentum, or energy), the pressure distribution at the brink is either assumed to be zero all over the end section or a correction factor with a positive value has to be inserted to the hydrostatic pressure distribution (Rajaratnam and Muralidhar 1964; Keller and Fong 1989; Dey 2002b).

Therefore, an elemental infinitesimal discharge (dQ) equation for the different channel cross-sections of the free over-fall is generated as:

$$dQ = C_f C_c C_v \left[2g \left(H_n - y - \frac{P_e}{\gamma} \right) \right]^{0.5} dA \quad (3.27)$$

where dQ = the elemental infinitesimal discharge; g = the acceleration due to gravity; γ = the specific weight of water; P_e = the mean pressure value at the end section; H_n = the total energy head at the upstream normal section; y = the flow depth at the distance x within the control volume measured from the brink towards upstream; and dA = the elemental infinitesimal flow area.

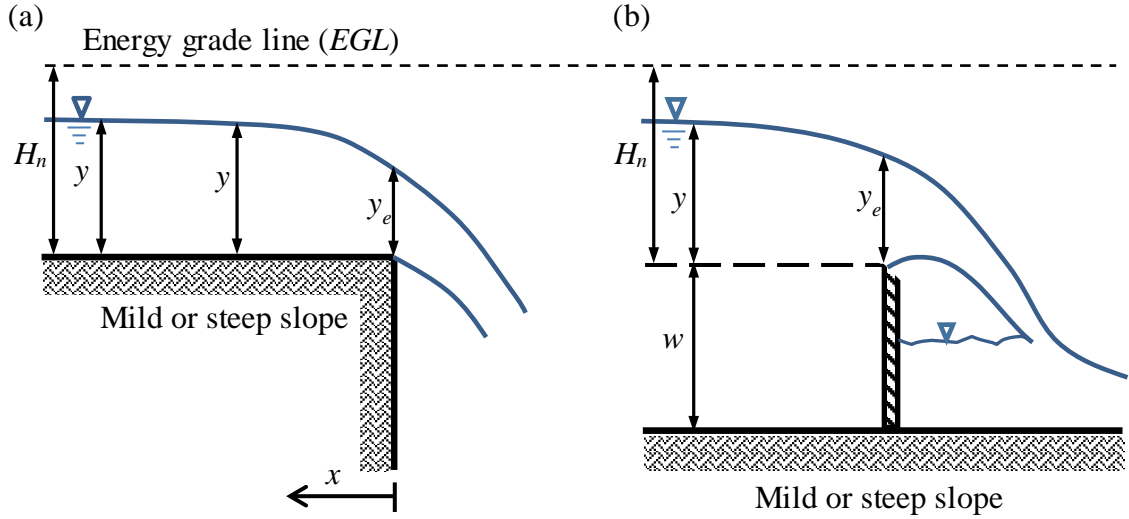


Figure 3.3: (a) Sketch of a free over-fall at sub- and supercritical flow regime; (b) flow over a sharp-crested weir with a sill 'w'

The longitudinal head losses along the relatively short sloping distances of the free over-falls are negligible. Hence, the longitudinal head loss correction coefficient (C_f) can be safely assumed to be unity. Due to the contraction of the falling nappe, the contraction correction coefficient is introduced so as to take into account the convergence of the streamline as $C_c = A_e/A_u$. As previously pointed out, the streamlines are considerably inclined towards the brink section along the flow direction; thus, the importance of the streamline curvature effect is either considered by some researchers like Murty Bhallamudi (1994), Dey (1998) and Dey (2003) or completely neglected as in the studies of Ahmad (2005), Ahmad (2012) and Vatankhah (2013). Hence in this study, a correction coefficient (C_v) is introduced into the sharp-crested weir equation. So, the equation of the discharge (Q) for an elemental tape of thickness dy at a height y measured from the channel bottom is given as:

$$Q = \frac{A_e}{A_n} C_v \int_0^{y_n} \left[2g \left(H_n - y - \frac{P_e}{\gamma} \right) \right]^{0.5} T dy \quad (3.28)$$

where Q = the flow discharge; A_e = the flow area at downstream the end section; A_n = the flow area at the upstream normal section; y_n = the upstream normal flow depth and T = the top width of water in contact with atmospheric pressure (the free surface flow width).

It should be noted that, if the end pressure effect and the streamline curvature at the vicinity of the brink are both neglected, the above equation reduces to:

$$Q = \frac{A_e}{A_n} \int_0^{y_n} (2g(H_n - y))^{0.5} T dy \quad (3.29)$$

3.3 Suggested Solution Methodologies

3.3.1 The Three Velocity Points Method

In order to eliminate the use the pressure effect in the solutions, a new method is proposed so as to generate the end depth ratio (EDR) relationship using the mass balance (continuity) equation between the upstream and the downstream sections. As shown in Fig. 3.4, to obtain a closer EDR value, the velocity distribution profile at the brink section is considered by sub-sectioning the end section into two parts at its geometric center (centroid). Hence, having 3 different velocity values at 3 different respective depths at the end section. Applying Bernoulli equation between the upstream section and the brink section for the three different velocity locations (at the top, at the geometric center and at the bottom) at the brink section, these velocity values are computed. The frictional head losses along the longitudinal cross-section within the examined portion which is short in comparison, are assumed negligible and also all the streamlines at the brink section are assumed to be parallel to each other.

Referring to Fig. 3.4, based on the Bernoulli equation, the selected velocity equations at the brink section can be expressed as:

$$v_{et} = \sqrt{2g(H_n - y_n)} \quad (3.30)$$

$$v_{ec} = \sqrt{2g(H_n - \bar{y})} \quad (3.31)$$

$$v_{eb} = \sqrt{2gH_n} \quad (3.32)$$

where EGL = the energy grade line, H_n = the total energy head with respect to the channels bottom, y_n = the flow depth at the upstream normal section, \bar{y} = the centroidal depth at the end section, measured from the channel bottom to the centroid of that relevant cross-section, v_{et} = the average velocity at the top of the end section, v_{ec} = the average velocity at the centroidal depth of the end section, v_{eb} = the average velocity at the bottom of the end section and g = the acceleration due to gravity. Note that the subscripts 'n' and 'e' denote the flow conditions at the upstream normal section and at the end section (brink), respectively. Similarly, the subscripts 'et', 'ec' and 'eb' refers to the top, the center and the bottom of the end section, respectively.

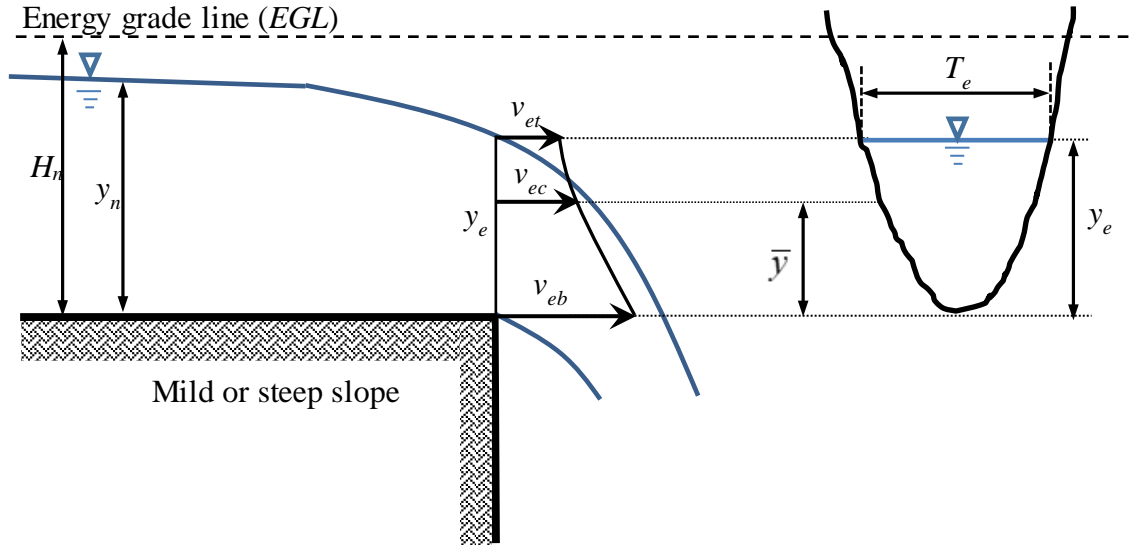


Figure 3.4: Sketch of a typical channel cross-section (transversal) of the free over-fall on a mild or steep (longitudinal) slope with the proposed three velocity locations for the velocity distribution profile at the brink ' y_e '

According to continuity equation, the average discharge (Q) is determined as:

$$Q = \frac{v_{et} + v_{ec}}{2} A_{et-ec} + \frac{v_{ec} + v_{eb}}{2} A_{ec-eb} \quad (3.33)$$

where A_{et-ec} is the sub-sectional flow area between the top and the centroid of the end section and A_{ec-eb} is the sub-sectional flow area between the centroid and the bottom of the end section.

Using Eqs. (3.30), (3.31) and (3.32), incorporating the upstream normal Froude number (Fr_n) based on Eq. (3.14) and inserting the proper equations of each sub-sectional flow area based on the defined channel cross-section into Eq. (3.33), the generalized end depth ratio (EDR) relationship can be computed.

3.3.2 The Infinite Number Velocity Points Method (n-Velocity Points Method)

The three velocity points method is mathematically expanded for infinite (pre-assumed) number of velocity points (np) so as to achieve more accurate results and

referred as n-velocity points method. As shown in Fig. 3.5, in order to have infinite (pre-assumed) number of velocity points, the velocity distribution profile at the brink section is sub-sectioned into $np-1$ parts. Applying the Bernoulli equation between the upstream section and the brink section for np number of velocity locations over the brink section, the respective velocity values are computed.

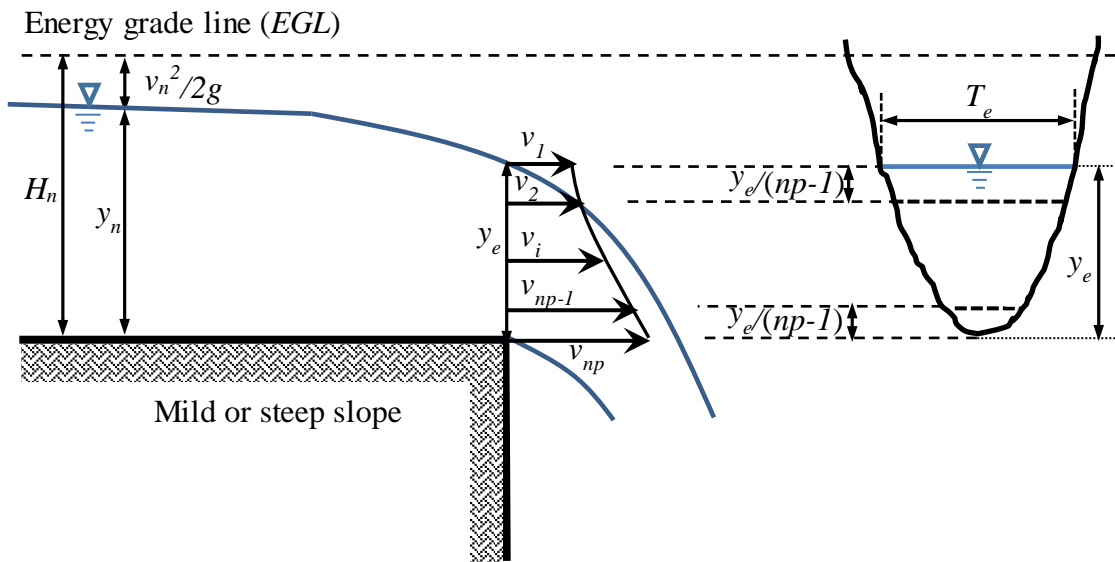


Figure 3.5: Sketch of a typical channel cross-section (transversal) of the free over-fall on a mild or steep (longitudinal) slope showing the representative sub-section ($np-1$) and how the velocity locations are established to form the velocity distribution profile at the brink ' y_e '

Referring to Fig. 3.5, based on the Bernoulli equation, the selected velocity equations at the brink section can be written as:

$$v_1 = \sqrt{2g \left(\frac{v_n^2}{2g} + \frac{0}{np-1} y_n \right)} \quad (3.34)$$

$$v_2 = \sqrt{2g \left(\frac{v_n^2}{2g} + \frac{1}{np-1} y_n \right)} \quad (3.35)$$

$$v_i = \sqrt{2g \left(\frac{v_n^2}{2g} + \frac{i-1}{np-1} y_n \right)} \quad (3.36)$$

$$v_{np-1} = \sqrt{2g \left(\frac{v_n^2}{2g} + \frac{np-2}{np-1} y_n \right)} \quad (3.37)$$

$$v_{np} = \sqrt{2g \left(\frac{v_n^2}{2g} + \frac{np-1}{np-1} y_n \right)} \quad (3.38)$$

where EGL = the energy grade line, H_n = the total energy head with respect to the channels bottom, y_n = the flow depth at the upstream normal section, v_i = the velocity at the top of the end section, v_{np} = the velocity at the bottom of the end section and g = the acceleration due to gravity. Note that the subscripts 'n' and 'e' denote the flow conditions at the upstream normal section and at the end section (brink), respectively.

According to continuity equation, the generalized average discharge (Q) is obtained as:

$$\begin{aligned} Q &= \frac{v_1+v_2}{2} A_{(1)to(2)} + \frac{v_2+v_3}{2} A_{(2)to(3)} + \dots + \frac{v_i+v_{i+1}}{2} A_{(i)to(i+1)} + \dots + \frac{v_{np-1}+v_{np}}{2} A_{(np-1)to(n)} \\ &= \sum_{i=1}^{np-1} \frac{v_i+v_{i+1}}{2} A_{(i)to(i+1)} \end{aligned} \quad (3.39)$$

where $A_{(1)to(2)}$ = the sub-sectional flow area between the top and the second points of the end section, $A_{(2)to(3)}$ = the sub-sectional flow area between the second and the third points of the end section, and $A_{(np-1)to(np)}$ = the sub-sectional flow area between the $np-1^{\text{th}}$ point and the bottom of the end section.

Using Eqs. (3.34), (3.35), (3.36), (3.37), and (3.38), incorporating the upstream Froude number based on Eq. (3.14) and inserting proper equations of each sub-sectional flow area based on the defined channel cross-section into Eq. (3.19), the end depth ratio (EDR) can be expressed mathematically as a series expansion.

Chapter 4

DIFFERENT ANALYTICAL SOLUTIONS OF THE END DEPTH RATIO (EDR) FOR VARIOUS CHANNEL CROSS-SECTIONS

4.1 General

This chapter presents both the previously applied different theoretical methods and the two proposed approaches for computing the end depth ratio (EDR) relationships of the free over-fall for the exponential, the generalized trapezoidal and the generalized flat base circular channel cross-sections for both sub- and super critical flow regimes.

The exponential channel is a general channel cross-section which is defined mathematically with a single exponential equation where three widely known prismatic shapes can be generated (rectangular, parabolic, and symmetric sided triangular).

The generalized trapezoidal channel cross-section is a geometric shape that is defined mathematically with a 2nd degree equation where six widely known prismatic channel cross-sectional shapes can be generated (rectangular, symmetric sided triangular, symmetric sided trapezoidal, semi-trapezoidal, symmetric sided inverted triangular (Δ) and semi-inverted triangular).

Similarly, the generalized circular channel cross-section having a flat base is a geometric shape that reduces to the circular, semi-inverted circular and partially full circular channel with varying flat base cross-sections (both for less than half full and more than half full).

4.2 The Channel Cross-sections

4.2.1 Exponential Channel Cross-sections

The exponential (power-law) channel cross-section on mild or steep slope shown in Fig. 4.1, is a channel of which its cross-section is defined mathematically with a single exponential equation (Eq. (4.1)) where, by changing the coefficient η_1 and the exponent η_2 , three widely known prismatic channel cross-section shapes can be generated (rectangular, parabolic, and triangular (symmetric)). The general flow cross-sectional area is expressed in such a way that, the flow depth 'y' becomes directly proportional to this area and is given as:

$$A = \eta_1 y^{\eta_2} \quad (4.1)$$

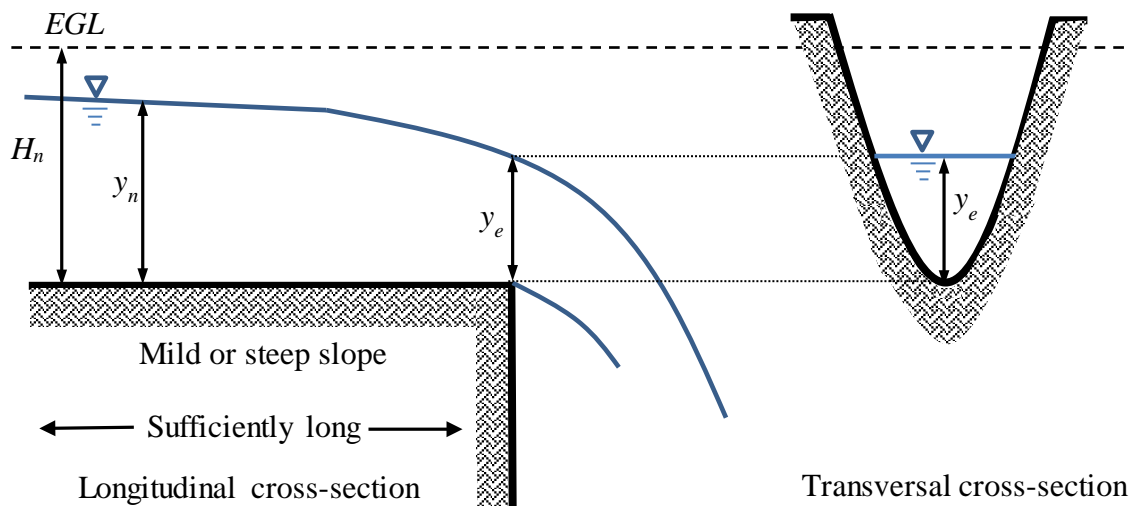
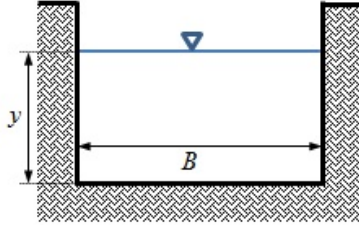
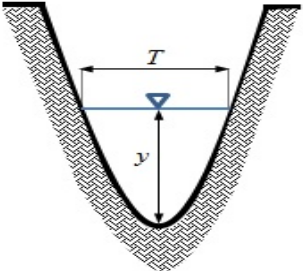
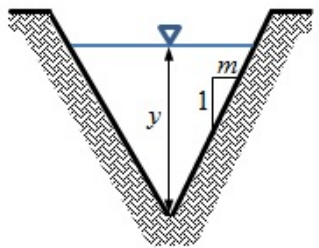


Figure 4.1: Sketch of the exponential channel cross-section (transversal) of the free over-fall on a mild or a steep (longitudinal) slope

The coefficient η_1 and the exponent η_2 are the parametric constants used for defining the channel cross-sectional shapes and their details are given in Table 4.1.

Table 4.1: The coefficient η_1 and the exponent η_2 constants that are used for generating the relevant cross-sections

Cross-sections Type	Cross-sections Shape	η_1	η_2
Rectangular		B	1
Parabolic		$2T/(3y^{0.5})$	1.5
Triangular (symmetric)		m	2

4.2.2 Generalized Trapezoidal Channel Cross-sections

The generalized trapezoidal channel cross-section is defined mathematically with 2nd degree equation (Eq. (4.2)) where, by changing the coefficients η_3 and η_4 and the exponent η_5 , six widely known prismatic channel cross-sectional shapes can be generated (rectangular, triangular (symmetric), trapezoidal (symmetric), semi-trapezoidal, inverted triangular (Δ) (symmetric) and semi-inverted triangular). This

equation is based on the general flow area that is directly proportional to the flow depth 'y'. The sketches of the two distinct generalized trapezoidal channel cross-sections with symmetric sides slopes 'm' (1 Vertical: m Horizontal) on mild or steep slope are shown in Figs. 4.2 (a) and (b).

$$A = \eta_3 y + (-1)^{\eta_5} \eta_4 y^2 \quad (4.2)$$

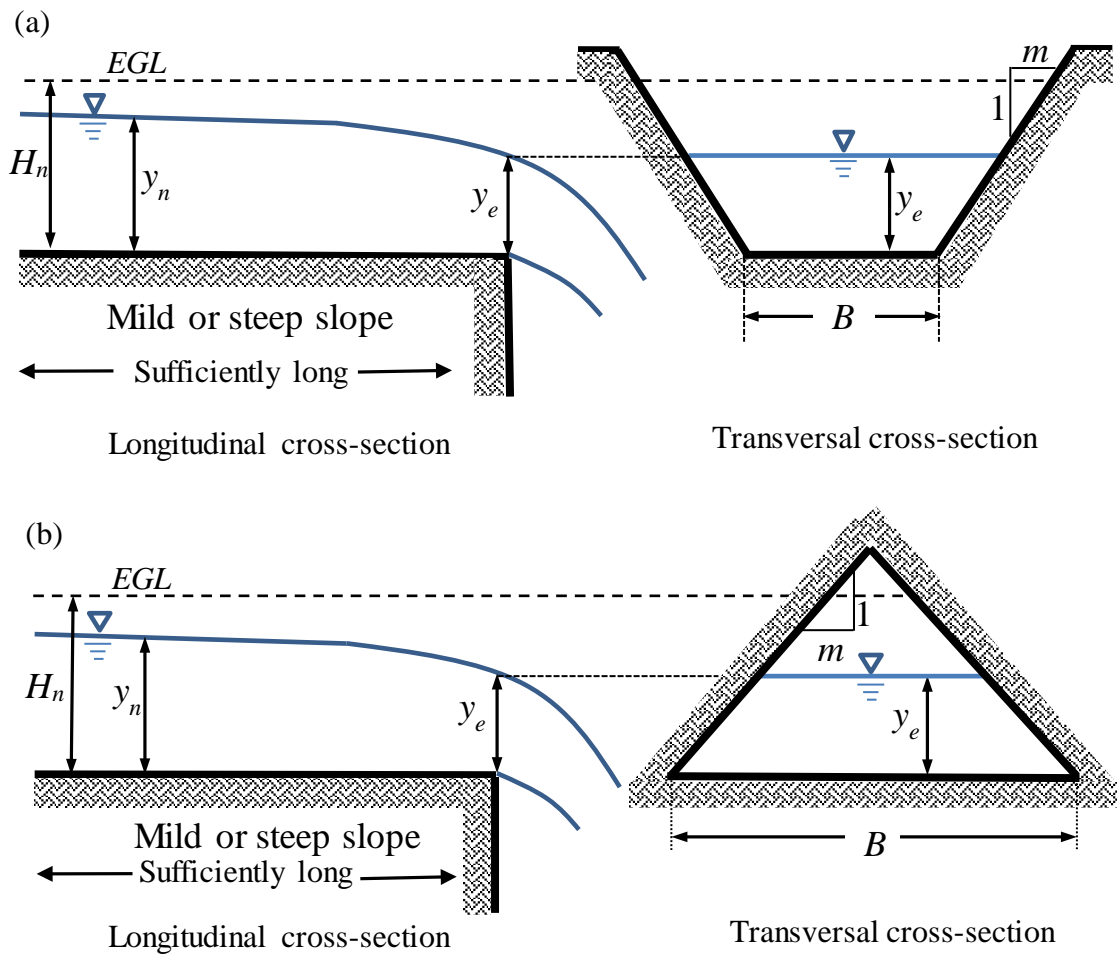
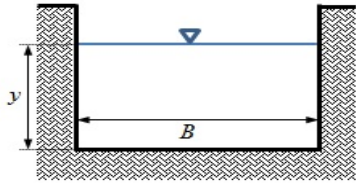
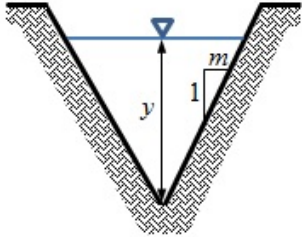
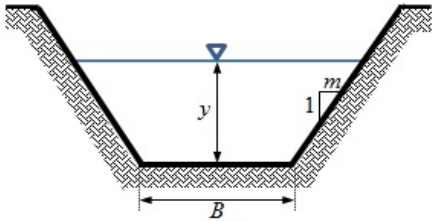
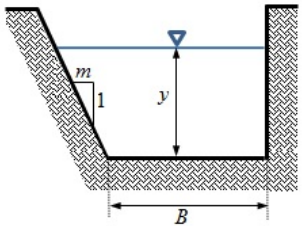
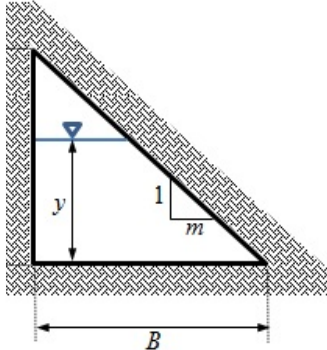


Figure 4.2: Sketch of the free over-fall at (a) the trapezoidal cross-section with symmetric sides; (b) the inverted-triangular (Δ -shaped) cross-section with symmetric sides (transversal) on mild or steep (longitudinal) slope

The coefficients η_3 and η_4 and the exponent η_5 are the parametric constants used for defining the channel cross-sectional shapes and their details are given in Table 4.2.

Table 4.2: The coefficients η_3 and η_4 and the exponent η_5 constants that are used for generating the relevant cross-sections

Cross-sections Type	Cross-section Shape	η_3	η_4	η_5
Rectangular		B	0	$-$
Triangular (symmetric)		0	m	0
Trapezoidal (symmetric)		B	m	0
Semi-trapezoidal		B	$m/2$	0
Semi-inverted triangular		B	$m/2$	1

4.2.3 Generalized Circular Channel Cross-sections

A generalized circular channel cross-section with flat base on mild or steep slope is shown in Fig. 4.3. This generalized circular channel represents a group of widely existing geometric cross-sectional shapes (the circular, the inverted semi-circular and partially full circular channel with varying flat base cross-sections (both for less than half full and more than half full)) where the flow cross-sectional area is related to the flow depth (y), the diameter (D), and the depth of the flat base from lower extremity of the generalized circular channel cross-section (Z), and defined as:

$$A = \frac{D^2}{4} (\varphi(\hat{I}) - \varphi(\hat{Z})) \quad (4.3)$$

$$\varphi(\hat{I}) = \sin^{-1} (2\hat{I} - 1) + 2(2\hat{I} - 1)(\hat{I} - \hat{I}^2)^{0.5} \quad (4.4)$$

$$\varphi(\hat{Z}) = \sin^{-1} (2\hat{Z} - 1) + 2(2\hat{Z} - 1)(\hat{Z} - \hat{Z}^2)^{0.5} \quad (4.5)$$

$$I = y + Z; \quad \frac{I}{D} = \frac{y}{D} + \frac{Z}{D}; \quad \hat{I} = \hat{y} + \hat{Z} \quad (4.6)$$

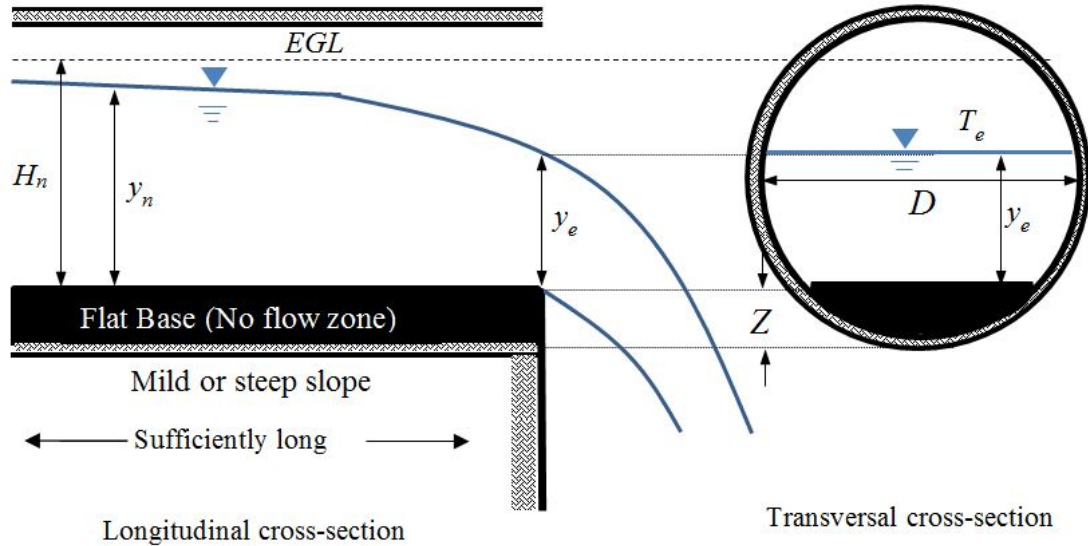


Figure 4.3: Sketch of free over-fall on the generalized circular channel cross-section (transversal) having flat base of the free over-fall on a mild or a steep (longitudinal) slope

4.3 End Depth Ratio (EDR) for Various Channel Cross-sections

4.3.1 Previously Applied Theories

4.3.1.1 The Energy Method

Using Eq. (3.17) along with the appropriate expressions for A_n , T_n and A_e for each cross-section, the generalized end depth ratio (EDR) which is the relationship between the end depth and the upstream depth (normal depth or critical depth), is computed for the exponential (Eq. (4.7)), the generalized trapezoidal (Eq. (4.9)) and the generalized circular channel cross-sections (Eq. (4.12)) separately, as follows:

$$\frac{2}{3} \text{EDR} + \frac{Fr_n^2}{2\eta_2} (\text{EDR}^{-2\eta_2} - 1) - 1 = 0 \quad (4.7)$$

where

$$\text{EDR} = \frac{y_e}{y_n} \quad (4.8)$$

Note that, Eq. (4.7) was already solved and presented in Subramanya (1994).

$$\frac{2}{3} \text{EDR} + \frac{(1 + (-1)^{\eta_5} N_n)^3 Fr_n^2}{(2 + 4(-1)^{\eta_5} N_n)(\text{EDR} + (-1)^{\eta_5} N_n \text{EDR}^2)^2} - \frac{(1 + (-1)^{\eta_5} N_n)^2 Fr_n^2}{(2 + 4(-1)^{\eta_5} N_n)} - 1 = 0 \quad (4.9)$$

where

$$\text{EDR} = \frac{y_e}{y_n} = \frac{N_e}{N_n} \quad (4.10)$$

$$N_n = \frac{\eta_3 y_n}{\eta_4}; N_e = \frac{\eta_3 y_e}{\eta_4} \quad (4.11)$$

$$\frac{2}{3} \text{EDR} + \frac{(\varphi(\hat{I}_n) - \varphi(\hat{Z}))^3 Fr_n^2}{16(\hat{I}_n - \hat{I}_n^2)^{0.5} (\varphi(\hat{I}_e) - \varphi(\hat{Z}))^2 \hat{y}_n} - \frac{(\varphi(\hat{I}_n) - \varphi(\hat{Z})) Fr_n^2}{16(\hat{I}_n - \hat{I}_n^2)^{0.5} \hat{y}_n} - 1 = 0 \quad (4.12)$$

where

$$\text{EDR} = \frac{y_e}{y_n} = \frac{\hat{y}_e}{\hat{y}_n} \quad (4.13)$$

$$\hat{y}_n = \frac{y_n}{D}; \hat{y}_e = \frac{y_e}{D}; \hat{Z} = \frac{Z}{D} \quad (4.14)$$

$$\hat{I}_e = \hat{y}_e + \hat{Z}; \hat{I}_n = \hat{y}_n + \hat{Z} \quad (4.15)$$

Eqs. (4.7), (4.9), and (4.12) are the general relationships and can be applied to either sub-critical or supercritical flow regime. In the case of sub-critical flow regimes,

$Fr_n = Fr_c = 1$, $N_n = N_c = \frac{my_c}{B}$, and $\hat{I}_n = \hat{I}_c = \hat{y}_c + \hat{Z}$. It should be noted that, the subscripts 'e', 'c' and 'n' are referring to the flow conditions at the end section, the critical section and the normal section, respectively.

4.3.1.2 Momentum Equation Coupled with the Free Vortex Theory

By inserting Eqs. (3.14), (3.25), and (3.26) into Eq. (3.3) and replacing the appropriate relationships for A_n , T_n and A_e of each channel cross-section type, the generalized EDR relationships are calculated for the exponential (Eq. (4.16)), the generalized trapezoidal (Eq. (4.17)) and the generalized circular channel cross-sections (Eq. (4.18)) as:

$$\left\{ 1 - \frac{4}{5} \left(1 + \frac{Fr_n^2}{2\eta_2} \right) + \frac{8}{35} \left[\left(1 + \frac{Fr_n^2}{2\eta_2} \right)^2 - \frac{\left(\frac{Fr_n^2}{2\eta_2} \right)^{3.5}}{\left(1 + \frac{Fr_n^2}{2\eta_2} \right)^{1.5}} \right] \right\} \text{EDR}^{(2\eta_2+1)} - \left[\frac{(\eta_2+1)Fr_n^2}{\eta_2} + 1 \right] \text{EDR}^{\eta_2} + \left[\frac{(\eta_2+1)Fr_n^2}{\eta_2} \right] = 0 \quad (4.16)$$

$$\begin{aligned}
& \left\{ 1 - \frac{4}{5} \left(1 + \frac{(1+(-1)^{n_5} N_n) Fr_n^2}{(2+4(-1)^{n_5} N_n)} \right) + \right. \\
& \left. \frac{8}{35} \left[\left(1 + \frac{(1+(-1)^{n_5} N_n) Fr_n^2}{(2+4(-1)^{n_5} N_n)} \right)^2 - \frac{\left(\frac{(1+(-1)^{n_5} N_n) Fr_n^2}{(2+4(-1)^{n_5} N_n)} \right)^{3.5}}{\left(1 + \frac{(1+(-1)^{n_5} N_n) Fr_n^2}{(2+4(-1)^{n_5} N_n)} \right)^{1.5}} \right] \right\} \\
& * \left(\frac{EDR^2}{2} + (-1)^{n_5} N_n \frac{EDR^3}{3} \right) \\
& + \frac{(1+(-1)^{n_5} N_n)^3 Fr_n^2}{(1+2(-1)^{n_5} N_n)(EDR + (-1)^{n_5} N_n EDR^2)} - (-1)^{n_5} \frac{N_n}{3} - \frac{1}{2} = 0 \tag{4.17}
\end{aligned}$$

$$\begin{aligned}
& (\varphi(\hat{I}_n) - \varphi(\hat{Z})) \left(\hat{I}_n - \frac{1}{2} \right) - \frac{8}{3} \left((\hat{Z} - \hat{Z}^2)^{1.5} - (\hat{I}_n - \hat{I}_n^2)^{1.5} \right) \\
& - k_e \left(\varphi(\hat{I}_e) - \varphi(\hat{Z}) \right) \left(\hat{I}_e - \frac{1}{2} \right) + \frac{8}{3} k_e \left((\hat{Z} - \hat{Z}^2)^{1.5} - (\hat{I}_e - \hat{I}_e^2)^{1.5} \right) \\
& - \frac{\left(\varphi(\hat{I}_n) - \varphi(\hat{Z}) \right)^2 Fr_n^2}{8(\hat{I}_n - \hat{I}_n^2)^{0.5}} - \left(\frac{\varphi(\hat{I}_n) - \varphi(\hat{Z})}{\varphi(\hat{I}_e) - \varphi(\hat{Z})} - 1 \right) = 0 \tag{4.18}
\end{aligned}$$

where

$$k_e = 1 - \frac{4}{5} \frac{\hat{H}_n}{\hat{y}_n} + \frac{8}{35} \left(\frac{\hat{H}_n}{\hat{y}_n} \right)^2 \left\{ 1 - \left[1 - \left(\frac{\hat{H}_n}{\hat{y}_n} \right)^{-1} \right]^{3.5} \right\} \tag{4.19}$$

$$\frac{\hat{H}_n}{\hat{y}_n} = 1 + \frac{\left(\varphi(\hat{I}_n) - \varphi(\hat{Z}) \right) Fr_n^2}{16(\hat{I}_n - \hat{I}_n^2)^{0.5} \hat{y}_n} \tag{4.20}$$

4.3.1.3 The Sharp Crested Weir Theory

4.3.1.3.1 The Continuity Equation

Fig. 4.4 shows a schematic representation of the free surface flow profile of the symmetric sided trapezoidal channel cross-section of the free over-fall. As discussed earlier, the flow over a free over-fall in any channel cross-section can be assumed to be similar to the flow over a sharp-crested weir of the same section with zero height (without a sill) (Anastasiadou-Partheniou and Hatzigiannakis 1995; Ferro 1999; Ahmad 2003; Vatankhah 2013; Vatankhah 2015). Therefore, the theoretical procedure that is applied to compute the discharge over a sharp-crested weir without a sill can also be used for the free over-fall to obtain the EDR relationships. From previous studies (Fathy & Shaarawi 1954, and Reploigle 1962) it is known that, the pressure distribution at the brink section forms a slightly skewed parabolic shape with its mean value considerably less than the hydrostatic one; therefore, the formed curve area of the actual pressure distribution is definitely smaller than the hydrostatic pressure profile area. Hence, contradictory to a sharp-crested weir, where the pressure distribution all over the end section (at the weir) is assumed to be zero (Ahmad 2003), a linear pressure distribution is proposed to form a right angle (but not isosceles) triangle having its height equal to the brink depth (y_e) and having its maximum value ($C_p y_e$) at the channel bed as shown in Fig. 4.4 (Delleur et al. 1956). Noting that, C_p is the brink pressure distribution coefficient which is less than a unity and was evaluated from experimental dataset of Rajaratnam and Muralidhar (1970). In accordance with the above proposed approach, the flow velocity at any depth at the brink section of the free over-fall can be computed by applying the energy equation between the upstream section and the brink section (see the Appendix for further mathematical details). Therefore using Eq. (A-2), an elemental infinitesimal

discharge (dQ) equation for an elemental tape of thickness dh_E at a height h_E below the energy grade line (EGL) for the trapezoidal free over-fall is generated as follows:

$$Q = \frac{A_e}{A_n} \frac{1}{\sqrt{1+k}} \int_{\frac{v_n^2}{2g}}^{H_n = y_n + \frac{v_n^2}{2g}} \left\{ 2g \left[(1-C_p)h_E + C_p(H_n - y_e) \right] \right\}^{0.5} [B + 2m(H_n - h_E)] dh_E \quad (4.21)$$

where Q = the flow discharge; A_e = the flow area at the brink; A_n = the flow area at the upstream; k = the local energy loss coefficient due to the streamline curvature at the vicinity of the brink; y_n = the upstream flow depth; v_n = the flow velocity at the upstream; C_p = the pressure coefficient; h_E = the vertical distance measured from the total energy head; H_n = the total energy head at the upstream section; y_e = the brink depth; B = the bottom width; m = the side slope (m :1; horizontal : vertical); and dh_E = the elemental infinitesimal depth. Note that the subscripts ‘ n ’ and ‘ e ’ denote the flow conditions at the upstream section and the end section, respectively.

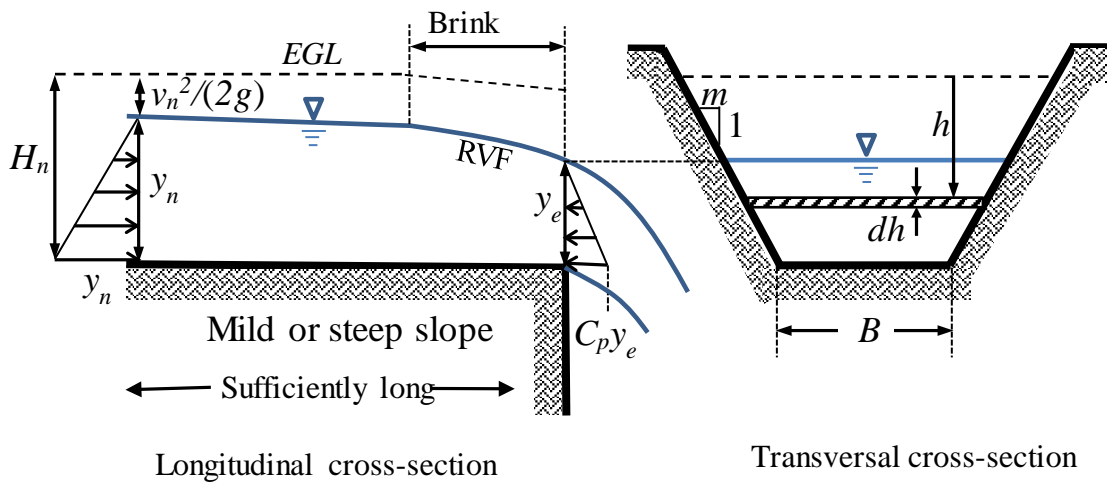


Figure 4.4: Sketch of a free over-fall along the longitudinal symmetric sides trapezoidal channel cross-section with the proposed brink pressure distribution and its transversal (cross-sectional) details

substantial at the free surface profile and zero at the bottom of the channel (Sharifi et al. 2009). Hence, the effect of the streamline curvature at the brink section is considered by introducing a correction factor only to the free-water surface. Subsequently, the following equation can be established to give the value of the discharge at the free over-fall as:

$$Q = \frac{\sqrt{8g} A_e}{15(1-C_p)^2 A_n} \left\{ \frac{1}{\sqrt{1+k}} \left[\begin{aligned} & \left(10m(C_p y_e - H_n) + 5B(C_p - 1) \right) \left(C_p(y_n - y_e) + \frac{v_n^2}{2g} \right)^{1.5} \\ & + 6m \left(C_p(y_n - y_e) + \frac{v_n^2}{2g} \right)^{2.5} \end{aligned} \right] - \left[5B(C_p - 1)(H_n - C_p y_e)^{1.5} - 4m(H_n - C_p y_e)^{2.5} \right] \right\} \quad (4.22)$$

By equating and simplifying Eqs. (4.22) and (3.14), an EDR equation for the generalized trapezoidal free over-fall is obtained as:

$$\begin{aligned} & N_n (\text{EDR})^2 + \text{EDR} \\ & + \frac{30(1-C_p)^2 (1+2N_n)^2 Fr_n}{\left\{ \left[5\psi_1(N_n)\psi_2^{1.5}(N_n) - 4N_n\psi_2^{2.5}(N_n) \right] - \frac{\psi_3^{1.5}(N_n)}{\sqrt{1+k}} \left[N_n(6\psi_3(N_n) - 10\psi_2(N_n)) + 5\psi_1(N_n) \right] \right\}} \\ & = 0 \end{aligned} \quad (4.23)$$

where

$$\text{EDR} = \frac{y_e}{y_n} = \frac{N_e}{N_n}; \quad N_e = \frac{m y_e}{B}; \quad N_n = \frac{m y_n}{B} \quad (4.24)$$

$$\psi_1(N_n) = (C_p - 1) \left(\frac{2 + 4N_n}{1 + N_n} \right) \quad (4.25)$$

$$\psi_2(N_n) = Fr_n^2 + (1 - C_p(\text{EDR})) \left(\frac{2 + 4N_n}{1 + N_n} \right) \quad (4.26)$$

$$\psi_3(N_n) = Fr_n^2 + C_p(1 - \text{EDR}) \left(\frac{2 + 4N_n}{1 + N_n} \right) \quad (4.27)$$

Eq. (4.23) can be simplified for rectangular and triangular channel cross-sections by taking $N_n = 0$ and $N_n = \infty$, respectively. So, substituting $N_n = 0$ and $N_n = \infty$ separately into Eq. (4.23) and simplifying, the EDR equation for the rectangular (Eq. (4.28)) and for the triangular (Eq. (4.29)) channel cross-sections are generated.

$$\text{EDR} - \frac{3(1 - C_p)Fr_n}{\left[Fr_n^2 + 2(1 - C_p\text{EDR}) \right]^{1.5} - \frac{1}{\sqrt{1+k}} \left[Fr_n^2 + 2C_p(1 - \text{EDR}) \right]^{1.5}} = 0 \quad (4.28)$$

$$\text{EDR}^2 - \frac{30(1 - C_p)^2 Fr_n}{\left\{ \begin{array}{l} \left[Fr_n^2 + 4(1 - C_p\text{EDR}) \right]^{2.5} \\ - \frac{\left[Fr_n^2 + 4C_p(1 - \text{EDR}) \right]^{1.5}}{\sqrt{1+k}} \left[Fr_n^2 + 4C_p(1 - \text{EDR}) + 10(1 - C_p) \right] \end{array} \right\}} = 0 \quad (4.29)$$

Since, the magnitude of the local energy loss coefficient (k) is not known, EDR cannot be computed for the given values of C_p and N_n , implying that the Eqs. (4.23), (4.28) and (4.29) are not sufficient to solve these equations at this step.

4.3.1.3.2 The Energy Equation

By applying the energy equation on the streamline at the vicinity of the brink section (between the upstream and the downstream sections), another independent equation

is generated that considers the local energy head loss (h_l) by taking into account the effect of the streamline curvature and given as:

$$H_n = d_e + \frac{v_e^2}{2g} + h_l \quad (4.30)$$

where d_e = the hydrostatic pressure head at the brink, v_e = the flow velocity at the end section (brink); and h_l = the local energy head loss.

Inserting Eq. (3.14) and $h_l = kv_e^2/2g$ into Eq. (4.30) and simplifying leads to:

$$\left\{ \frac{d_e}{y_n} - \left[\frac{(1+N_n)Fr_n^2}{2+4N_n} + 1 \right] \right\} (N_n \text{EDR}^2 + \text{EDR})^2 + \frac{(1+k)(1+N_n)^3 Fr_n^2}{2+4N_n} = 0 \quad (4.31)$$

To obtain a relationship for an imaginary equivalent hydrostatic pressure head at the brink (d_e) based on $C_p y_e$ by using the experimental data of Rajaratnam and Muralidhar (1970), the suggested volume of the linearly varying pressure distribution as detailed in Fig. 4.4 is equated with the volume of the hydrostatic pressure distribution with the depth d_e . Hence, Eq. (4.32) is obtained for the generalized trapezoidal channel cross-sections.

$$2N_n \left[C_p \text{EDR}^3 - \left(\frac{d_e}{y_n} \right)^3 \right] + 3 \left[C_p \text{EDR}^2 - \left(\frac{d_e}{y_n} \right)^2 \right] = 0 \quad (4.32)$$

Eqs. (4.31) and (4.32) are reduced to a single 3rd degree polynomial, for the rectangular channel cross-sections by substituting $N_n = 0$.

$$C_p^{\frac{1}{2}} \text{EDR}^3 - \left(1 + \frac{Fr_n^2}{2}\right) \text{EDR}^2 + (1+k) \frac{Fr_n^2}{2} = 0 \quad (4.33)$$

Similarly, for the triangular channel cross-sections, a single 5th degree polynomial is obtained by substituting $N_n = \infty$.

$$C_p^{\frac{1}{3}} \text{EDR}^5 - \left(1 + \frac{Fr_n^2}{4}\right) \text{EDR}^4 + (1+k) \frac{Fr_n^2}{4} = 0 \quad (4.34)$$

Since, an independent equation is established using the energy equation, the aforementioned equations (Eqs. (4.23), (4.28) and (4.29)) can be solved by using the pressure coefficient (C_p) values suggested by Rajaratnam and Muralidhar (1970) where,

$$C_p = \begin{pmatrix} 0.281 - 0.1184N_c & 0 \leq N_c < 0.79 \\ 0.1875 & 0.79 \leq N_c \leq 2.34 \\ 0.2136 - 0.01116N_c & 2.34 < N_c \leq 10.00 \\ 0.102 & 10 < N_c \leq \infty \end{pmatrix} \quad (4.35)$$

where $N_c = my_c/B$.

4.3.2 The Suggested Approaches

4.3.2.1 Three Velocity Points Method

Using Eqs. (3.30), (3.31), and (3.32) and substituting the upstream Froude number Fr_n from Eq. (3.14) and the proper relationships of the flow area for each cross-section into Eq. (3.33), the generalized EDR relationships are obtained based on this new approach for the exponential (Eq. (4.36)), the generalized trapezoidal (Eq. (4.37)) and the generalized circular channel cross-sections (Eq. (4.40)) as:

$$\text{EDR} = \left[\frac{2Fr_n}{Fr_n + \sqrt{Fr_n^2 + \frac{2\eta_2}{\eta_2 + 1}} + \left(\sqrt{Fr_n^2 + 2\eta_2} - Fr_n \right) \left(\frac{\eta_2}{\eta_2 + 1} \right)^{\eta_2}} \right]^{\frac{1}{\eta_2}} \quad (4.36)$$

$$f_1(N_n) + f_2(N_n) - 36 \left[N_n^2 \text{EDR}^2 + 2(-1)^{\eta_5} N_n \text{EDR} + 1 \right] * \frac{\left[1 + (-1)^{\eta_5} N_n \right]^{1.5} Fr_n}{\left[0.5 + (-1)^{\eta_5} N_n \right]^{0.5}} = 0 \quad (4.37)$$

$$f_1(N_n) = \left[20(-1)^{\eta_5} N_n^3 \text{EDR}^4 + 60N_n^2 \text{EDR}^3 + 57(-1)^{\eta_5} N_n \text{EDR}^2 + 18\text{EDR} \right] \cdot \left[\sqrt{\frac{(1 + (-1)^{\eta_5} N_n) Fr_n^2}{2 + 4(-1)^{\eta_5} N_n}} + \sqrt{\frac{(1 + (-1)^{\eta_5} N_n) Fr_n^2}{2 + 4(-1)^{\eta_5} N_n} + \frac{3 + 2(-1)^{\eta_5} N_n}{6 + 6(-1)^{\eta_5} N_n}} \right] \quad (4.38)$$

where

$$f_2(N_n) = \left[16(-1)^{\eta_5} N_n^3 \text{EDR}^4 + 48N_n^2 \text{EDR}^3 + 51(-1)^{\eta_5} N_n \text{EDR}^2 + 18\text{EDR} \right] \cdot \left[\sqrt{1 + \frac{(1 + (-1)^{\eta_5} N_n) Fr_n^2}{2 + 4(-1)^{\eta_5} N_n}} + \sqrt{\frac{(1 + (-1)^{\eta_5} N_n) Fr_n^2}{2 + 4(-1)^{\eta_5} N_n} + \frac{3 + 2(-1)^{\eta_5} N_n}{6 + 6(-1)^{\eta_5} N_n}} \right] \quad (4.39)$$

$$\left[\sqrt{\frac{(\varphi(\hat{I}_n) - \varphi(\hat{Z})) Fr_n^2}{16(\hat{I}_n - \hat{I}_n^2)^{0.5}}} + \sqrt{\frac{(\varphi(\hat{I}_n) - \varphi(\hat{Z})) Fr_n^2}{16(\hat{I}_n - \hat{I}_n^2)^{0.5}} + \left(\hat{I}_n - \frac{1}{2} - \frac{8 \left((\hat{Z}_{fb} - \hat{Z}^2)^{1.5} - (\hat{I}_n - \hat{I}_n^2)^{1.5} \right)}{\varphi(\hat{I}_n) - \varphi(\hat{Z})} \right)} \right] \cdot (\varphi(\hat{I}_e) - \varphi(\hat{I}_e - \hat{y}_e)) + \left[\sqrt{\hat{y}_n + \frac{(\varphi(\hat{I}_n) - \varphi(\hat{Z})) Fr_n^2}{16(\hat{I}_n - \hat{I}_n^2)^{0.5}}} + \sqrt{\frac{(\varphi(\hat{I}_n) - \varphi(\hat{Z})) Fr_n^2}{16(\hat{I}_n - \hat{I}_n^2)^{0.5}} + \left(\hat{I}_n - \frac{1}{2} - \frac{8 \left((\hat{Z} - \hat{Z}^2)^{1.5} - (\hat{I}_n - \hat{I}_n^2)^{1.5} \right)}{\varphi(\hat{I}_n) - \varphi(\hat{Z})} \right)} \right] \cdot (\varphi(\hat{I}_e - \hat{y}_e) - \varphi(\hat{Z})) - \frac{(\varphi(\hat{I}_n) - \varphi(\hat{Z}))^{1.5} Fr_n}{2(\hat{I}_n - \hat{I}_n^2)^{0.25}} = 0 \quad (4.40)$$

where

$$\hat{y}_e = \hat{I}_e - \frac{1}{2} - \frac{8}{3} \frac{((\hat{Z} - \hat{Z}^2)^{1.5} - (\hat{I}_e - \hat{I}_e^2)^{1.5})}{\varphi(\hat{I}_e) - \varphi(\hat{Z})} \quad (4.41)$$

4.3.2.2 Infinite Number (n-) Velocity Points Method

Using Eqs. (3.34), (3.35), (3.36), (3.37), and (3.38) and substituting the upstream Froude number Fr_n from Eq. (3.14) and the proper relationships of the flow area for each cross-section into Eq. (3.39), the generalized EDR relationships are expressed based on this new approach as series expansion for the exponential (Eq. (4.42)), the generalized trapezoidal (Eq. (4.43)) and the generalized circular channel cross-sections (Eq. (4.44)) as:

$$\text{EDR} = \left\{ \frac{\sqrt{2}(np-1)^{\eta_2} Fr_n}{\eta_2^{\frac{1}{2}} \sum_{i=1}^{np-1} \left[\left(\sqrt{\frac{Fr_n^2}{2\eta_2} + \frac{i-1}{np-1}} + \sqrt{\frac{Fr_n^2}{2\eta_2} + \frac{i}{np-1}} \right) ((np-i)^{\eta_2} - (np-i-1)^{\eta_2}) \right]} \right\}^{\frac{1}{\eta_2}} \quad (4.42)$$

$$\sum_{i=1}^{np-1} \left[\left(\sqrt{\frac{(1+(-1)^{\eta_5} N_n) Fr_n^2}{(2+4(-1)^{\eta_5} N_n)} + \frac{i-1}{np-1}} + \sqrt{\frac{(1+(-1)^{\eta_5} N_n) Fr_n^2}{(2+4(-1)^{\eta_5} N_n)} + \frac{i}{np-1}} \right) \cdot \left(\frac{\text{EDR}}{np-1} + (-1)^{\eta_5} \frac{N_n \text{EDR}^2 (2np-2i-1)}{(np-1)^2} \right) \right] - \frac{\sqrt{2}(1+(-1)^{\eta_5} N_n)^{1.5} Fr_n}{(1+2(-1)^{\eta_5} N_n)^{\frac{1}{2}}} = 0 \quad (4.43)$$

$$\begin{aligned}
& \sum_{i=1}^{np-1} \left[\left(\sqrt{\frac{(\varphi(\hat{I}_n) - \varphi(\hat{Z})) Fr_n^2}{4(\hat{I}_n - \hat{I}_n^2)^{0.5}} + \frac{i-1}{np-1}} + \sqrt{\frac{(\varphi(\hat{I}_n) - \varphi(\hat{Z})) Fr_n^2}{4(\hat{I}_n - \hat{I}_n^2)^{0.5}} + \frac{i}{np-1}} \right) \right. \\
& \quad \left. \cdot \left(\varphi\left(\frac{np-i}{np-1} \hat{y}_e + \hat{Z}\right) - \varphi\left(\frac{np-i-1}{np-1} \hat{y}_e + \hat{Z}\right) \right) \right] \\
& - \frac{(\varphi(\hat{I}_n) - \varphi(\hat{Z}))^{1.5} Fr_n}{(\hat{I}_n - \hat{I}_n^2)^{0.25}} = 0
\end{aligned} \tag{4.44}$$

Chapter 5

RESULTS AND DISCUSSION

5.1 Introduction

In this chapter, the variation of the end depth ratio (EDR) and the end depth discharge (EDD) values for different channel cross-sections are investigated through the proposed methodologies and presented within four main sections. The first section deals with the solution of the proposed methodologies for computing the EDR and the EDD of the exponential channel cross-sections for both sub- and super critical flow regimes. The second section details the solution of the suggested methodologies for the EDR and the EDD relationships of the generalized trapezoidal channel cross-sections for both regimes (Abrari et al, 2018). In this section, also the results of semi-trapezoidal and inverted semi-triangular channel cross-sections based on different approaches (energy (Abrari et al, 2017b), free vortex theory (Abrari et al, 2016), three velocity points (Abrari et al, 2017a) and infinite number velocity points) are determined since they were not studied earlier. The third section deals with the solutions of the computed EDR and EDD relationships for the circular channel cross-sections with flat base for both sub- and super critical flow regimes. This chapter ends with the direct prediction of the discharges from the known values of the end depths for all the above-mentioned channel cross-sections in both flow regimes. As previously stated, in sub-critical flow regimes, the end depth value is related to the critical depth, since the critical section occurs somewhere upstream of the end section. However in super critical flow regimes, due to the lack of the critical

depth occurrence within the studied control volume of the approaching flow, the water depth at the end section has been correlated to the longitudinal channel bed slope (S) and the channel bed roughness (n) through the semi-empirical Manning-Strickler equation.

5.2 Exponential Channel Cross-sections

5.2.1 EDR for Sub-critical Flow Regimes

When the approaching flow is in sub-critical regime, the critical section exists at the upstream of the end section provided that the channel is longitudinally long enough. Using Eq. (4.36), the end depth ratio (EDR), being the ratio of the end depth to the critical depth, can be determined based on the three velocity points method for the rectangular, the parabolic, and the triangular channel cross-sections by inserting $Fr_n = Fr_c = 1$ and incorporating with the appropriate value of the exponent η_2 as shown in Table 4.1. Therefore, by substituting $\eta_2 = 1, 1.5,$ and $2,$ EDR values of $0.719, 0.772,$ and 0.806 for the rectangular (unconfined nappe), the parabolic and the triangular (symmetric sides) channel cross-sections are obtained respectively. Also, substituting $Fr_n = Fr_c = 1$ and number of point (np) = ∞ for the infinite number velocity points method into Eq. (4.42), the EDR values are found to be $0.715, 0.777,$ and 0.817 for the rectangular, the parabolic, and the triangular channel cross-sections respectively.

5.2.2 EDD for Sub-critical Flow Regimes

Similarly, the discharge relationship of the exponential channel based on the Froude number of the normal depth (Fr_n) can be written as:

$$Q = \frac{g^{0.5} \eta_1 y_n^{(\eta_2+0.5)}}{\eta_2^{0.5}} Fr_n \quad (5.1)$$

Substituting y_n from Eqs. (4.16), (4.36), and (4.42) into Eq. (5.1), the following general end depth discharge (EDD) relationships which are the direct prediction of the discharge for the given end depth (y_e) based on the three velocity points method (Eq. (5.2)), the infinite number velocity points method (Eq. (5.3)), and the free vortex theory (Eq. (5.4)), for flows in sub- and super critical regimes at free over-fall in exponential channel cross-section are obtained only since the solution based on energy method is available in the literature:

$$Q = \frac{g^{0.5} \eta_1 Fr_n}{\eta_2^{0.5}} \left[\frac{Fr_n}{Fr_n + \sqrt{Fr_n^2 + \frac{2\eta_2}{\eta_2 + 1}} + \left(\sqrt{Fr_n^2 + 2\eta_2} - Fr_n \right) \left(\frac{\eta_2}{\eta_2 + 1} \right)^{\eta_2}} \right]^{-\left(1 + \frac{0.5}{\eta_2}\right)} \cdot y_e^{(\eta_2+1)} \quad (5.2)$$

$$Q = \frac{g^{0.5} \eta_1 Fr_n}{\eta_2^{0.5}} \left[\frac{\sqrt{2}(n-1)^{\eta_2} Fr_n}{\eta_2^2 \sum_{i=1}^{np-1} \left[\left(\sqrt{\frac{Fr_n^2}{2\eta_2} + \frac{i-1}{np-1}} + \sqrt{\frac{Fr_n^2}{2\eta_2} + \frac{i}{np-1}} \right) \left((np-i)^{\eta_2} - (np-i-1)^{\eta_2} \right) \right]} \right]^{-\left(1 + \frac{0.5}{\eta_2}\right)} \cdot y_e^{(\eta_2+1)} \quad (5.3)$$

$$\left\{ 1 - \frac{4}{5} \left(1 + \frac{\eta_1 Fr_n^2}{2\eta_2} \right) + \frac{8}{35} \left[\left(1 + \frac{\eta_1 Fr_n^2}{2\eta_2} \right)^2 - \frac{\left(\frac{\eta_1 Fr_n^2}{2\eta_2} \right)^{3.5}}{\left(1 + \frac{\eta_1 Fr_n^2}{2\eta_2} \right)^{1.5}} \right] \right\} \text{EDR}^{(2\eta_2+1)} - \left[\frac{(\eta_2+1)\eta_1 Fr_n^2}{\eta_2} + 1 \right] \text{EDR}^{\eta_2} + \frac{(\eta_2+1)\eta_1 Fr_n^2}{\eta_2} = 0 \quad (5.4)$$

where

$$Fr_n = \frac{QT_n^{0.5}}{g^{0.5} A_n^{1.5}} = \left(\frac{y_c}{y_n} \right)^{\eta_2+0.5} \quad (5.5)$$

Substituting $Fr_n = Fr_c = 1$, the defined values of the exponent η_2 for the rectangular, the parabolic and the triangular sections and inserting $np = \infty$ into these general equations, the EDD relationships for the above mentioned cross-sections were computed from the two above mentioned suggested methodologies and detailed as well in Table 5.1, since Beirami et al. (2006) computed the EDR and the EDD relationships of the exponential channel cross-sections for sub-critical flow regimes.

Table 5.1: Computed EDR values and EDD relationships based on the two suggested methods of this study for the exponential channel cross-section

Cross-section	Methods	Nappe Type	EDR (y_e/y_c)	EDD (m^3/s)
Rectangular	n-velocity points method	U	0.715	$1.654 g^{0.5} \eta_1 y_e^{1.5}$
	Three velocity points method	U	0.719	$1.639 g^{0.5} \eta_1 y_e^{1.5}$
Parabolic	n-velocity points method	U	0.777	$1.351 g^{0.5} \eta_1 y_e^2$
	Three velocity points method	U	0.772	$1.370 g^{0.5} \eta_1 y_e^2$
Triangular	n-velocity points method	U	0.817	$1.171 g^{0.5} \eta_1 y_e^{2.5}$
	Three velocity points method	U	0.806	$1.212 g^{0.5} \eta_1 y_e^{2.5}$

U: unconfined nappe

5.2.3 EDR for Super Critical Flow Regimes

In super critical flow regime where the longitudinal channel slope is steep, the critical water depth ' y_c ' does not exist at the control volume (between the upstream (normal) section and the downstream (end) section), since the critical depth it is greater than the uniform (normal) water depth. So, the water level at the end depth ' y_e ' depends on the upstream Froude number ' Fr_n ' instead of the critical flow depth and ' Fr_c '. As the upstream Froude number is a function of the channel bed slope ' S ', the functional relationship of y_e can be written as:

$$y_e = y_e(y_c, S) \quad (5.6)$$

Note that, the ratio of y_e/y_c is related to the EDR and the upstream Froude number ' Fr_n ' by the following equation:

$$\varepsilon_e = \frac{y_e}{y_c} = \frac{\text{EDR}}{Fr_n^{(\eta_2+0.5)}} \quad (5.7)$$

The upstream Froude number ' Fr_n ' in the Eq. (5.5) is divided by the Froude number of the fictitious critical cross-section to obtain as:

$$Fr_n = \left(\frac{T_n}{T_c} \right)^{0.5} \left(\frac{A_c}{A_n} \right)^{1.5} \quad (5.8)$$

where T_c = the top width of the flow at the fictitious critical water depth section and A_c = the cross-sectional area of the flow at that fictitious section. Since the critical water depth does not exist within the control volume section, to overcome this, the semi-empirical equation suggested by Manning-Strickler for open channels is introduced that gives the following relationship as:

$$Fr_n = \left(\frac{S}{S_c} \right)^{\frac{1}{2}} \left(\frac{T_n}{T_c} \right)^{\frac{1}{2}} \left(\frac{A_n}{A_c} \right)^{\frac{1}{6}} \left(\frac{P_c}{P_n} \right)^{\frac{2}{3}} \quad (5.9)$$

where P_n = the channels wetted perimeter at the normal depth section, P_c = the channels wetted perimeter at the fictitious critical depth section, S_c = the fictitious critical slope of the channels, and S = the channels bed slope as defined earlier.

Equating Eqs. (5.8) and (5.9), gives:

$$\tilde{S} = \frac{S}{S_c} = \left(\frac{A_c}{A_n} \right)^{\frac{10}{3}} \left(\frac{P_n}{P_c} \right)^{\frac{4}{3}} \quad (5.10)$$

Replacing the corrected form of the foregoing parameters into Eq. (5.10), \tilde{S} for the rectangular (Eq. (5.11a)), the parabolic (Eq. (5.11b)), and the triangular (Eq. (5.11c)) channel cross-sections are given in a simplified form as:

$$\tilde{S}_{rec} = \left(\frac{1 + 2y_n/B}{1 + 2y_c/B} \right)^{\frac{4}{3}} \left(\frac{y_c}{y_n} \right)^{\frac{10}{3}} \quad (5.11a)$$

$$\tilde{S}_{par} = \left\{ \frac{T_n \left[\sqrt{1 + \left(\frac{4y_n}{T_n} \right)^2} + \frac{T_n}{4y_n} \ln \left(\frac{4y_n}{T_n} + \sqrt{1 + \left(\frac{4y_n}{T_n} \right)^2} \right) \right]}{T_c \left[\sqrt{1 + \left(\frac{4y_c}{T_c} \right)^2} + \frac{T_c}{4y_c} \ln \left(\frac{4y_c}{T_c} + \sqrt{1 + \left(\frac{4y_c}{T_c} \right)^2} \right) \right]} \right\}^{\frac{4}{3}} \left(\frac{T_c y_c}{T_n y_n} \right)^{\frac{10}{3}} \quad (5.11b)$$

$$\tilde{S}_{tri} = \left(\frac{y_c}{y_n} \right)^{\frac{16}{3}} \quad (5.11c)$$

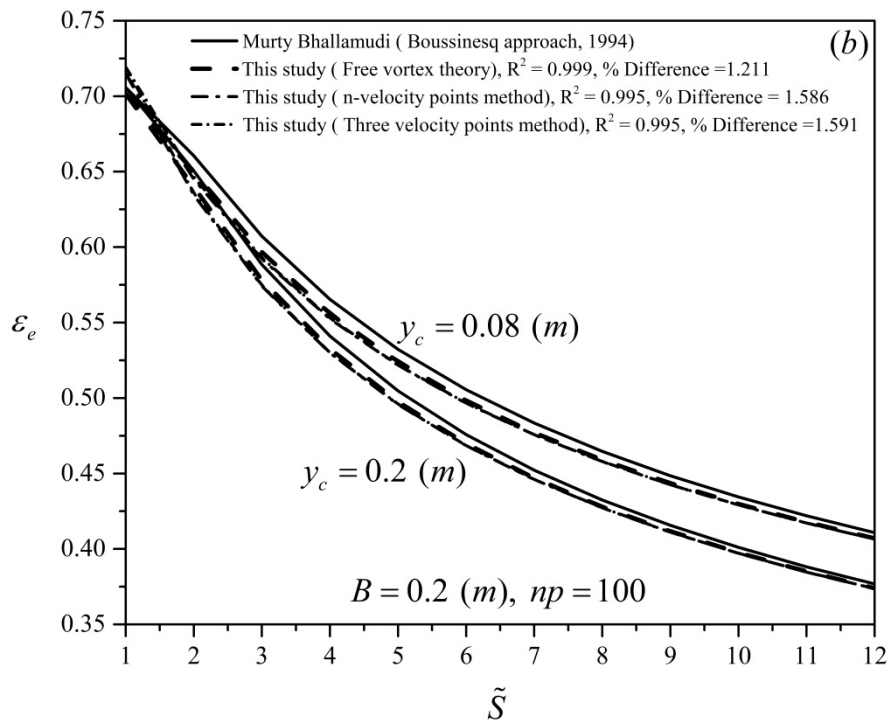
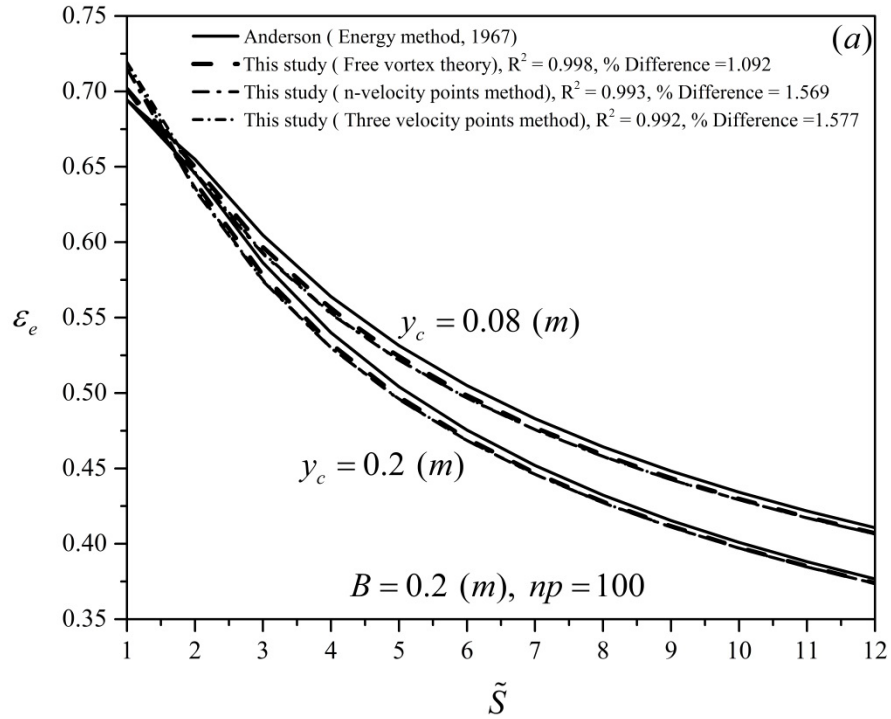
5.2.3.1 EDR of Rectangular Channel Cross-sections

To evaluate y_n for the given values of y_c , B and \tilde{S} , Eq. (5.11a) was solved numerically. Subsequently Fr_n is calculated from Eq. (5.5) and y_e numerically determined from Eqs. (4.16), (4.36), and (4.42) for free vortex theory (to strengthen the suggested new methods), the three velocity points method, and the infinite number velocity points method, respectively. Then, the ratio of y_e/y_c ' \mathcal{E}_e ' is estimated from Eq. (5.7) for the rectangular channel cross-sections by using the relevant value of η_2 . The result of \mathcal{E}_e compared with the theoretical study of Anderson, (1967) based on the energy method, Murty Bhallamudi, (1994) using the Boussinesq approach, and Ferro, (1999) through the sharp-crested weir theory are shown graphically in Fig. 5.1(a), (b), and (c) for the rectangular channel cross-section in super critical flow regimes, respectively. These graphical representations involve number of curves since the effect of different bed slopes ' S ' are coupled in the solution; unlike the sub-critical flow regime cases where the critical slope interferes only. In order to show the accuracy of the suggested methods, the two statistical measuring indices (Mean Absolute Relative Error (MARE) and Correlation coefficient (R^2)) were determined and shown as well in these figures. For best relationship, the value of MARE should be close to zero and the value of R^2 should approach to unity. As shown in Fig. 5.1(c), the curve for infinite number velocity points method are overlapping with the study of Ferro (1999), since as the number of points (np) approaches to an infinity number, the series expansion equation converges to the equation of the sharp-crested weir theory.

A comparison of the computed results of the EDR values for the rectangular channel cross-sections obtained from the suggested theoretical methods of the current study

with the relevant experimental study by Jagannadha Rao, (1961) is given in Fig. 5.2.

The verification of this study with the relevant experimental data sets varies slightly from the observations.



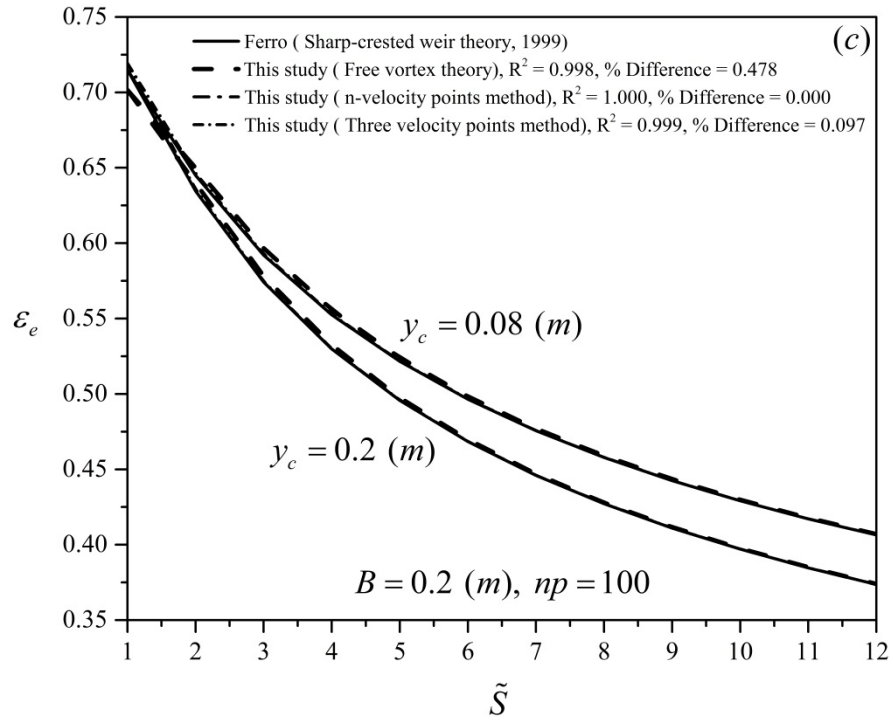


Figure 5.1: Comparison between the variation of ε_e on \tilde{S} for 0.08 (m) $\leq y_c \leq 0.2$ (m) and $B = 0.2$ (m) of the two suggested theoretical approaches and the theoretical solution of the free vortex theory with the study of (a) Anderson (1967); (b) Murty Bhallamudi (1994); and (c) Ferro (1999) in rectangular channel cross-sections

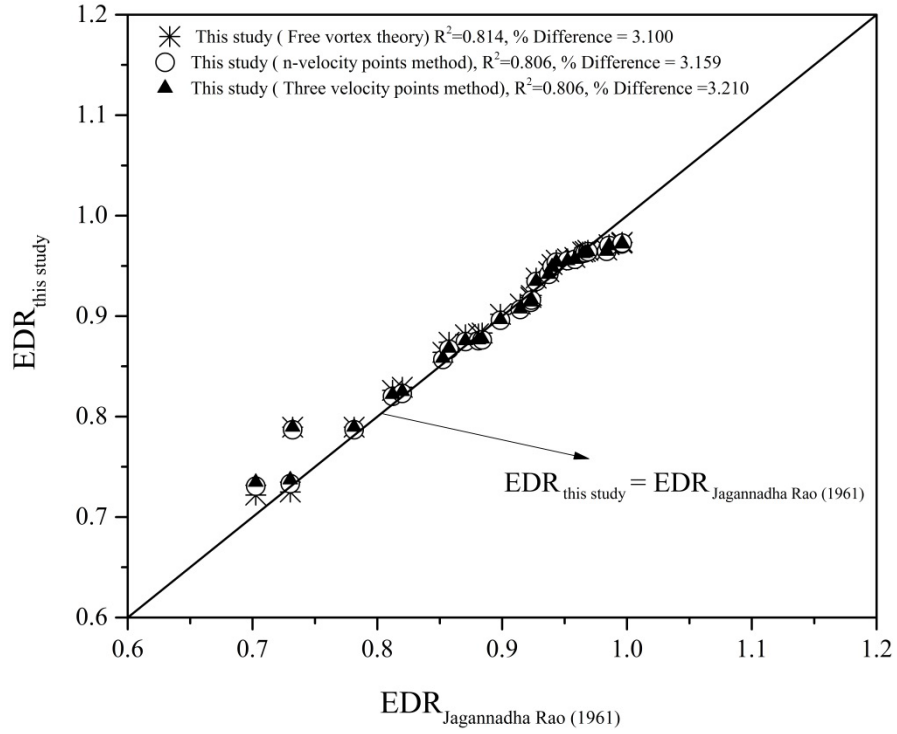
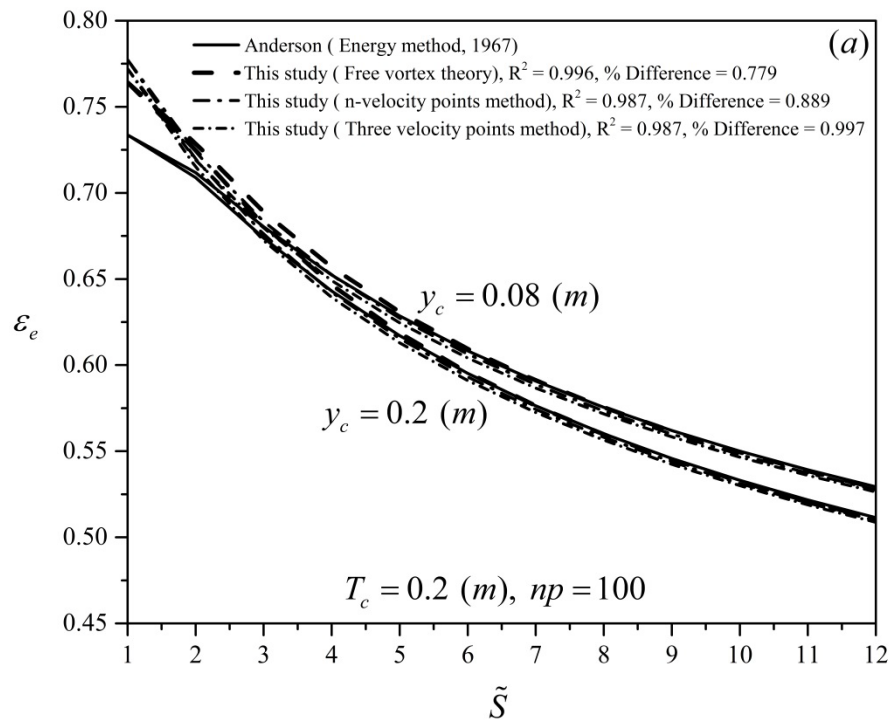


Figure 5.2: Comparison between the computed EDR values of the two suggested theoretical approaches and the free vortex theory with the experimental data set of the EDR of Jagannadha Rao (1961) in rectangular channels

5.2.3.2 EDR of Parabolic Channel Cross-sections

Similarly, in order to evaluate y_n for the given values of y_c , T_c and \tilde{S} , Eq. (5.11b) was solved numerically. Subsequently Fr_n is calculated from Eq. (5.5) and the value of y_e numerically determined from Eqs. (4.16), (4.36), and (4.42) for the free vortex theory, the three velocity points method, and the infinite number velocity points method, respectively. Then, ε_e is calculated from Eq. (5.7) for the parabolic channel cross-sections by inserting the relevant value of η_2 . The result of ε_e compared with the theoretical study of Anderson, (1967) based on the energy method, Murty Bhallamudi, (1994) using Boussinesq approach, and the sharp-crested weir theory (solved by the authors for strengthening the suggested methods) are shown graphically in Figs. 5.3(a), (b), and (c) respectively. These graphical representations

involve number of curves since the effect of different bed slopes ‘ S ’ are coupled in the solution; unlike the sub-critical flow regime cases where the critical slope interferes only. In order to investigate the correctness of the suggested methods, the two statistical measuring indices (Mean Absolute Relative Error (MARE) and Correlation coefficient (R^2)) are provided in these figures as well. As shown in Fig. 5.3(c), the curves of the infinite number velocity points method are overlapping with the sharp-crested weir theory, since as the number of points (np) approaches to infinity, this series expansion method converges to the sharp-crested weir theory.



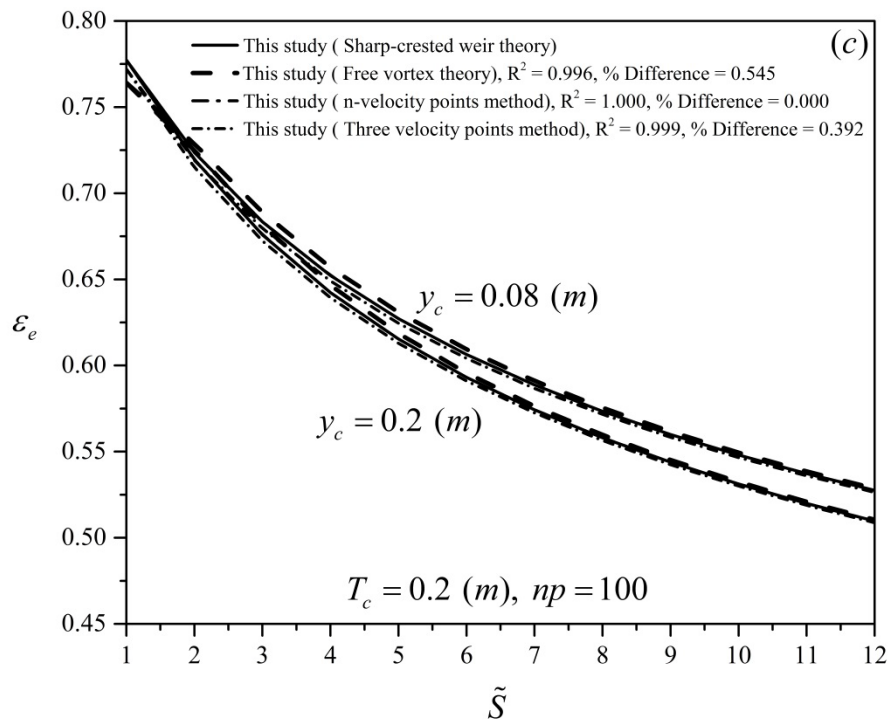
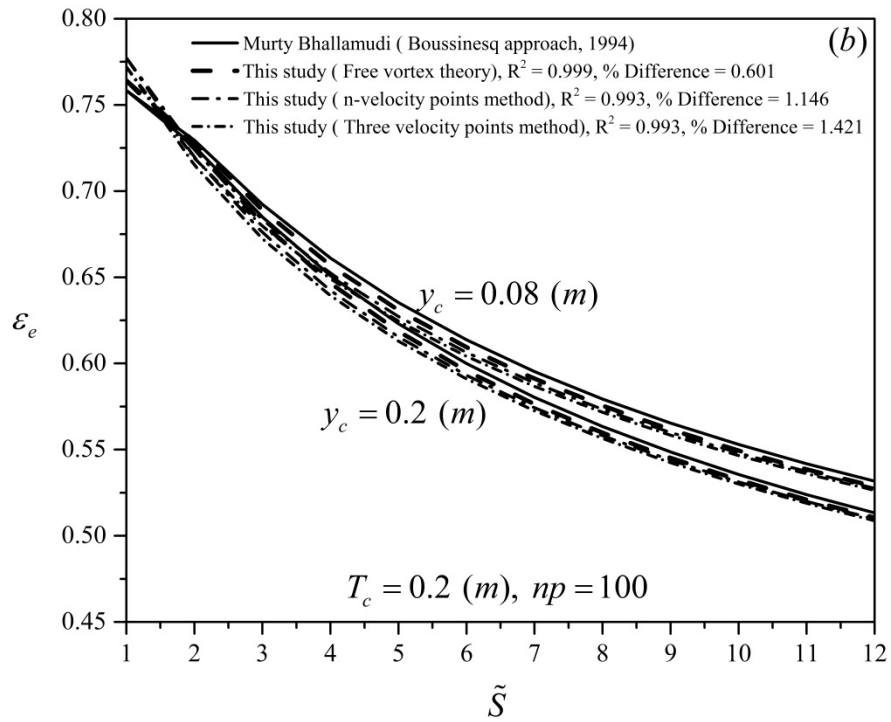
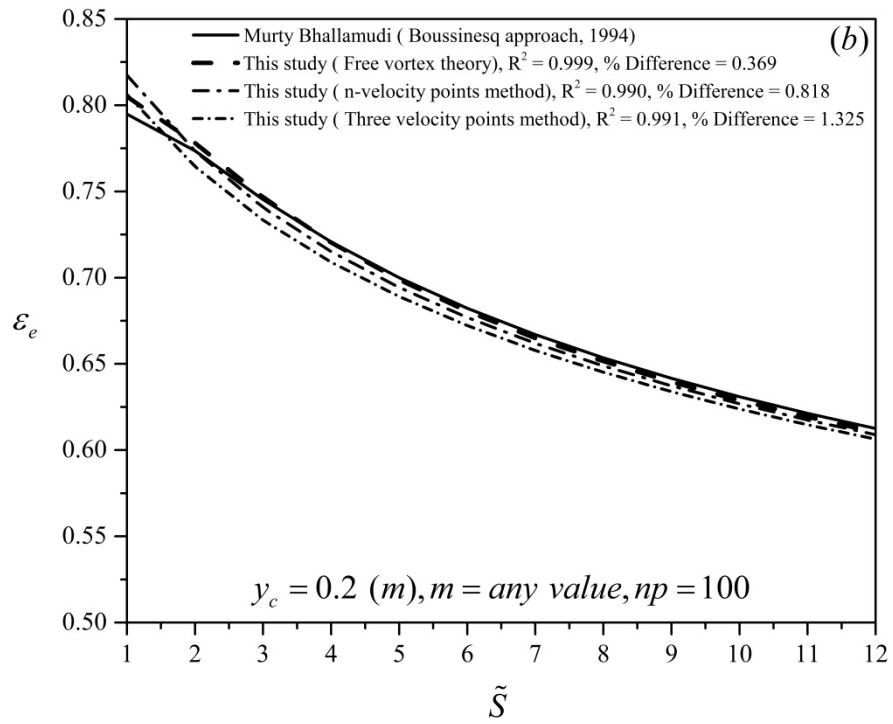
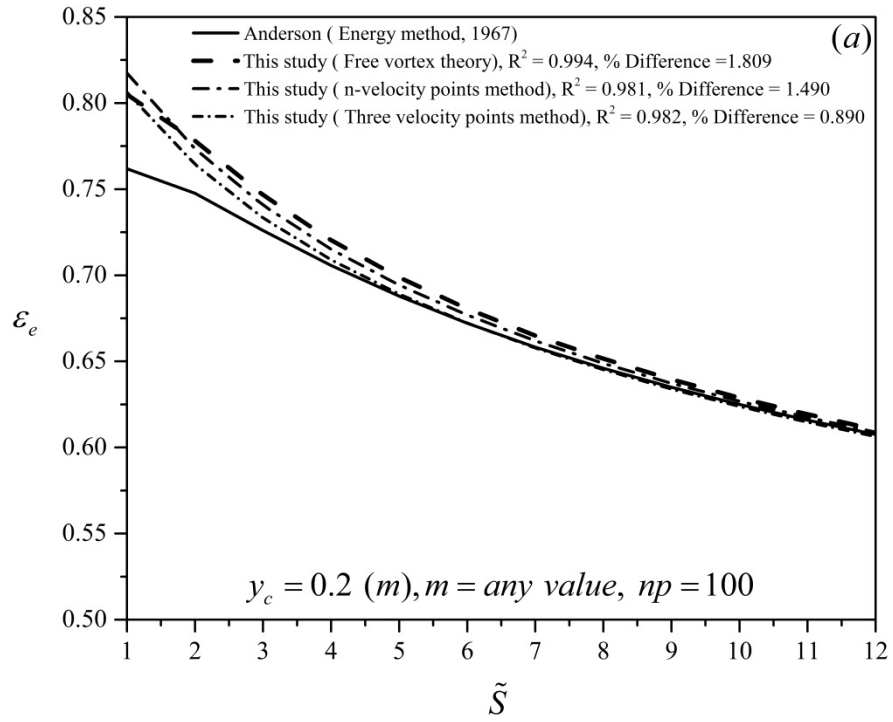


Figure 5.3: Comparison between the variation of ε_e on \tilde{S} for $0.08 (m) \leq y_c \leq 0.2 (m)$ and $T_c = 0.2 (m)$ of the two suggested theoretical approaches and the theoretical solution of free vortex theory with the study of (a) Anderson (1967); (b) Murty Bhallamudi (1994); and (c) the theoretical solution of the sharp-crested weir theory in parabolic channel cross-sections

5.2.3.3 EDR of Triangular Channel Cross-sections

In a similar way, to evaluate y_n for the given values of y_c and \tilde{S} , Eqs. (5.11c) was solved numerically. Subsequently Fr_n is calculated from Eq. (5.5) and y_e numerically determined from Eqs. (4.16), (4.36), and (4.42) for the free vortex theory, the three velocity points method, and the infinite number velocity points method, respectively. Then, ε_e is estimated from Eq. (5.7) for the triangular channel cross-sections by using the relevant values of η_2 . The result of ε_e compared with the theoretical study of Anderson, (1967) based on the energy method, Murty Bhallamudi (1994) using the Boussinesq approach, and Ferro, (1999) through the sharp-crested weir theory are shown in Figs. 5.4(a), (b) and (c) for triangular channel cross-sections in super critical flow regimes, respectively. In order to show the accuracy of the suggested methods, the two statistical measuring indices (Mean Absolute Relative Error (MARE) and correlation coefficient (R^2)) were provided as well in these figures. As shown in Fig. 5.4(c), the curve for infinite number velocity points method are overlapping with the study of Ferro (1999), since as the number of points (np) approaches to infinity, due to the same reasoning discussed in the earlier section.



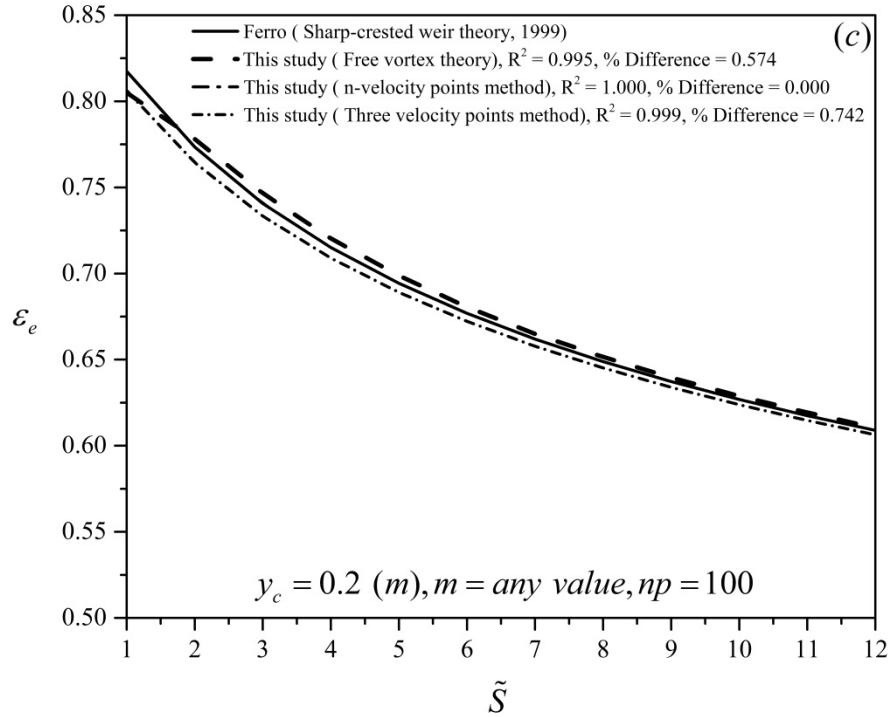


Figure 5.4: Comparison between the variation of ε_e versus \tilde{S} for any value of m and $y_c=0.2$ and the theoretical study of (a) Anderson, (1967); (b) Murty Bhallamudi (1994); and (c) Ferro (1999) in triangular channel cross-sections

The experimental data of Rajaratnam and Muralidhar (1964) is considered for verifying the computed EDR of the suggested method of this study for the triangular free over-falls and is presented in Fig. 5.5. The verification of this study with the relevant experimental data sets varies slightly from the observations. This variation is probably due to the fluctuation of the measured data set of Rajaratnam and Muralidhar (1964) since, the studied cross-sectional shape characteristics at very low discharges are forming very shallow water depths where the occurred wetted perimeter at different discharge values due to the inner wall roughness effecting the measurements significantly.

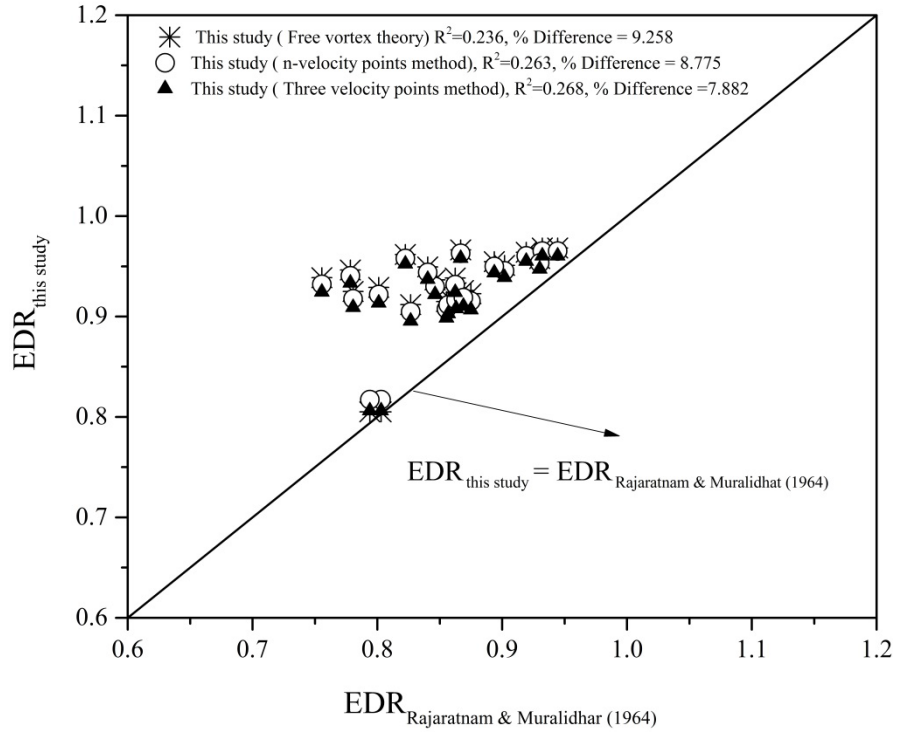


Figure 5.5: Comparison of the computational EDR values of the two suggested theoretical approaches and the free vortex theory of this study with the experimental data set of the EDR value by Rajaratnam and Muralidhar, (1964) in triangular channel cross-sections

5.2.4 EDD of Super Critical Flow Regimes

To utilize the free over-fall as a flow measuring device, it is essential to estimate the discharge value only by using the flow depth at the end section. Therefore, by substituting $y_n = y_e / EDR$ into Eq. (5.1), the generalized equation of the EDD is obtained:

$$Q = \left[\frac{g^{0.5} \eta_1 y_e^{(\eta_2+0.5)}}{\eta_2^{0.5} EDR^{(\eta_2+0.5)}} \right] Fr_n \quad (5.12)$$

In super critical flow regimes, as the discharge is dependent on y_e and Fr_n , so it is not explicitly possible to estimate the discharge from the given value of the end depth measurement only (unlike to sub-critical flow regimes). Hence, a second

measurement at the upstream is unavoidable. In essence, if both y_e and y_n are known, the upstream Froude number at the normal section ' Fr_n ' can be calculated directly using Eqs. (4.16), (4.36), and (4.42). Subsequently, y_e and Fr_n may be used to estimate the discharge from Eq. (5.12). Since, it is difficult to determine the location of the normal section properly, the known values of the relative channel bed slope (\tilde{S}) using Eqs. (5.11a), (5.11b), and (5.11c), the semi-empirical Manning-Strickler equation is coupled with the end depth measurements.

5.2.4.1 EDD of Rectangular Channel Cross-sections

Therefore, to evaluate y_c , y_n , and Fr_n for the given value of y_e and \tilde{S} , Eqs. (5.5), (5.11a), and (4.36) for the three velocity points method, Eqs. (5.5), (5.11a), and (4.42) for the infinite number velocity points, and Eqs. (5.5), (5.11a), and (4.16) for the free vortex theory method were solved numerically. Eventually by substituting the appropriate value of η_2 , the discharge (Q) values for the rectangular channel cross-sections were computed using Eqs. (5.2), (5.3), and (5.4) for the three velocity points method, for the Infinite number velocity points method, and for the free vortex theory respectively.

5.2.4.2 EDD of Parabolic Channel Cross-sections

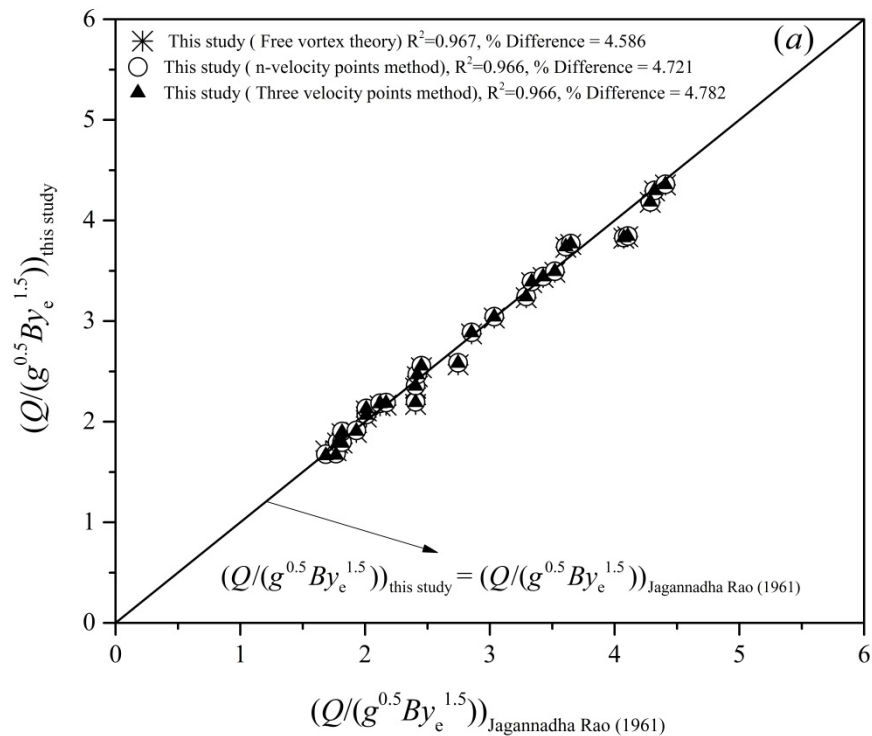
Since no earlier experimental data are available in the literature, the generated relevant theoretical equations for this cross-section were not validated.

5.2.4.3 EDD of Triangular Channel Cross-sections

For the triangular channel cross-sections, in order to investigate y_c , y_n , and Fr_n for the given value of y_e and \tilde{S} , Eqs. (5.5), (5.11c), and (4.36) for the three velocity points method, Eqs. (5.5), (5.11c), and (4.42) for the infinite number velocity points method and Eqs. (5.5), (5.11c), and (4.16) for the free vortex theory were solved

numerically. Finally by inserting the relevant value of η_2 , for the triangular channel cross-sections the discharge (Q) values were computed using Eqs. (5.2), (5.3), and (5.4) for the three velocity points method, for the infinite number velocity points method, and for the free vortex theory respectively.

In order to verify the calculated discharge values, a comparison has been made for the exponential channels with relevant experimental results existing in the literature. In Figures 5.6(a) and 5.6(b), the observed data sets of Jagannadha Rao (1961) for the rectangular channels and the experimental data of Rajaratnam and Muralidhar (1964) for the triangular channels are compared with the calculated discharge values of the generated equations. Figures 5.6(a) and 5.6(b) reveal that, the calculated values of the discharge giving little discrepancies with the experimental data sets due to the same reason discussed earlier.



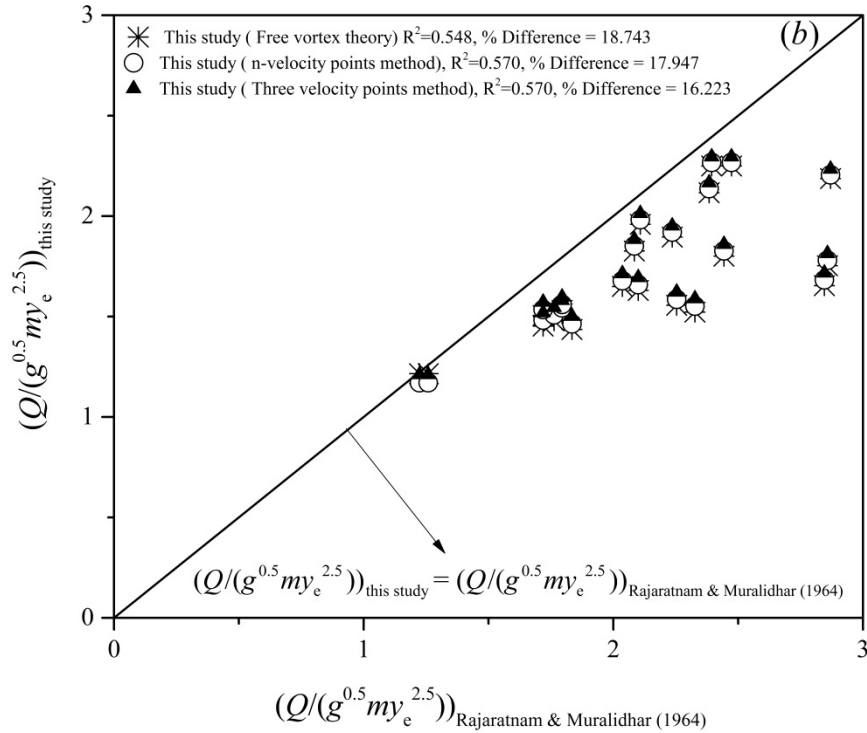


Figure 5.6: Comparison between the experimentally determined non-dimensional discharge values with the computed non-dimensional discharge values of the two suggested approaches and the free vortex theory for (a) rectangular; and (b) triangular channel cross-sections

5.3 Generalized Trapezoidal Channel Cross-sections

5.3.1 EDR for Sub-critical Flow Regimes

As previously stated, in sub-critical flow regimes the EDR is the ratio between the end depth ' y_e ' and the upstream critical depth ' y_c '. Hence, by measuring the end depth, the discharge ' Q ' value can be computed, since there is a unique relationship between the critical depth and the discharge value based on Froude number at that critical depth ' Fr_c '.

5.3.1.1 EDR of Trapezoidal Channel Cross-sections

By substituting $Fr_n = Fr_c = 1$ and $N_n = N_c$ into Eqs. (4.9), (4.37) and (4.43) separately, the EDR equations of the generalized trapezoidal channel cross-sections for sub-critical flow regimes other than the two proposed methods (the three velocity

points Eq. (5.15) and the infinite number velocity points Eq. (5.18)), the energy method Eq. (5.13) is also computed (since this approach was not applied in earlier studies for this cross-section type, so as to strengthen the above mentioned two proposed methods) are generated:

$$\frac{2}{3}\text{EDR} + \frac{(1 + (-1)^{n_5} N_c)^3}{(2 + 4(-1)^{n_5} N_c)(\text{EDR} + (-1)^{n_5} N_c \text{EDR}^2)^2} - \frac{(1 + (-1)^{n_5} N_c)^2}{(2 + 4(-1)^{n_5} N_c)} - 1 = 0 \quad (5.13)$$

where

$$\text{EDR} = \frac{y_e}{y_c} = \frac{N_e}{N_c}; N_e = \frac{\eta_4 y_e}{\eta_3}; N_c = \frac{\eta_4 y_c}{\eta_3} \quad (5.14)$$

$$f_1(N_c) + f_2(N_c) - 36 \left[N_c^2 \text{EDR}^2 + 2(-1)^{n_5} N_c \text{EDR} + 1 \right] * \frac{\left[1 + (-1)^{n_5} N_c \right]^{1.5}}{\left[0.5 + (-1)^{n_5} N_c \right]^{0.5}} = 0 \quad (5.15)$$

where

$$f_1(N_c) = \left[20(-1)^{n_5} N_c^3 \text{EDR}^4 + 60N_c^2 \text{EDR}^3 + 57(-1)^{n_5} N_c \text{EDR}^2 + 18\text{EDR} \right] \cdot \left[\sqrt{\frac{(1 + (-1)^{n_5} N_c)}{2 + 4(-1)^{n_5} N_c}} + \sqrt{\frac{(1 + (-1)^{n_5} N_c)}{2 + 4(-1)^{n_5} N_c} + \frac{3 + 2(-1)^{n_5} N_c}{6 + 6(-1)^{n_5} N_c}} \right] \quad (5.16)$$

$$f_2(N_c) = \left[16(-1)^{n_5} N_c^3 \text{EDR}^4 + 48N_c^2 \text{EDR}^3 + 51(-1)^{n_5} N_c \text{EDR}^2 + 18\text{EDR} \right] \cdot \left[\sqrt{1 + \frac{(1 + (-1)^{n_5} N_c)}{2 + 4(-1)^{n_5} N_c}} + \sqrt{\frac{(1 + (-1)^{n_5} N_c)}{2 + 4(-1)^{n_5} N_c} + \frac{3 + 2(-1)^{n_5} N_c}{6 + 6(-1)^{n_5} N_c}} \right] \quad (5.17)$$

$$\sum_{i=1}^{np-1} \left[\left(\sqrt{\frac{(1+(-1)^{\eta_5} N_c)}{(2+4(-1)^{\eta_5} N_c)} + \frac{i-1}{np-1}} + \sqrt{\frac{(1+(-1)^{\eta_5} N_c)}{(2+4(-1)^{\eta_5} N_c)} + \frac{i}{np-1}} \right) \cdot \left(\frac{\text{EDR}}{np-1} + (-1)^{\eta_5} \frac{N_c \text{EDR}^2 (2n-2i-1)}{(np-1)^2} \right) \right] - \frac{\sqrt{2}(1+(-1)^{\eta_5} N_c)^{1.5}}{(1+2(-1)^{\eta_5} N_c)^{0.5}} = 0 \quad (5.18)$$

Since the equations defining the generalized trapezoidal channel cross-sections for the energy, the three velocity points and the infinite number velocity points methods (Eq. (5.13), Eq. (5.15), and Eq. (5.18) respectively) are revealing no single representative EDR value, unlike to the rectangular, the parabolic and the triangular channel cross-sections, other than the flow depth at the brink section ' y_e ', the channels side slopes ratio (m) and the channels bed width (B) were also introduced as dependent (influencing) parameters so as to achieve a group of mathematical solutions. Using these effective channel parameters (y_e , m , and B), a comparison of the computed EDR values of the theoretical studies of Murty Bhallamudi (1994), Beirami et al. (2006), and Vatankhah (2013) and the experimental data sets of Diskin (1961), Keller and Fong (1989), and Pagliara and Viti (1995) were used by applying the appropriate values of η_3 , η_4 , and η_5 that are given in Table 4.2 and detailed in Figs. (5.7, 5.8a, and 5.8b).

As depicted in Fig. 5.7, comparison of the computed EDR values for this study with the above mentioned theoretical approaches revealed that, there is a close agreement with the theoretical study of Murty Bhallamudi (1994) and Beirami et al. (2006) since to some extent, the effects of the streamline curvature and the pressure coefficient at the end section were considered in these studies. The computed low correlation values (R^2) in the theoretical studies compared with the experimental data

set are probably due to the fluctuations of the measured data set as discussed earlier sections since, the studied cross-sectional shape characteristics at very low discharges are forming very shallow water depths and the formed wetted perimeter at different discharge values due to the inner wall roughness is effecting the measurements significantly.

Similar computations were carried out in order to check the accuracy of the computed EDR values of the two proposed methods (the three velocity points and the infinite number velocity points) and presented in Figs 5.8 (a) and (b) respectively. It is clearly observed that, there is a close agreement with the theoretical study of Vatankhah (2013), since to some extent; the application of the continuity equation is used in both studies. As the statistical measure indices indicates, the slight deviations of the EDR values computed by Murty Bhallamudi (1994) and Beirami et al. (2006) are probability due to the effects of the streamline curvature and the assumed negligible effect of the pressure coefficient at the end section.

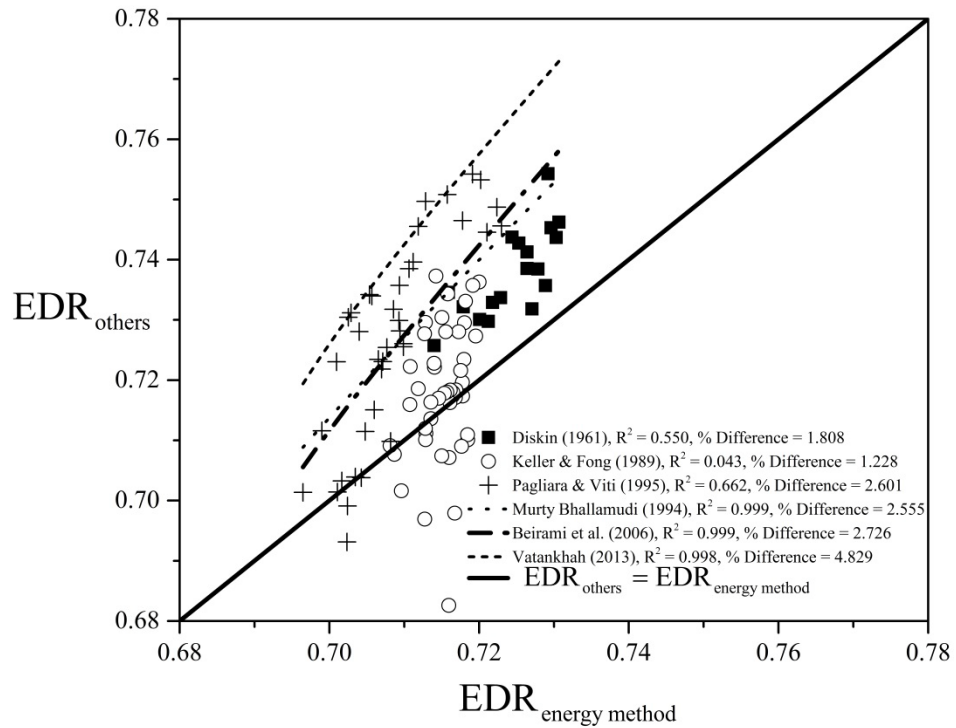
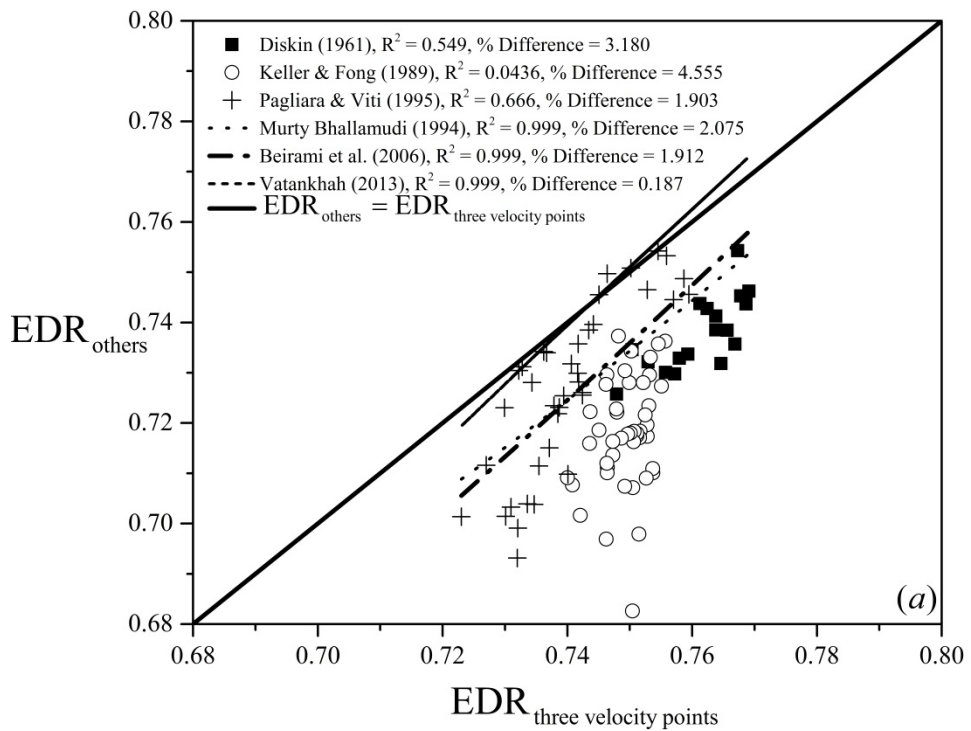


Figure 5.7: Comparison between the relevant theoretical and experimental EDR results of the previous studies and the computed EDR results of the energy method of the trapezoidal channel cross-section with symmetric sides at sub-critical flow regime



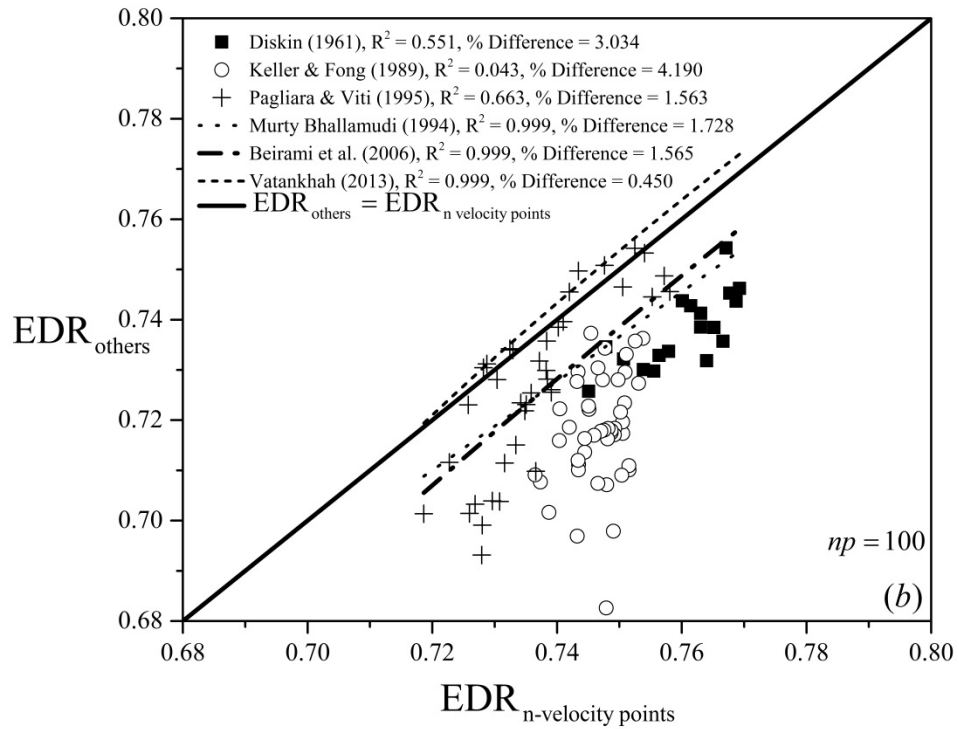


Figure 5.8: Comparison between the relevant theoretical and experimental EDR results of the previous studies and the computed EDR results of the (a) three velocity points method; and (b) infinite number velocity points method of the trapezoidal channel cross-section with symmetric sides at sub-critical flow regime

5.3.1.2 EDR of Inverted Triangular Channel Cross-sections

Due to the similar reason as discussed for the trapezoidal channel cross-section case, for the inverted-triangular (Δ -shaped) channel cross-section, the effective channel parameters (y_e , m , and B) were introduced so as to compute the EDR values based on three different theoretical methods. For their comparisons, the experimental study of Dey and Ravi Kumar (2002) and the theoretical study of Beirami et al. (2006) based on the free vortex theory were used and are tabulated in Table 5.2. As can be seen, the computed EDR values of the suggested methods are in well agreement with the observed data set of Dey and Ravi Kumar (2002) and the theoretical study of Beirami et al. (2006).

Table 5.2: Comparison between the computed EDR values of the different suggested methods of this study with the observed data of Dey and Ravi Kumar (2002) and the theoretical study by Beirami et al. (2006)

B (m)	m	y_e (m)	EDR _{obs} (Dey & Ravi Kumar)	EDR _{com} (Beirami et al.)	EDR (3 v p)	EDR (n-v p)	EDR (energy)
0.18	0.57735	0.073952	0.7112	0.6903	0.7040	0.7024	0.7050
0.18	0.57735	0.070242	0.7195	0.6879	0.7025	0.7007	0.7012
0.18	0.57735	0.065035	0.7053	0.6858	0.7014	0.6992	0.6971
0.18	0.57735	0.060889	0.6892	0.6849	0.7012	0.6986	0.6946
0.18	0.57735	0.056118	0.7155	0.6846	0.7015	0.6986	0.6925
0.18	0.57735	0.053437	0.6812	0.6847	0.7019	0.6988	0.6916
0.18	0.57735	0.048153	0.7051	0.6853	0.7030	0.6996	0.6904
0.18	0.57735	0.044256	0.7011	0.6861	0.7040	0.7004	0.6899
0.18	0.57735	0.039657	0.6832	0.6873	0.7054	0.7016	0.6896
0.18	0.57735	0.037677	0.6999	0.6879	0.7060	0.7022	0.6895
0.18	0.57735	0.035417	0.7041	0.6886	0.7069	0.7028	0.6895
0.18	0.57735	0.033422	0.6855	0.6892	0.7075	0.7034	0.6896
0.18	0.57735	0.031083	0.6921	0.6900	0.7083	0.7042	0.6897
0.18	0.57735	0.027888	0.6991	0.6911	0.7094	0.7052	0.6900
0.18	0.57735	0.024334	0.7122	0.6924	0.7107	0.7064	0.6904
0.18	0.57735	0.021481	0.6961	0.6934	0.7117	0.7074	0.6908
0.18	0.57735	0.019314	0.6988	0.6942	0.7125	0.7082	0.6910
0.18	0.57735	0.015853	0.7012	0.6956	0.7137	0.7094	0.6915
0.18	0.57735	0.012206	0.7057	0.6969	0.7150	0.7107	0.6921
0.18	0.57735	0.008745	0.6911	0.6983	0.7163	0.7119	0.6927
0.12	0.57735	0.052824	0.6922	0.6951	0.7074	0.7062	0.7115
0.12	0.57735	0.050226	0.7057	0.6914	0.7047	0.7033	0.7065
0.12	0.57735	0.045207	0.6878	0.6867	0.7019	0.6998	0.6992
0.12	0.57735	0.044167	0.7191	0.6861	0.7016	0.6994	0.6980
0.12	0.57735	0.042432	0.6927	0.6854	0.7013	0.6989	0.6962
0.12	0.57735	0.041393	0.6971	0.6851	0.7012	0.6987	0.6953
0.12	0.57735	0.039491	0.7019	0.6847	0.7013	0.6986	0.6938
0.12	0.57735	0.037236	0.7123	0.6846	0.7016	0.6986	0.6924
0.12	0.57735	0.035677	0.6811	0.6846	0.7019	0.6988	0.6916
0.12	0.57735	0.033339	0.7181	0.6850	0.7026	0.6993	0.6907
0.12	0.57735	0.03126	0.6821	0.6855	0.7033	0.6999	0.6902
0.12	0.57735	0.029098	0.7044	0.6862	0.7042	0.7006	0.6898
0.12	0.57735	0.027623	0.7163	0.6868	0.7049	0.7011	0.6896
0.12	0.57735	0.025025	0.7011	0.6879	0.7061	0.7022	0.6895
0.12	0.57735	0.023123	0.6921	0.6888	0.7070	0.7031	0.6896
0.12	0.57735	0.021221	0.7151	0.6898	0.7080	0.7039	0.6897
0.12	0.57735	0.018363	0.6824	0.6912	0.7095	0.70534	0.6900
0.12	0.57735	0.016285	0.7052	0.6923	0.7106	0.7064	0.6903
0.12	0.57735	0.013946	0.6911	0.6936	0.7119	0.7076	0.6908

5.3.1.3 EDR of Semi-trapezoidal and Semi-inverted Triangular Channel Cross-sections

Since no earlier experimental data are available in the literature, the generated relevant theoretical equations for these cross-sections were not validated.

5.3.2 EDD for Sub-critical Flow Regimes

The discharge ' Q ' relationship of the generalized trapezoidal channel cross-section based on the definition of the normal (uniform) flow depth of the Froude number (Fr_n) for both sub- and super critical flow regimes can be written as:

$$Q = \frac{g^{0.5} [\eta_3 y_n + (-1)^{\eta_5} \eta_4 y_n^2]^{1.5}}{[\eta_3 + 2(-1)^{\eta_5} \eta_4 y_n]^{0.5}} Fr_n \quad (5.19)$$

By substituting $Fr_n = Fr_c = 1$ and $y_n = y_c$ into Eq. (5.19), the discharge can be computed for sub-critical flow regimes as:

$$Q = \frac{g^{0.5} [\eta_3 y_c + (-1)^{\eta_5} \eta_4 y_c^2]^{1.5}}{[\eta_3 + 2(-1)^{\eta_5} \eta_4 y_c]^{0.5}} \quad (5.20)$$

To estimate the discharge ' Q ' from the known end depth, the direct discharge equations in terms of the end depth values were proposed for the flows at sub-critical regimes. To have common parameters for comparison; due to different ' B ' and ' m ' values; after the determination of the upstream critical depth (y_c), a general dimensionless discharge (Q^*) value was obtained by substituting $N_c = \eta_4 y_c / \eta_3$ into Eq. (5.20) that yields:

$$Q^* = \frac{Q \eta_4^{1.5}}{g^{0.5} \eta_3^{2.5}} = \frac{\left[N_c + (-1)^{\eta_5} N_c^2 \right]^{1.5}}{\left[1 + 2(-1)^{\eta_5} N_c \right]^{0.5}} \quad (5.21)$$

Since in most of the practical problems, the end depth is known and it is desirable to compute the discharge directly with respect to this end depth, $N_c = N_e/EDR$ was inserted to Eq. (5.21) so as to generate a dimensionless discharge value (Q^*) in terms of N_e :

$$Q^* = \frac{\left[\left(\frac{N_e}{EDR} \right) + (-1)^{\eta_5} \left(\frac{N_e}{EDR} \right)^2 \right]^{1.5}}{\left[1 + 2(-1)^{\eta_5} \left(\frac{N_e}{EDR} \right) \right]^{0.5}} \quad (5.22)$$

5.3.2.1 EDD of Trapezoidal Channel Cross-sections

Inserting the calculated EDR Eq. (5.13) into Eq. (5.22) for $\eta_3=B$, $\eta_4=m$ and $\eta_5=0$, the EDD relationship was obtained for the trapezoidal channel cross-sections with symmetric sides at sub-critical regime based on the energy method. Using the non-dimensional discharge values $Q^* = Qm^{1.5}/(g^{0.5}B^{2.5})$, the theoretical results obtained from the energy method and the experimental data sets of Diskin (1961), Keller and Fong (1989), and Pagliara and Viti (1995) and the theoretical studies of Murty Bhallamudi (1994), Beirami et al. (2006), and Vatankhah (2013) for the trapezoidal channels with symmetric sides were compared with the two statistical measuring indices (MARE and R) as detailed graphically in Fig. 5.9. It is clearly observed that, there is a high correlation among these studies.

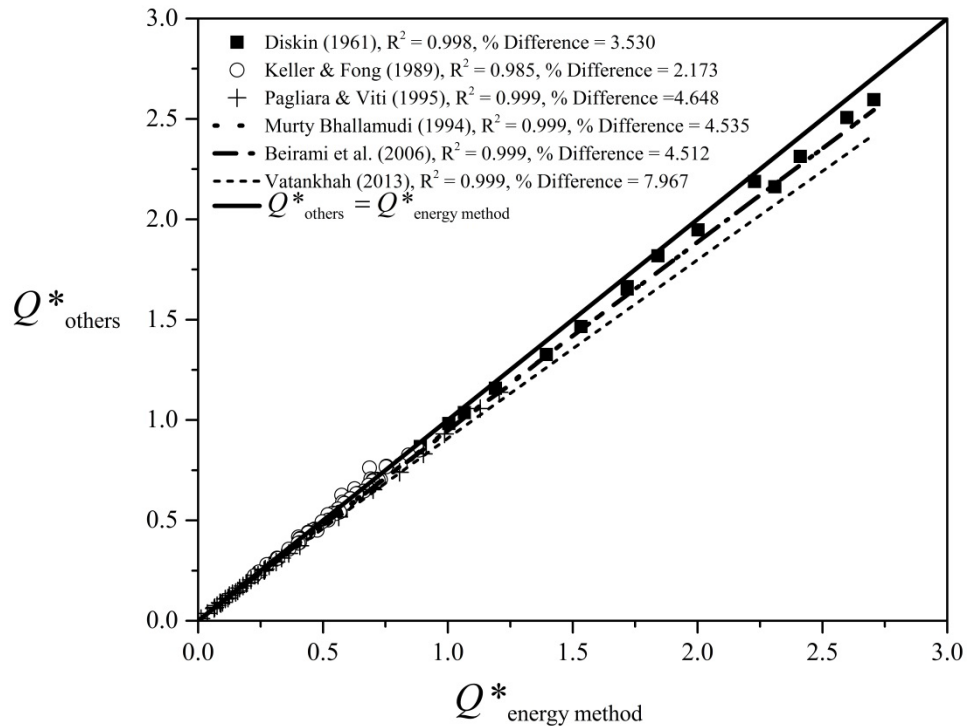


Figure 5.9: Comparison between the non-dimensional discharge (Q^*) values obtained from the energy method and the other relevant theoretical and experimental results for the trapezoidal channel cross-section with symmetric sides at sub-critical flow regimes

To assess the correctness of the three velocity points method and the infinite number velocity points methods of the predicted non-dimensional discharge (Q^*) values, Eqs. (5.15), (5.18), and (5.22) were used. Figures 5.10(a) and (b) are presenting the comparison of this non-dimensional discharge values in sub-critical flow regime for both the experimental data sets of Diskin (1961), Keller and Fong (1989), and Pagliara and Viti (1995) and the theoretical studies of Murty Bhallamudi (1994), Beirami et al. (2006), and Vatankhah (2013). Similarly, the same statistical measuring indices are used for their correctness evaluations and shown in Figures 5.10(a) and (b). It is also observed that, there exists a close agreement between the computed non-dimensional discharge (Q^*) values and the other theoretical and experimental studies results for both proposed approaches.

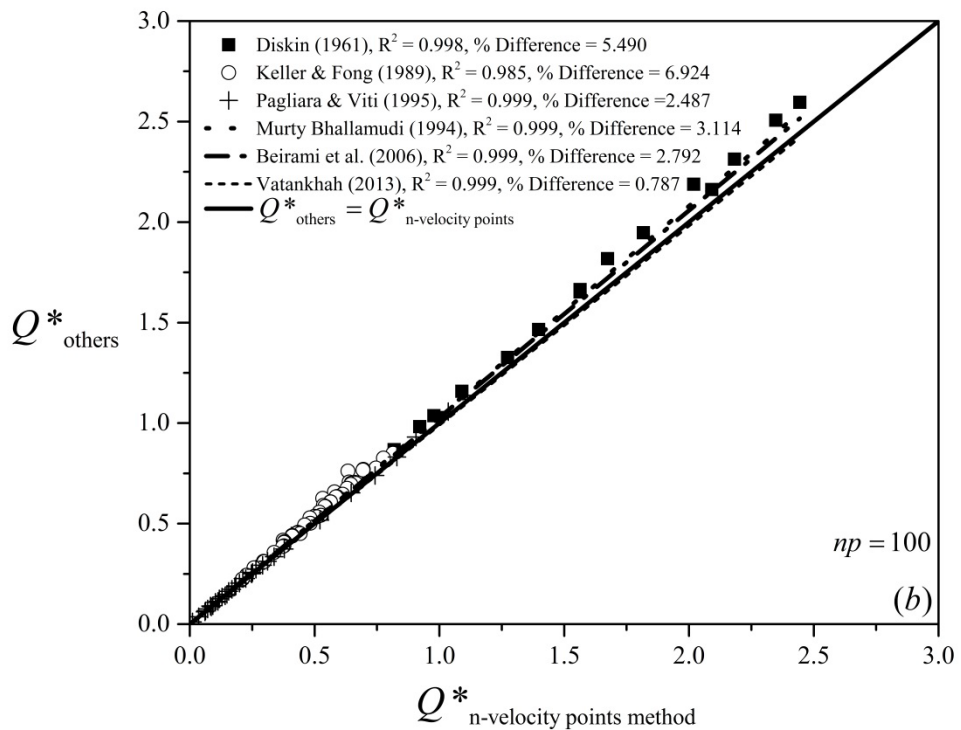
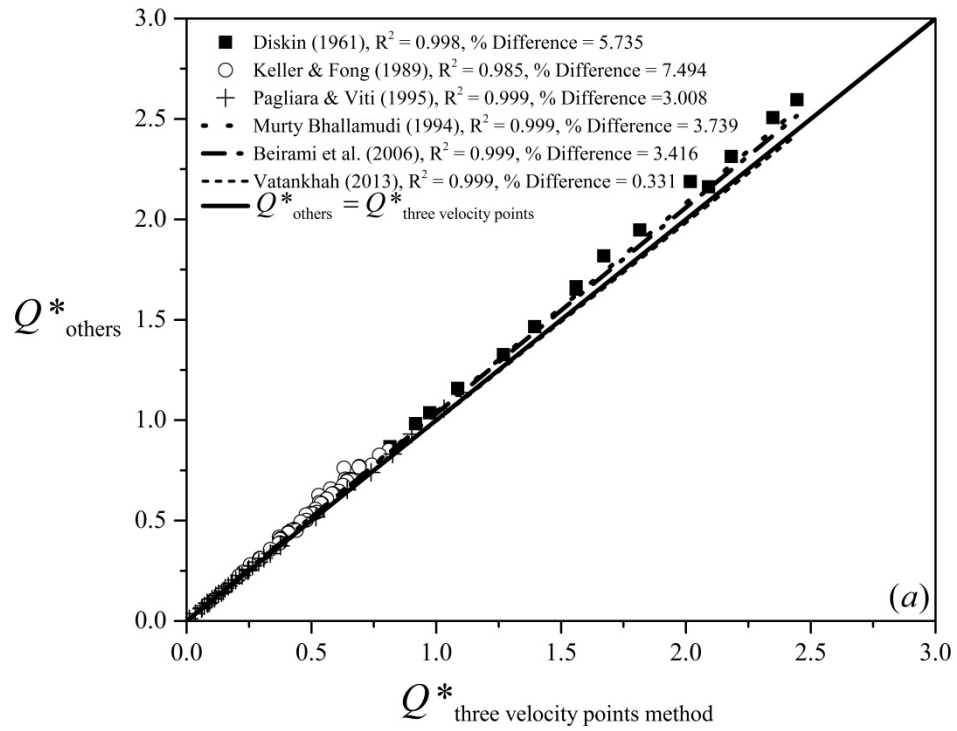
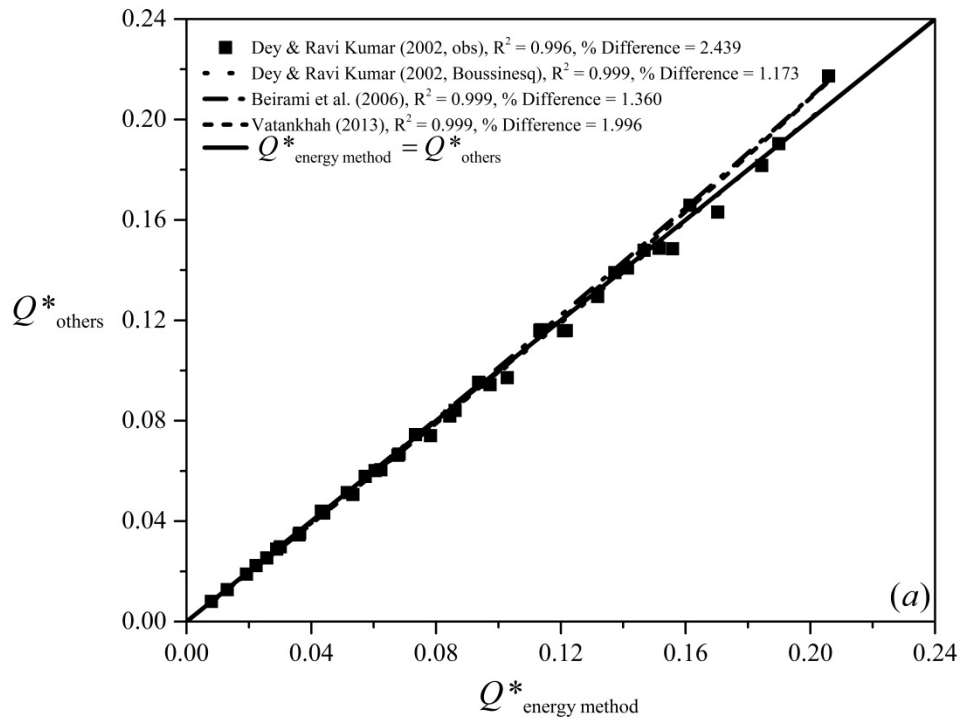


Figure 5.10: Comparison between the non-dimensional discharge (Q^*) values obtained based on the (a) three velocity points method; and (b) infinite number velocity points method and the other relevant theoretical and experimental results for the trapezoidal channel cross-sections with symmetric sides at sub-critical flow regimes

5.3.2.2 EDD of Inverted Triangular Channel Cross-sections

Inserting the calculated EDR of Eq. (5.13) into Eq. (5.22) for $\eta_3=B$, $\eta_4=m$ and $\eta_5=1$, EDD relationship was obtained for the inverted triangular channel cross-sections with symmetric sides at sub-critical regime based on the energy method, the three velocity points method, and the infinite number velocity points method. For on the non-dimensional discharge (Q^*) values $Q^*= Qm^{1.5}/(g^{0.5}B^{2.5})$, the theoretical results of the above mentioned approaches and the relevant experimental data sets of Dey and Ravi Kumar (2002) and the thoretical studies of Murty Bhallamudi (1994), Beirami et al. (2006), and Vatankhah (2013) were used to investigate the accuracy with the same statistical measuring indices as detailed earlier and presented in Figures 5.11 (a), (b), and (c). The proposed methods results are showing very small deviations with the other theoretical and experimental findings.



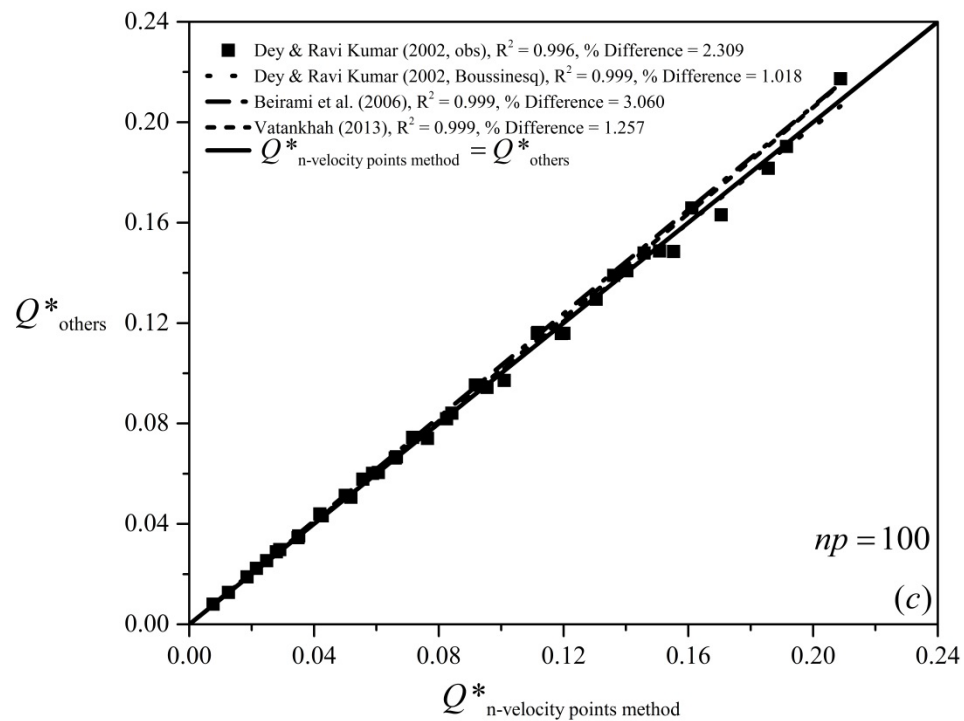
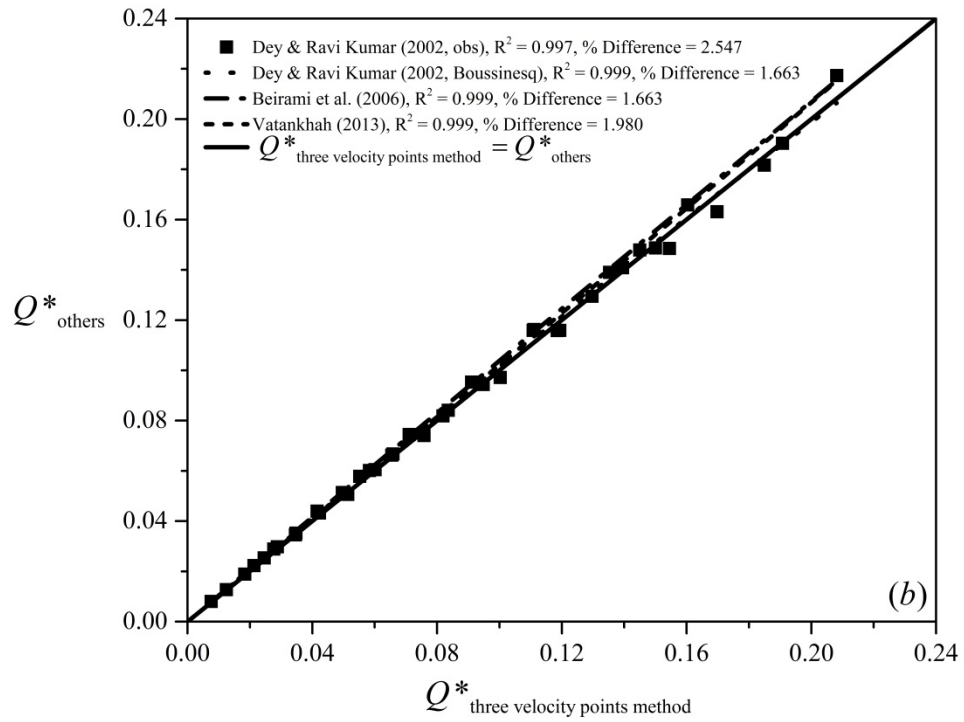


Figure 5.11: Comparison between the non-dimensional discharge (Q^*) values with (a) the energy method; (b) the three velocity points method; and (c) the infinite number velocity points and the other relevant theoretical and experimental results for the inverted-triangular channel cross-sections at sub-critical flow regimes

5.3.2.3 EDD of Semi-trapezoidal and Semi-inverted Triangular Channel Cross-sections

Since no earlier experimental data are available in the literature, the generated relevant theoretical equations for these cross-sections were not validated.

5.3.3 EDR for Super Critical Flow Regimes

As previously stated, in super critical flow regimes, the normal depth is always less than the critical depth, and the critical section never exists within this reach (upstream of the end section). Therefore, to express a relationship for the flow depth at the end section (y_e), the upstream Froude number (Fr_n), which is a function of the channel bed slope (S), must be used.

The ratio between the flow depth at the end section (y_e) and the critical depth (y_c) is defined as:

$$\varepsilon_e = \frac{y_e}{y_c} = \frac{N_e}{N_c} \quad (5.23)$$

Dividing the upstream Froude number (Fr_n) of Eq. (3.14) by the critical Froude number ($Fr_c = 1$) gives the following ratio:

$$Fr_n = \left(\frac{1 + 2N_n}{1 + 2N_c} \right)^{1/2} \left(\frac{N_c + N_c^2}{N_n + N_n^2} \right)^{3/2} \quad (5.24)$$

Substituting the upstream Froude number (Fr_n) from Eq. (3.14) into Manning's equation and then dividing by the critical Froude number ($Fr_c = 1$) yields:

$$Fr_n = \left(\frac{S}{S_c} \right)^{1/2} \left(\frac{1+2N_n}{1+2N_c} \right)^{1/2} \left(\frac{N_n + N_n^2}{N_c + N_c^2} \right)^{1/6} \left[\frac{1+2N_n\sqrt{1+m^2}}{1+2N_c\sqrt{1+m^2}} \right]^{2/3} \quad (5.25)$$

Equating Eqs. (5.24), and (5.25) yields the relative slope (\tilde{S}):

$$\tilde{S} = \frac{S}{S_c} = \left(\frac{X_c + X_c^2}{X_n + X_n^2} \right)^{10/3} \left[\frac{1+2X_n\sqrt{1+m^2}}{1+2X_c\sqrt{1+m^2}} \right]^{4/3} \quad (5.26)$$

5.3.3.1 EDR of Trapezoidal Channel Cross-sections

To evaluate N_n for the given values of N_c and \tilde{S} , Eq. (5.26) is solved numerically and Fr_n is calculated from Eq. (5.24). Then, a numerical method is used to compute N_e separately from Eq. (4.9) for the energy method (since this approach was not available in the literature for these cross-sections), from Eq. (4.17) for the free vortex theory (since this approach was not available in the literature for these cross-sections), from Eq. (4.37) for the three velocity points method, and from Eq. (4.39) for the infinite number velocity points method. Subsequently, the ratio between the flow depth at end section and the critical depth (ε_e) is obtained by inserting Eq. (5.23) to each method. The theoretical studies of Murty Bhallamudi (1994) and the sharp-crested weir theory are graphically compared with the predicted values of ε_e . Variations in ε_e with respect to the relative slope (\tilde{S}) for different values of N_c is presented in Figs. 5.12 (a) and (b). As a general trend, it is clearly observed that, as the relative slope (\tilde{S}) increases, the magnitude of the ε_e decreases. Also as can be seen from Fig. 5.12 (a), a close agreement with Murty Bhallamudi (1994) was observed for the energy method and the free vortex theory since, somehow, the streamline curvature and the end pressure effects were considered while deriving

these studies. Also, the statistical measuring indices are showing that, the computed curves based on the three velocity points method and the infinite number velocity points method are agreeing well with the sharp-crested weir theory, since to some extent, the continuity equation is used in these all studies as given in Fig. 5.12 (b).

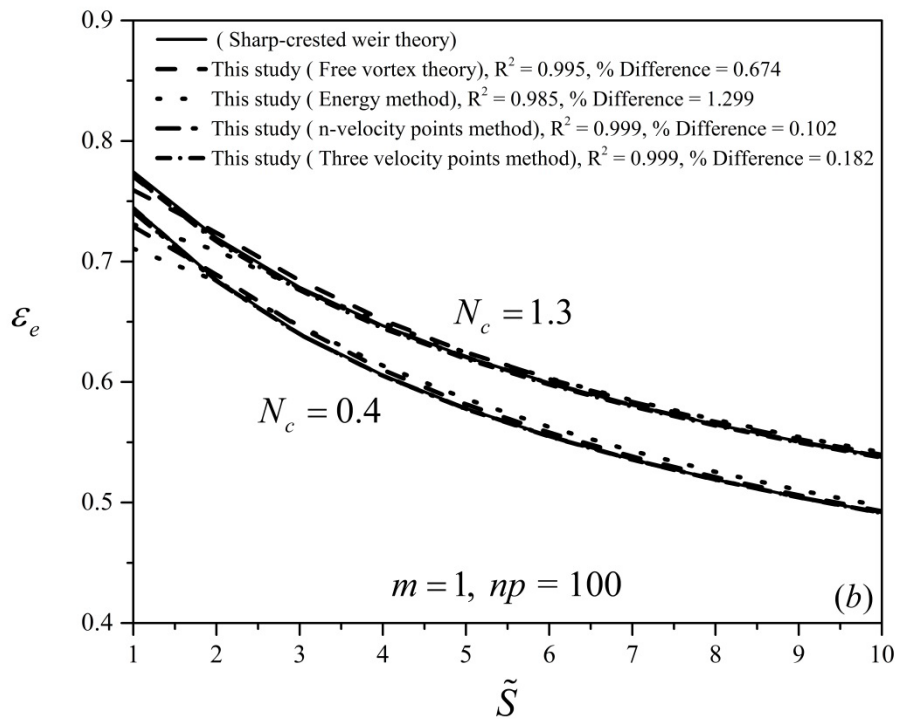
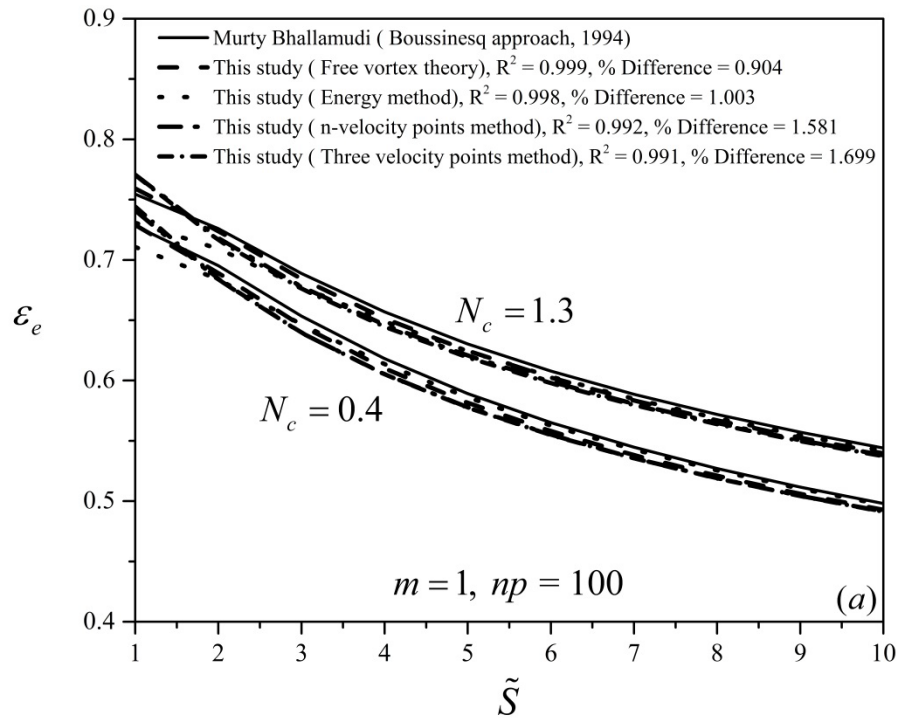


Figure 5.12: Comparison between the ε_e values obtained based on four theoretical methods and the ε_e values of the (a) Boussinesq approach by Murty Bhallamudi (1994); and (b) sharp-crested weir theory for the trapezoidal channel cross-sections at supercritical regimes

Similar comparisons are made with the relevant experimental data sets of Pagliara and Viti (1995) and shown in Fig. 5.13. The results obtained by four of the theoretical methods are varying slightly from the observations of the data of Pagliara and Viti (1995). This discrepancy is probably due to the effect of the streamline curvature that was not encountered while deriving in relevant theories. Furthermore, a comparison of the computed EDR values of the suggested four methods with the theoretical studies of Murty Bhallamudi (1994) and the sharp-crested weir theory in the range of data sets of Pagliara and Viti (1995) are also presented in Figs. 5.14 (a) and (b), respectively. Good agreements can be seen based on the earlier mentioned statistical measuring indices.

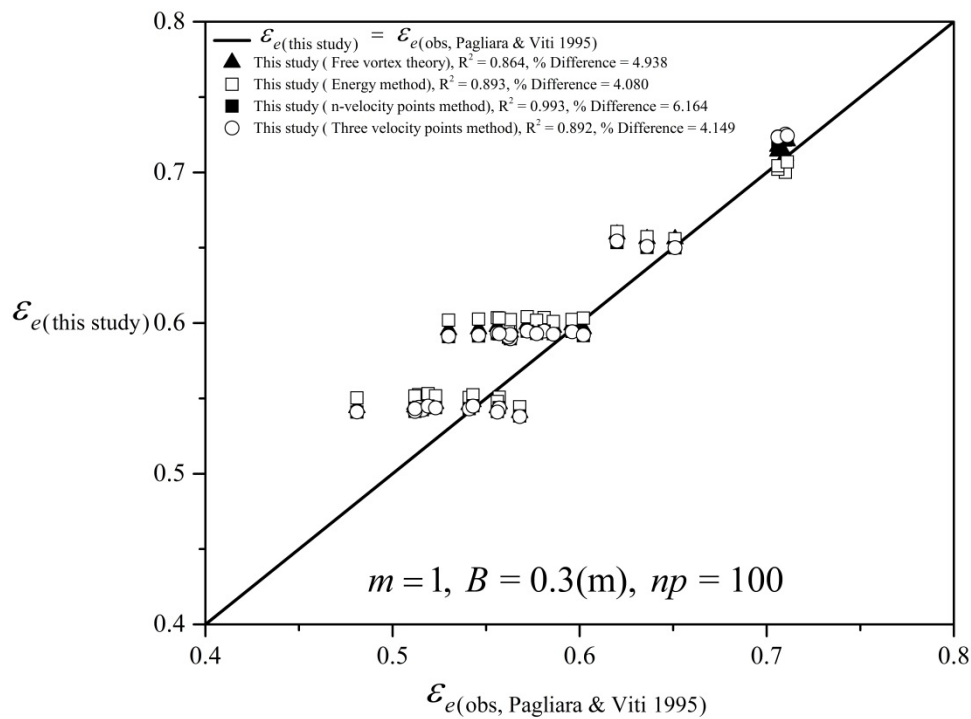


Figure 5.13: Comparison between \mathcal{E}_e values based on four suggested methods and \mathcal{E}_e values based on the experimental data sets of Pagliara and Viti (1995) in trapezoidal channel cross-sections at super critical flow regimes

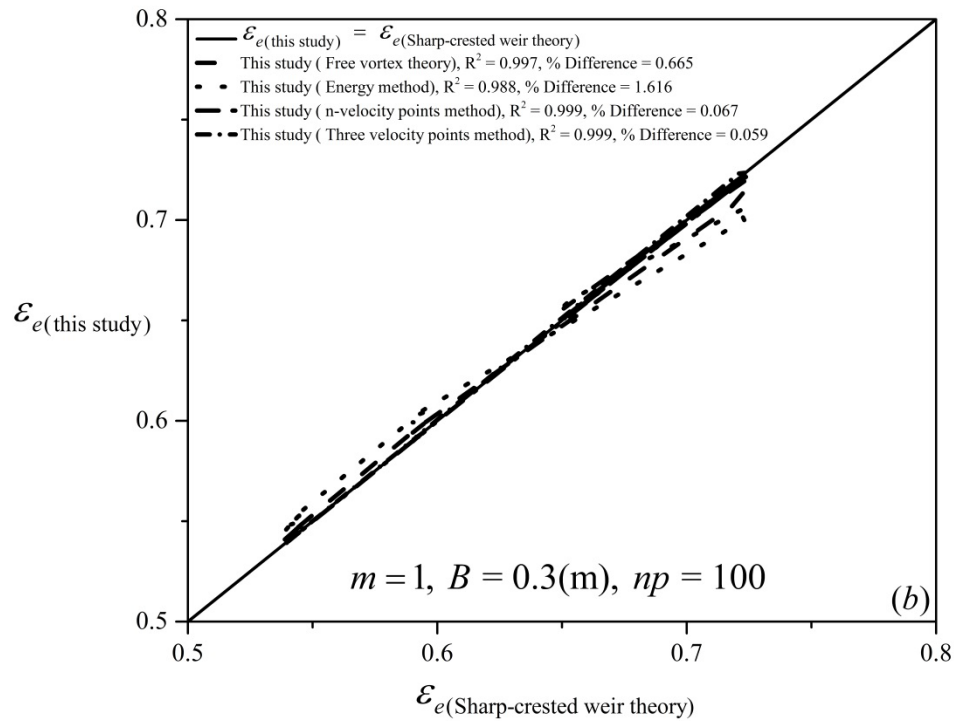
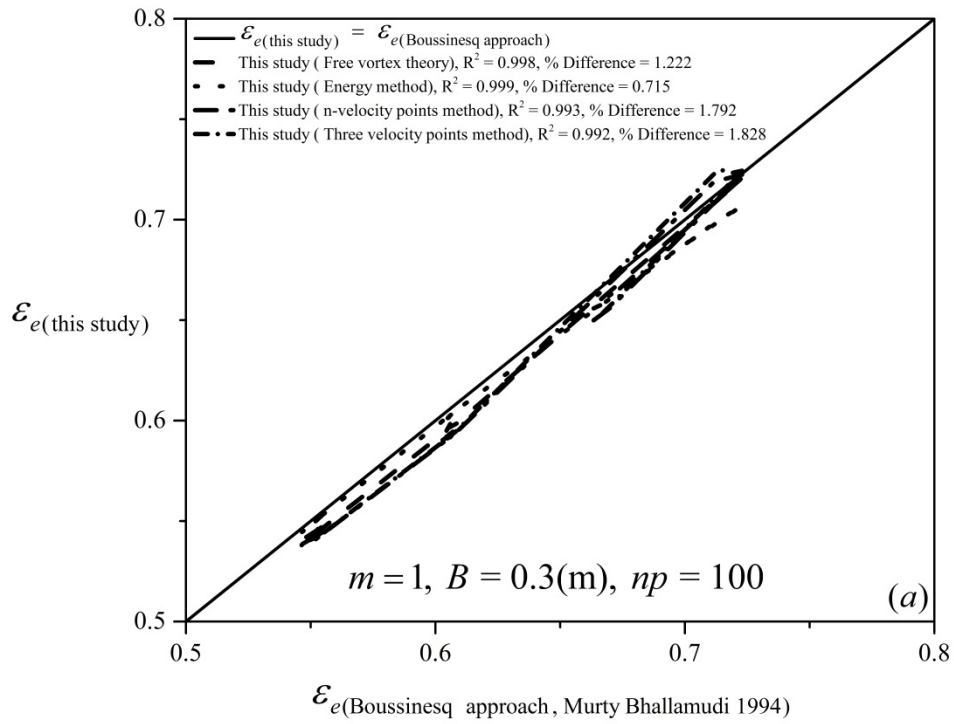
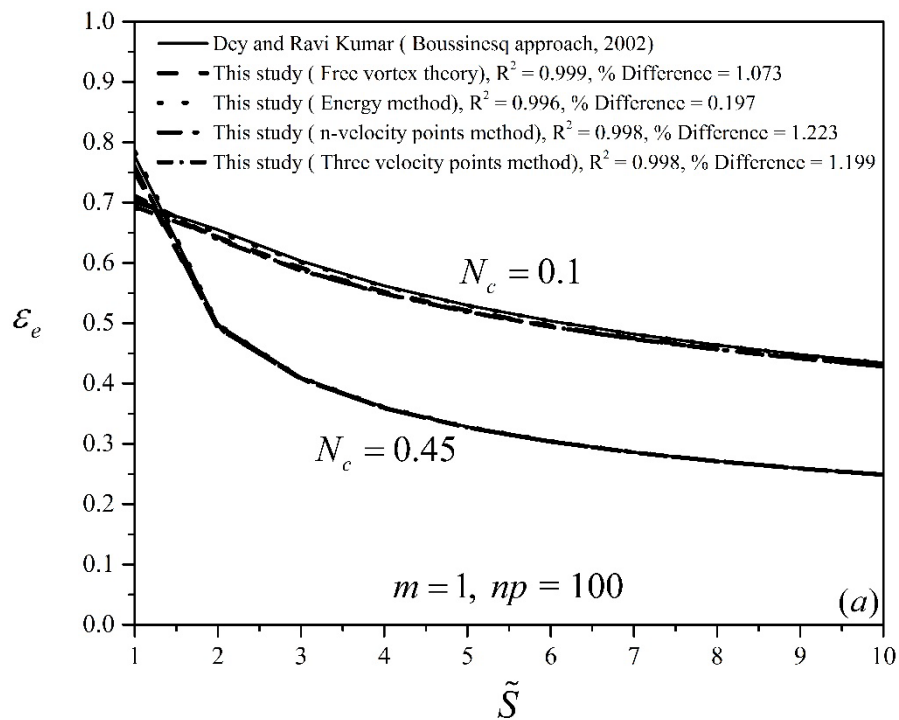


Figure 5.14: Comparison between ε_e values based on four suggested methods and ε_e values obtained based on the theoretical study (a) of Murty Bhallamudi (1994); and (b) the sharp-crested weir theory in trapezoidal channel cross-sections in super critical regimes

5.3.3.2 EDR of Inverted Triangular Channel Cross-sections

In a similar way for the inverted triangular channel cross-sections, the ratio between the flow depth at end section and the critical depth (ε_e) is obtained using Eq. (5.23) for the four suggested methods. Variation of ε_e with respect to the relative slope (\tilde{S}) for different values of N_c is presented in Figs. 5.15(a) and (b). As a general trend, it is easily observed that, as the relative slope (\tilde{S}) increases, the magnitude of the ε_e decreases. Since no experimental data sets are available in the literature for this channel cross-section, the theoretical study of Dey and Ravi Kumar (2002) are generated and graphically compared with the predicted values of ε_e and presented in Figs. 5.15 (a) and (b). Based on the statistical measuring indices, there exists close agreements with both of the theoretical studies of Dey and Ravi Kumar (2002).



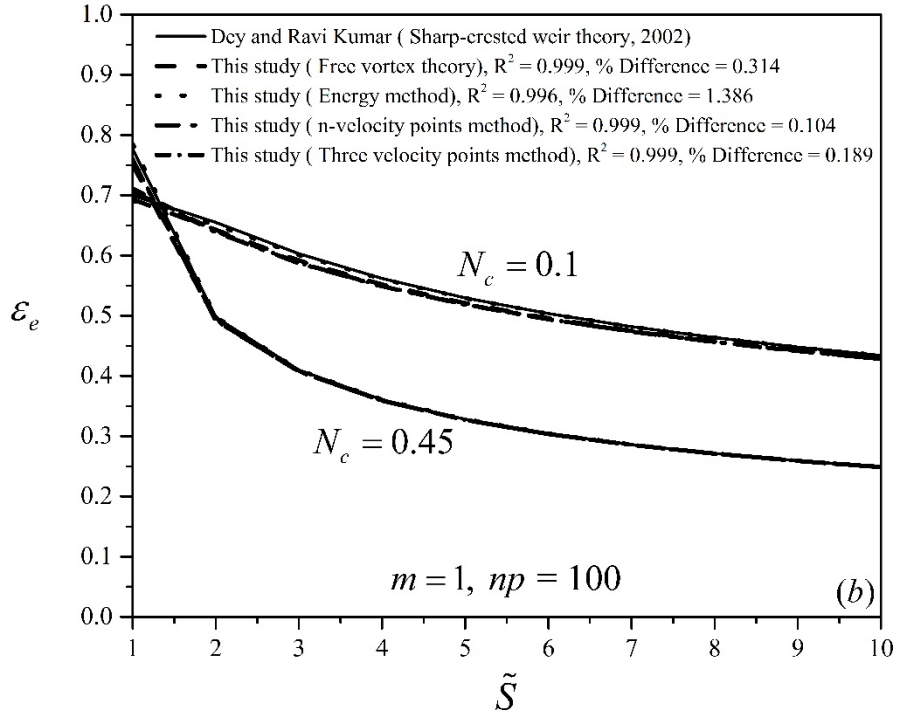


Figure 5.15: Comparison between ε_e and \tilde{S} values based on the suggested four methods for the range of $0.1 \leq N_c \leq 0.45$ and $m = 1$ with the (a) Boussinesq approach by Dey and Ravi Kumar (2002); and (b) sharp-crested weir theory by Dey and Ravi Kumar (2002) for inverted triangular channel cross-sections in super critical flow regimes

5.3.3.3 EDR of Semi-trapezoidal and Semi-inverted Triangular Channel Cross-sections

Since no earlier experimental data are available in the literature, the generated relevant theoretical equations for these cross-sections were not validated.

5.3.4 EDD for Super Critical Flow Regime

The EDR values varying with respect to N_n for the generalized trapezoidal channel in both sub- and super critical flow regimes. By substituting $N_n = \eta_4 y_n / \eta_3$ and $N_n = N_e / EDR$ into Eq. (5.20), the dimensionless discharge (Q^*) in a generalized trapezoidal channel cross-section is determined.

$$Q^* = \frac{Q \eta_4^{1.5}}{g^{0.5} \eta_3^{2.5}} = \frac{(N_n + (-1)^{\eta_5} N_n^2)^{1.5} Fr_n}{(1 + 2(-1)^{\eta_5} N_n)^{0.5}} = \frac{\left[\frac{N_e}{EDR} + (-1)^{\eta_5} \left(\frac{N_e}{EDR} \right)^2 \right]^{1.5} Fr_n}{\left(1 + 2(-1)^{\eta_5} \frac{N_e}{EDR} \right)^{0.5}} \quad (5.27)$$

To evaluate N_n for the given values of N_e and \tilde{S} , Eq. (5.26) is solved numerically and Fr_n is calculated from Eq. (5.24). Then, a numerical method is used to compute N_e separately from Eq. (4.9) for the energy method, Eq. (4.17) for the free vortex theory, Eq. (4.37) for the three velocity points method, and Eq. (4.39) for the infinite number velocity points method.

5.3.4.1 EDD of Trapezoidal Channel Cross-sections

As expressed in Eq. (5.27), the discharge (Q) value is related to the end depth (y_e) and the upstream Froude number (Fr_n) in a super critical flow regime. Hence, an explicit solution of the discharge (Q) is not possible. To overcome this problem, Eqs. (4.9), (5.23), (5.25), and (5.26) for the energy method, Eqs. (4.17), (5.23), (5.25), and (5.26) for the free vortex theory, Eqs. (4.37), (5.23), (5.25), and (5.26) for the three velocity points method and Eqs. (4.39), (5.23), (5.25), and (5.26) for the infinite number velocity points method are solved simultaneously to evaluate Fr_n and N_n values for the given values of N_e and \tilde{S} . Then, Eq. (5.27) is used to compute the non-dimensional discharge (Q^*) values for each method, separately.

To evaluate the correctness of these four approaches graphically, a comparison between the computed values of Q^* and the relevant experimental results of Pagliara and Viti (1995) is used and presented in Fig. 5.16. The results indicate that, most of

the Q^* values predicted by these suggested approaches having a high correlation coefficient with the observed data sets of Pagliara and Viti (1995).

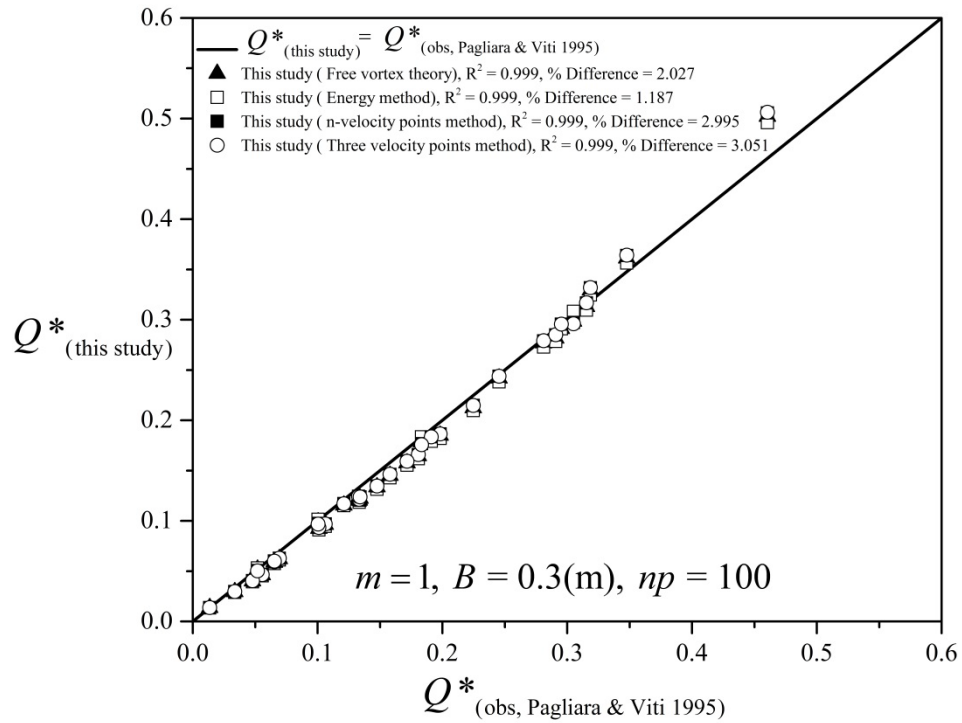


Figure 5.16: Comparison between the computed non-dimensional discharges (Q^*) of the proposed four methods and the experimental data sets of Q^* by Pagliara and Viti (1995) for the trapezoidal channel cross-sections at super critical flow regime

In order to check the correctness of the proposed methods of these methods, the computed discharge in the range of the experimental data sets of Pagliara and Viti (1995) and the theoretical study of Murty Bhallamudi (1994) based on Boussinesq approach were statistically studied and presented in Fig. 5.17 (a). To strengthen the results of these suggested methods, the sharp-crested weir theory was also applied for this cross-section (since this approach were not applied previously for this cross-section at super critical regime) and the generated relationship was also compared graphically with the relevant data sets as detailed in Fig. 5.17 (b). Figs. 5.17 (a) and

(b) indicating the correctness of the proposed methods with the other theoretical approaches based on the two statistical measuring indices (R^2 and MARE).

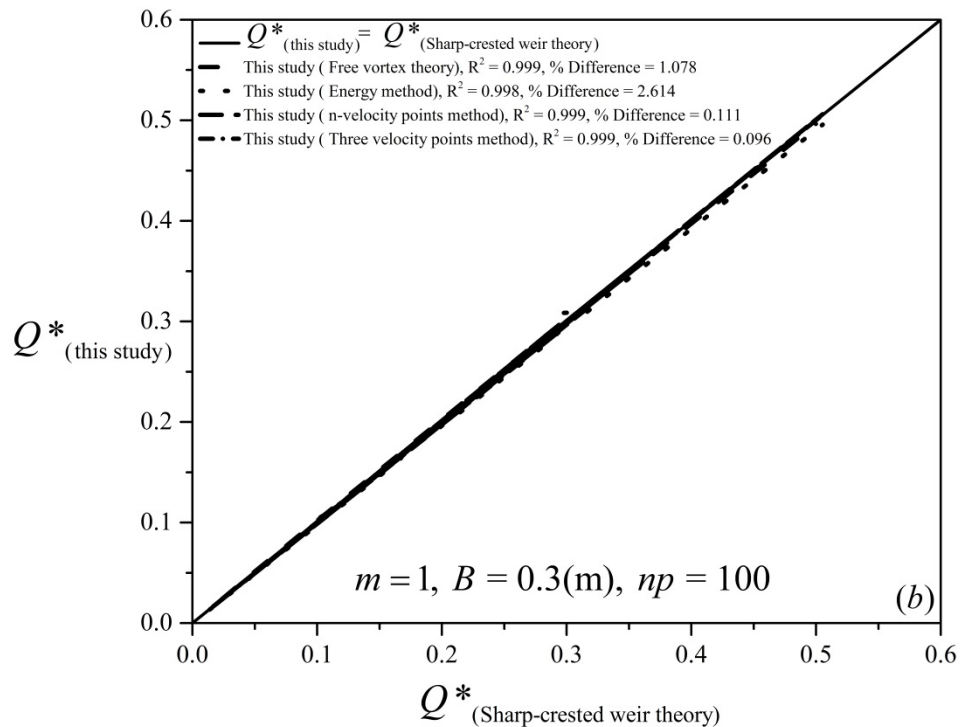
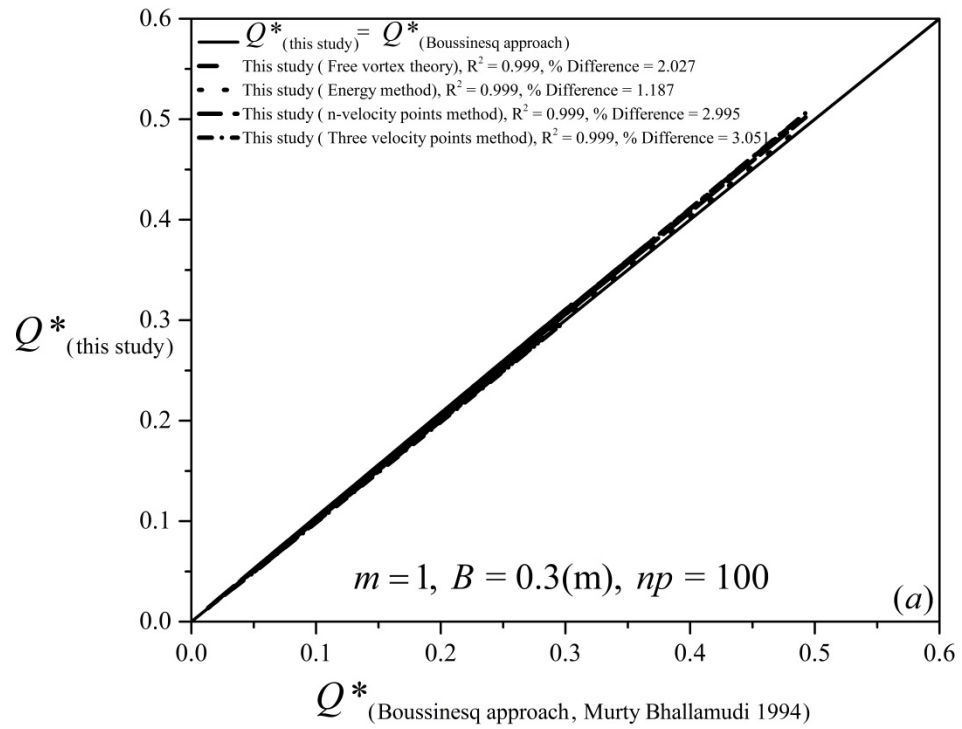


Figure 5.17: Comparison between the computed non-dimensional discharges (Q^*) of the suggested four methods and the theoretical Q^* results of the (a) Boussinesq approach of Murty Bhallamudi (1994); and (b) sharp-crested weir theory for the trapezoidal channel cross-sections at super critical flow regimes

5.3.4.2 EDD of Inverted Triangular, Semi-trapezoidal and Semi-inverted Triangular Channel Cross-sections

Since no earlier experimental data are available in the literature, the generated relevant theoretical equations for these cross-sections could not be validated.

5.4 Generalized Circular Channel Cross-sections with Flat-base

As discussed in Chapter 4, for the generalized circular channel cross-sections with flat base as the value of the height of the flat base (Z) changes, different types of circular channel cross-section with flat-base can be generated. In this study, the values of $\hat{Z} = Z/D$ are selected to be 0 (circular cross-section without a flat-base), 0.25, 0.33, 0.5 (inverted semi-circular cross-section), and 0.66. For comparison, experimental data sets of Sterling and Knight (2001) were gathered due to the personal communication with Dr. Mark Sterling which is acknowledged.

5.4.1 EDR for Sub-critical Flow Regimes

For the circular channel cross-sections also the EDR is the ratio between the end depth flow and the upstream critical depth for sub-critical regimes. Therefore, by substituting $Fr_n = Fr_c = 1$, $\hat{y}_n = \hat{y}_c$, $\hat{H}_n = \hat{H}_c$, and $\hat{I}_n = \hat{I}_c$ into Eqs. (4.12), (4.18), (4.40), and (4.44) separately, the EDR equations of the generalized circular channel cross-sections with flat base in sub-critical flow regimes based on the energy method (Eq. (5.28)), the free vortex theory (Eq. (5.29)), the three velocity points method (Eq. (5.32)), and the infinite number velocity points (Eq. (5.34)) were obtained.

$$\frac{2}{3} \text{EDR} + \frac{(\varphi(\hat{I}_c) - \varphi(\hat{Z}))^3}{16(\hat{I}_c - \hat{I}_c^2)^{0.5} (\varphi(\hat{I}_c) - \varphi(\hat{Z}))^2 \hat{y}_c} - \frac{(\varphi(\hat{I}_c) - \varphi(\hat{Z}))}{16(\hat{I}_c - \hat{I}_c^2) \hat{y}_c} - 1 = 0 \quad (5.28)$$

$$\begin{aligned}
& (\varphi(\hat{I}_c) - \varphi(\hat{Z}))\left(\hat{I}_c - \frac{1}{2}\right) - \frac{8}{3}\left((\hat{Z} - \hat{Z}^2)^{1.5} - (\hat{I}_c - \hat{I}_c^2)^{1.5}\right) - k_e(\varphi(\hat{I}_e) - \varphi(\hat{Z}))\left(\hat{I}_e - \frac{1}{2}\right) \\
& + \frac{8}{3}k_e\left((\hat{Z} - \hat{Z}^2)^{1.5} - (\hat{I}_e - \hat{I}_e^2)^{1.5}\right) - \frac{(\varphi(\hat{I}_c) - \varphi(\hat{Z}))^2}{8(\hat{I}_c - \hat{I}_c^2)^{0.5}} - \left(\frac{\varphi(\hat{I}_c) - \varphi(\hat{Z})}{\varphi(\hat{I}_e) - \varphi(\hat{Z})} - 1\right) = 0
\end{aligned} \tag{5.29}$$

where

$$k_e = 1 - \frac{4\hat{H}_c}{5\hat{y}_c} + \frac{8}{35}\left(\frac{\hat{H}_c}{\hat{y}_c}\right)^2 \left\{ 1 - \left[1 - \left(\frac{\hat{H}_c}{\hat{y}_c}\right)^{-1} \right]^{3.5} \right\} \tag{5.30}$$

$$\frac{\hat{H}_c}{\hat{y}_c} = 1 + \frac{(\varphi(\hat{I}_c) - \varphi(\hat{Z}))}{16(\hat{I}_c - \hat{I}_c^2)^{0.5}\hat{y}_c} \tag{5.31}$$

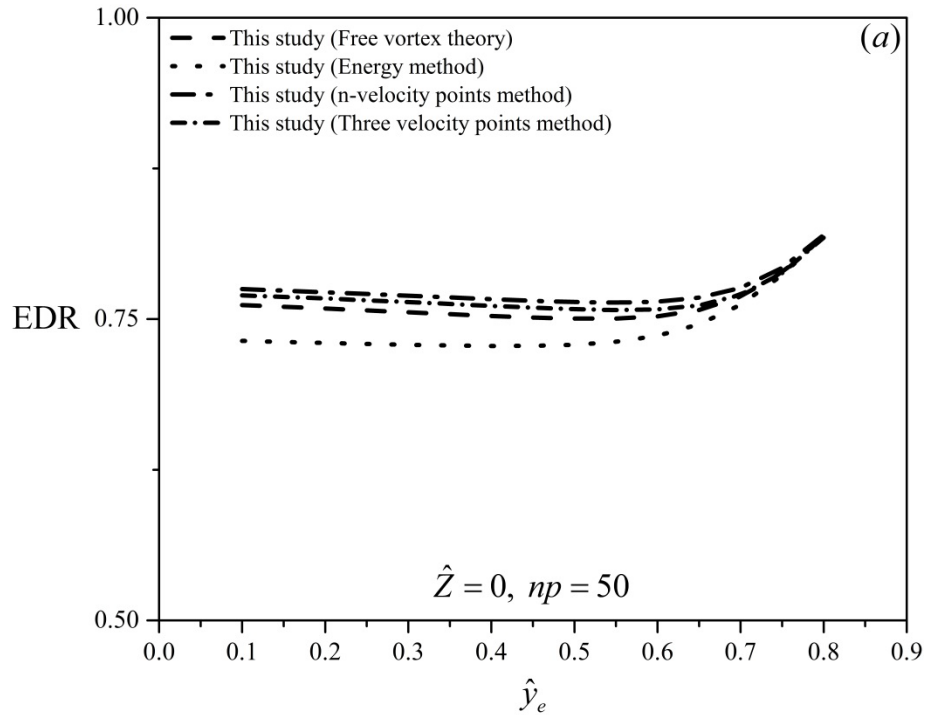
$$\begin{aligned}
& \left[\sqrt{\frac{(\varphi(\hat{I}_c) - \varphi(\hat{Z}))}{16(\hat{I}_c - \hat{I}_c^2)^{0.5}}} + \sqrt{\frac{(\varphi(\hat{I}_c) - \varphi(\hat{Z}))}{16(\hat{I}_c - \hat{I}_c^2)^{0.5}} + \left(\hat{I}_c - \frac{1}{2} - \frac{8}{3} \frac{((\hat{Z} - \hat{Z}^2)^{1.5} - (\hat{I}_c - \hat{I}_c^2)^{1.5})}{\varphi(\hat{I}_c) - \varphi(\hat{Z})}\right)} \right] \\
& \cdot (\varphi(\hat{I}_e) - \varphi(\hat{I}_e - \hat{y}_e)) + \\
& \left[\sqrt{\hat{y}_c + \frac{(\varphi(\hat{I}_c) - \varphi(\hat{Z}))}{16(\hat{I}_c - \hat{I}_c^2)^{0.5}}} + \sqrt{\frac{(\varphi(\hat{I}_c) - \varphi(\hat{Z}))}{16(\hat{I}_c - \hat{I}_c^2)^{0.5}} + \left(\hat{I}_c - \frac{1}{2} - \frac{8}{3} \frac{((\hat{Z} - \hat{Z}^2)^{1.5} - (\hat{I}_c - \hat{I}_c^2)^{1.5})}{\varphi(\hat{I}_c) - \varphi(\hat{Z})}\right)} \right] \\
& \cdot (\varphi(\hat{I}_e - \hat{y}_e) - \varphi(\hat{Z}_{fb})) - \frac{(\varphi(\hat{I}_c) - \varphi(\hat{Z}))^{1.5}}{2(\hat{I}_c - \hat{I}_c^2)^{0.25}} = 0
\end{aligned} \tag{5.32}$$

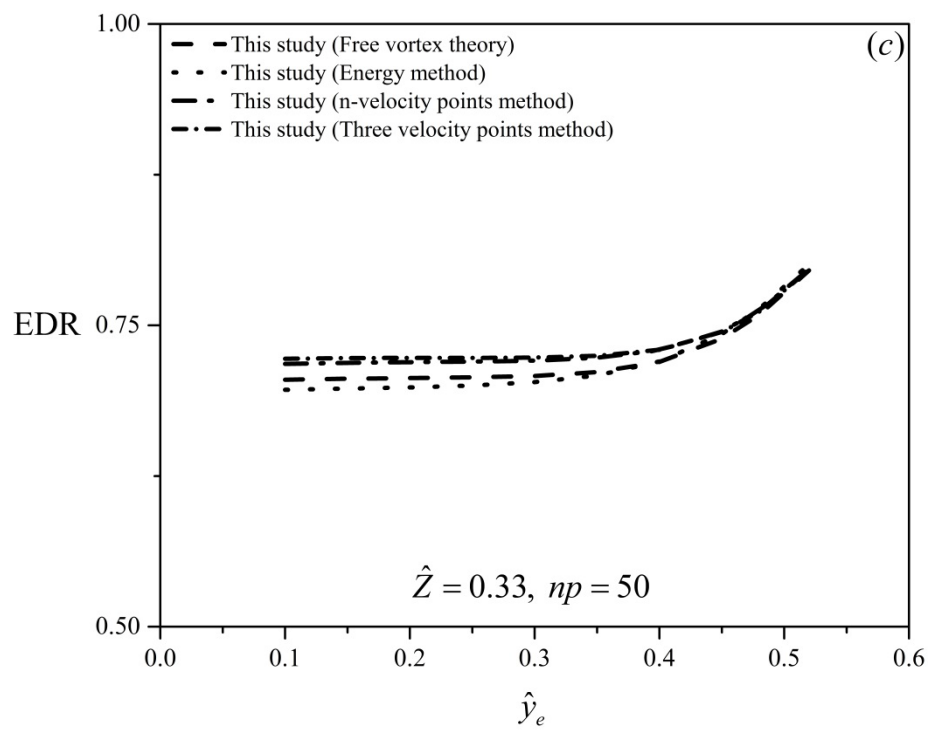
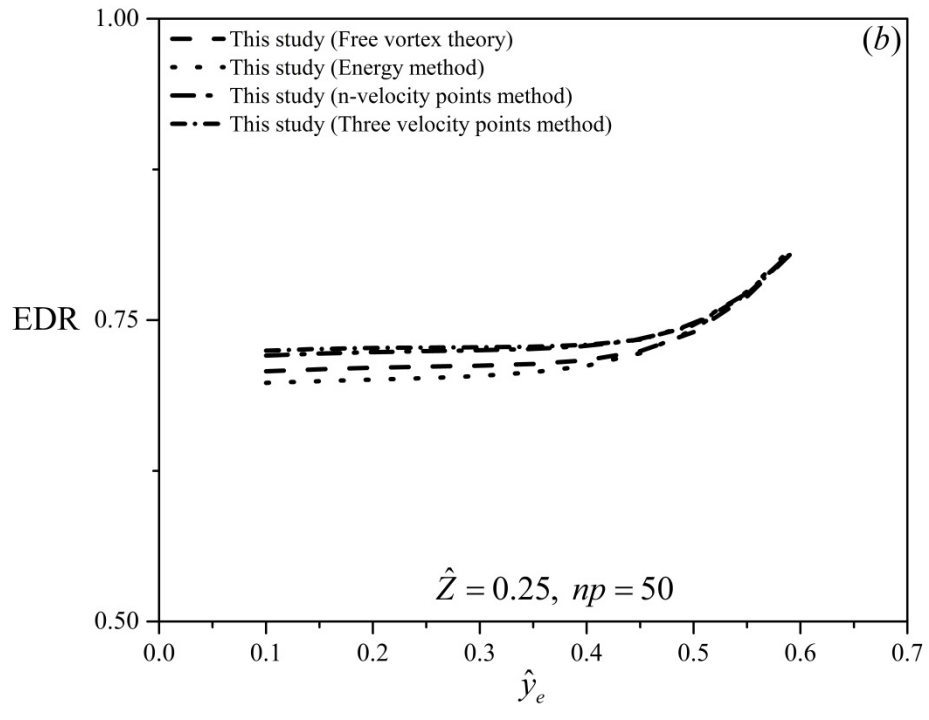
where

$$\hat{y}_e = \hat{I}_e - \frac{1}{2} - \frac{8}{3} \frac{((\hat{Z}_{fb} - \hat{Z}_{fb}^2)^{1.5} - (\hat{I}_e - \hat{I}_e^2)^{1.5})}{\varphi(\hat{I}_e) - \varphi(\hat{Z}_{fb})} \tag{5.33}$$

$$\sum_{i=1}^{np-1} \left[\left(\sqrt{\frac{(\varphi(\hat{I}_c) - \varphi(\hat{Z}))}{16(\hat{I}_c - \hat{I}_c^2)^{0.5}} + \frac{i-1}{np-1}} + \sqrt{\frac{(\varphi(\hat{I}_c) - \varphi(\hat{Z}))}{16(\hat{I}_c - \hat{I}_c^2)^{0.5}} + \frac{i}{np-1}} \right) \cdot \left(\varphi\left(\frac{n-i}{np-1} \hat{y}_e + \hat{Z}\right) - \varphi\left(\frac{np-i-1}{np-1} \hat{y}_e + \hat{Z}\right) \right) \right] - \frac{(\varphi(\hat{I}_c) - \varphi(\hat{Z}))^{1.5}}{2(\hat{I}_c - \hat{I}_c^2)^{0.25}} = 0 \quad (5.34)$$

To evaluate the EDR values of the above mentioned channel cross-sections based on different suggested methods, Eq. (5.28) for the energy method, Eq. (5.29) for the free vortex theory, Eq. (5.32) for the three velocity points method and Eq. (5.34) for the infinite number velocity points were solved separately for the given values of the \hat{y}_e and presented in Figs. 5.18 (a), (b), (c), (d), and (e) respectively. It is easily observed from these figures that, the proposed methods are in close agreement for different flat-base values of the channel cross-sections. Note that for infinite number velocity points method the value of 50 was used as the upper limit of the series expansion.





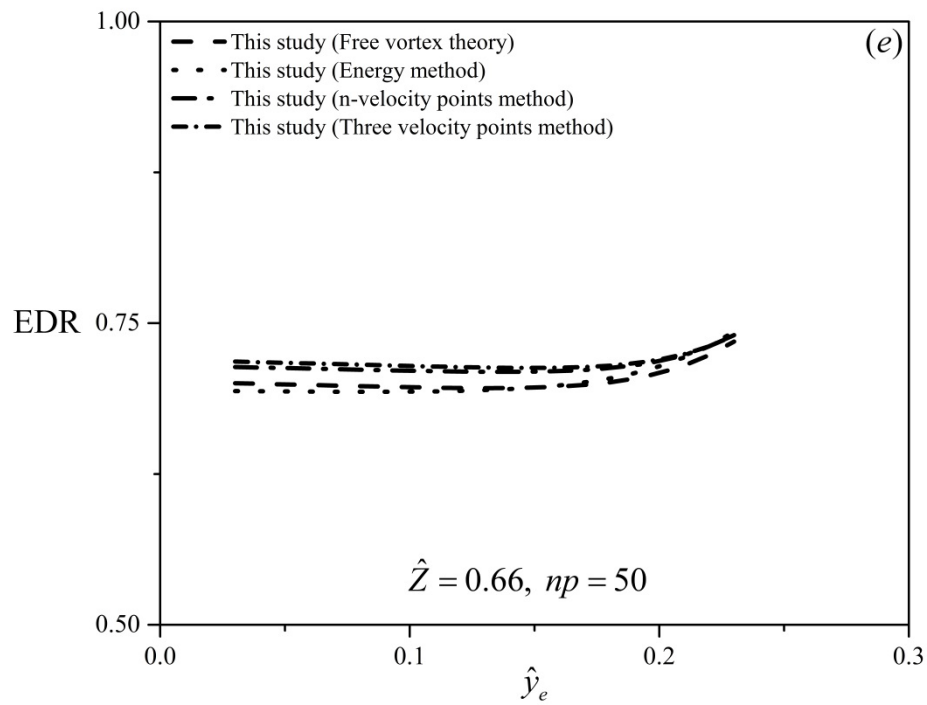
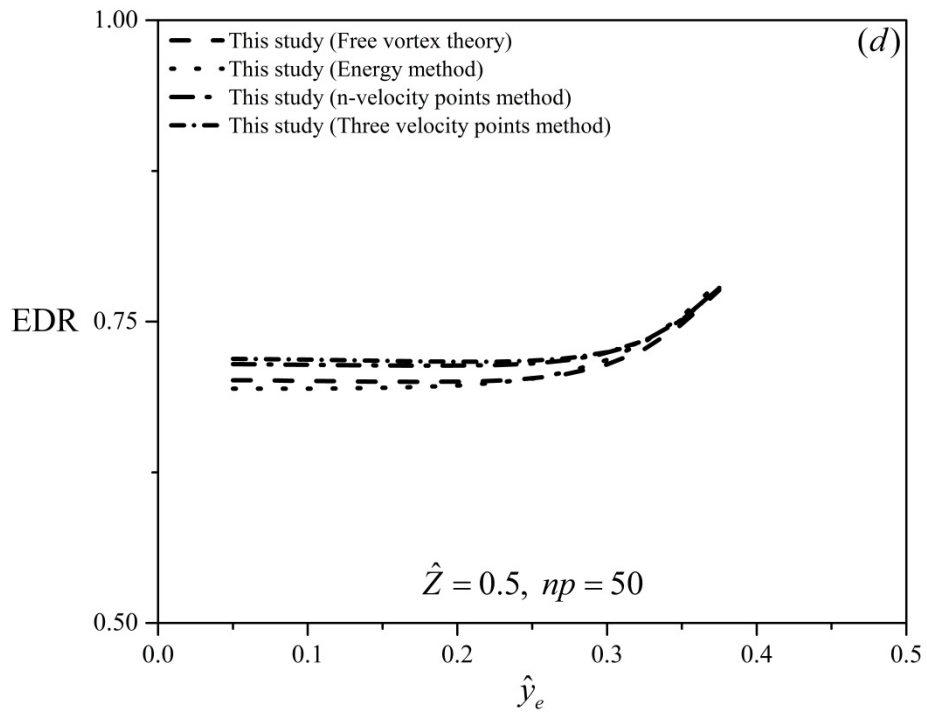


Figure 5.18: EDR values based on the proposed methods of circular channel cross-section with flat-base for (a) $\hat{Z} = 0$; (b) $\hat{Z} = 0.25$; (c) $\hat{Z} = 0.33$; (d) $\hat{Z} = 0.5$; and (e) $\hat{Z} = 0.66$ at sub-critical flow regimes

5.4.2 EDD for Sub-critical Flow Regimes

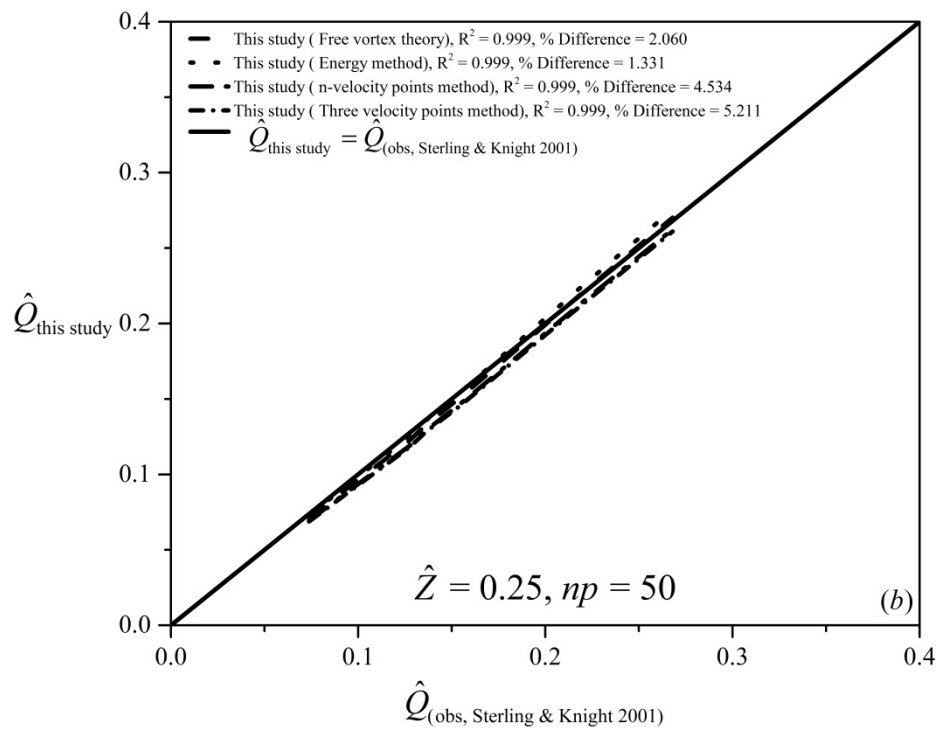
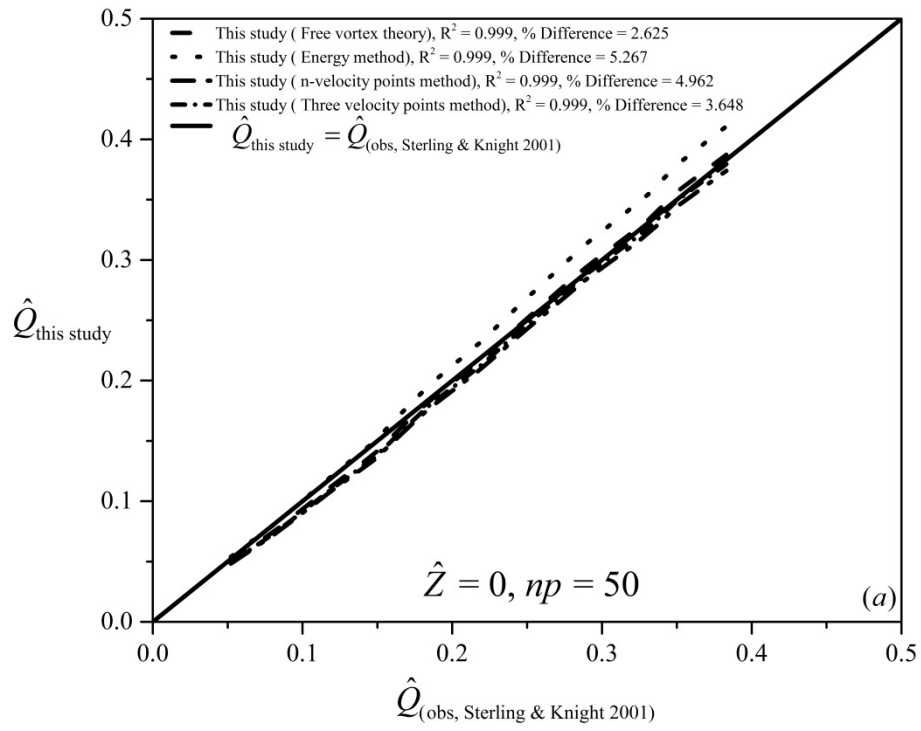
The non-dimensional discharge (\hat{Q}) relationship of the circular channel cross-sections with flat-base based on the definition of the normal Froude number (Fr_n) for both sub- and supercritical flow regimes can be written as:

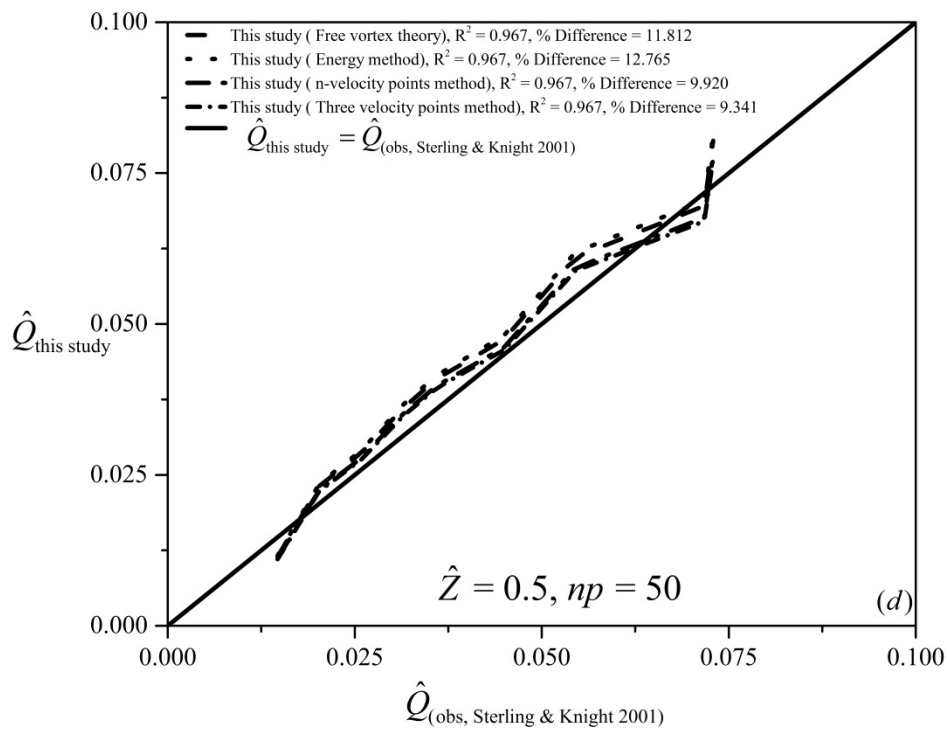
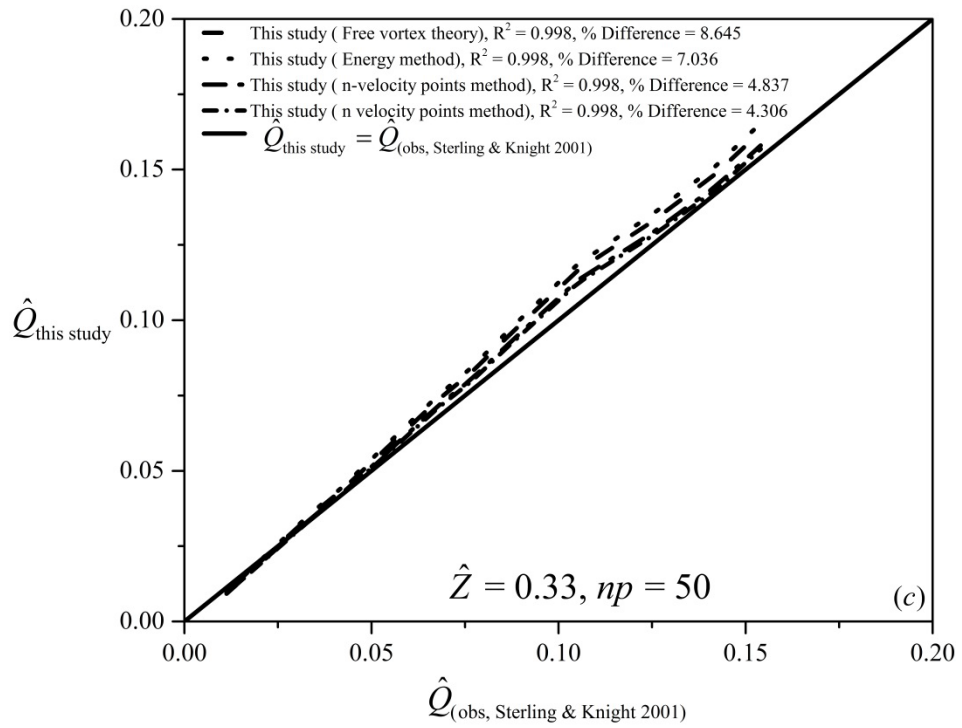
$$\hat{Q} = \frac{Q}{g^{0.5} D^{2.5}} = \frac{(\varphi(\hat{I}_n) - \varphi(\hat{Z}))^{1.5}}{8\sqrt{2}(\hat{I}_n - \hat{I}_n^2)^{0.25}} Fr_n \quad (5.35)$$

By substituting $Fr_n = Fr_c = 1$ and $\hat{I}_n = \hat{I}_c$ into Eq. (5.35), the discharge for sub-critical flow regimes is computed as:

$$\hat{Q} = \frac{Q}{g^{0.5} D^{2.5}} = \frac{(\varphi(\hat{I}_c) - \varphi(\hat{Z}))^{1.5}}{8\sqrt{2}(\hat{I}_c - \hat{I}_c^2)^{0.25}} \quad (5.36)$$

In order to obtain the \hat{I}_c values using different suggested methods, Eq. (5.28) for the energy method, Eq. (5.29) for the free vortex theory, Eq. (5.32) for the three velocity points method, and Eq. (5.34) for the infinite number velocity points were computed separately for the given values of the \hat{y}_e based on Sterling and Knight (2001) data sets. Then, the non-dimensional discharges (\hat{Q}) were computed from Eq. (5.36) for these methods separately and presented in Figures 5.19 (a), (b), (c), (d), and (e). The results of these different methods showing small deviations with the experimental data sets of Sterling (1998) for $\hat{Z} = 0$, $\hat{Z} = 0.25$, and $\hat{Z} = 0.33$. However, the computed discharges values have a lack of compatibility with the experimental observations of Sterling (1998) for $\hat{Z} = 0.5$, and $\hat{Z} = 0.66$ due to the assumption of the suggested approaches and the small cross-section flow depth ratio.





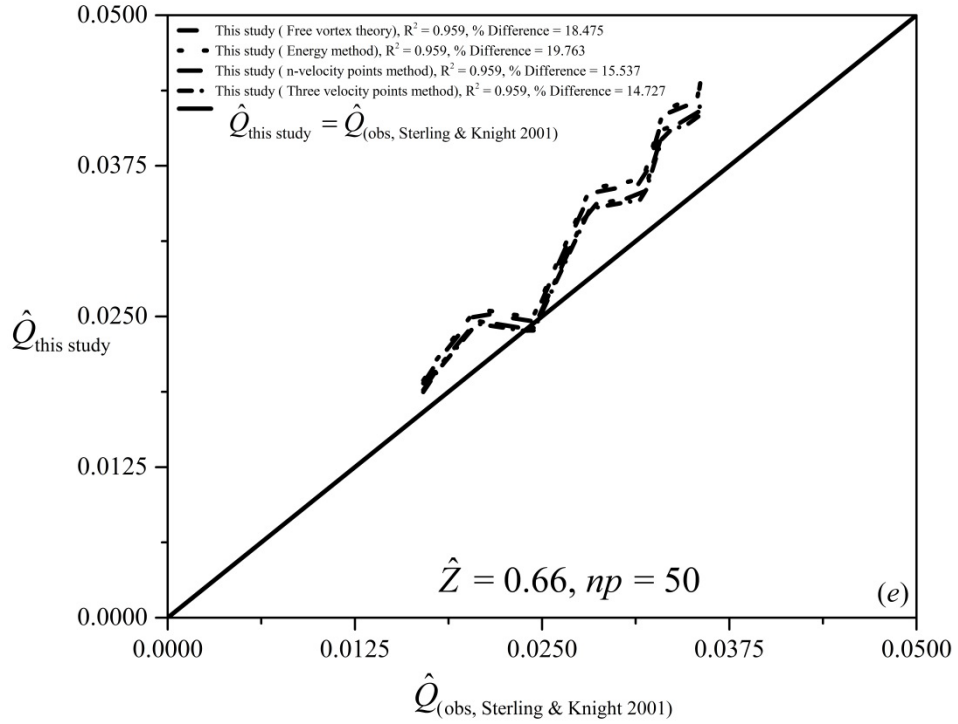


Figure 5.19: Comparison between the non-dimensional discharges (\hat{Q}) values of the suggested methods for the circular channel cross-section with flat-base and the experimental data set of Sterling (1998) for (a) $\hat{Z} = 0$; (b) $\hat{Z} = 0.25$; (c) $\hat{Z} = 0.33$; (d) $\hat{Z} = 0.5$; and (e) $\hat{Z} = 0.66$ at sub-critical flow regimes

5.4.3 EDR for Super Critical Flow Regimes

Similar to the exponential and the generalized trapezoidal channel cross-sections, the ratio between the flow depth at the brink (y_e) and the critical depth (y_c) is defined as:

$$\varepsilon_e = \frac{y_e}{y_c} = \frac{\hat{y}_e}{\hat{y}_c} \quad (5.37)$$

Dividing the upstream Froude number (Fr_n) of Eq. (3.14) by the critical Froude number ($Fr_c = 1$) the following ratio is generated:

$$Fr_n = \left(\frac{\hat{I}_n - \hat{I}_n^2}{\hat{I}_c - \hat{I}_c^2} \right)^{1/2} \left(\frac{\varphi(\hat{I}_c) - \varphi(\hat{Z})}{\varphi(\hat{I}_n) - \varphi(\hat{Z})} \right)^{3/2} \quad (5.38)$$

Substituting the upstream Froude number (Fr_n) from Eq. (3.14) into Manning's equation and then dividing by the critical Froude number ($Fr_c = 1$) yields:

$$Fr_n = \left(\frac{S}{S_c} \right)^{1/2} \left(\frac{\hat{I}_n - \hat{I}_n^2}{\hat{I}_c - \hat{I}_c^2} \right)^{1/2} \left(\frac{\varphi(\hat{I}_n) - \varphi(\hat{Z})}{\varphi(\hat{I}_c) - \varphi(\hat{Z})} \right)^{1/3} \cdot \left(\frac{2\sqrt{\hat{Z} - \hat{Z}^2} + \cos^{-1}(1 - 2\hat{I}_n) - \cos^{-1}(1 - \hat{Z})}{2\sqrt{\hat{Z} - \hat{Z}^2} + \cos^{-1}(1 - 2\hat{I}_c) - \cos^{-1}(1 - \hat{Z})} \right)^{2/3} \quad (5.40)$$

Equating Eqs. (5.39), and (5.40) yields the relative slope (\tilde{S}):

$$\tilde{S} = \frac{S}{S_c} = \left(\frac{\varphi(\hat{I}_n) - \varphi(\hat{Z})}{\varphi(\hat{I}_c) - \varphi(\hat{Z})} \right)^{10/3} \left(\frac{2\sqrt{\hat{Z} - \hat{Z}^2} + \cos^{-1}(1 - 2\hat{I}_c) - \cos^{-1}(1 - \hat{Z})}{2\sqrt{\hat{Z} - \hat{Z}^2} + \cos^{-1}(1 - 2\hat{I}_n) - \cos^{-1}(1 - \hat{Z})} \right)^{4/3} \quad (5.41)$$

To evaluate \hat{y}_n for the given values of \hat{y}_c and \tilde{S} , Eq. (5.41) is solved numerically for different value of $\hat{Z} = 0, 0.25, \text{ and } 0.5$. Then, Fr_n is calculated from Eq. (5.40). Subsequently, a numerical method is used to compute \hat{y}_e separately from Eq. (4.12) for the energy method, Eq. (4.18) for the free vortex theory, Eq. (4.40) for the three velocity points method, and Eq. (4.44) for the infinite number velocity points method. Eventually, the ratio between the flow depth at end section (y_e) and the critical depth (y_c), ε_e is obtained using Eq. (5.37) for each approach. Comparison of ε_e with respect to the relative slope (\tilde{S}) for different values of N_c and \hat{Z} and the theoretical study of Dey (2002) based on the Boussinesq approach and the sharp-crested weir theory are presented in Figs. 5.20 (a) and (b) for $\hat{Z} = 0$, Figs. 5.21 (a) and (b) for $\hat{Z} = 0.25$, and Figs. 5.22 (a) and (b) for $\hat{Z} = 0.5$. As a general trend, it is observed that, as the relative slope (\tilde{S}) increases, the magnitude of the ε_e decreases.

Also, based on statistical measuring indices, close agreements can be seen among the compared curves within the figure. Note that for infinite number velocity points method the value of 100 was used as the upper limit of the series expansion.

In order to evaluate \hat{y}_n , \hat{y}_c , and Fr_n for the given values of \hat{y}_e , \tilde{S} , and \hat{Z} Eqs. (5.28), (5.37), (5.38), and (5.41) for the energy method, Eqs. (5.29), (5.37), (5.38), and (5.41) for the free vortex theory, Eqs. (5.32), (5.37), (5.38), and (5.41) for the three velocity points method, and Eqs. (5.34), (5.37), (5.38), and (5.41) for the infinite number velocity points method were solved separately. Then, the ratio between the flow depth at end section and the critical depth (ε_e) is obtained using Eq. (5.37) for each method in the range of experimental data sets of Sterling and Knight (2001) study for $\hat{Z} = 0$ and 0.5. As shown in Figs. 5.23 (a) and (b) and Figs. 5.24 (a) and (b), the two statistical measuring indices (R^2 and MARE) were indicating close agreements implying the correctness of the proposed methods.

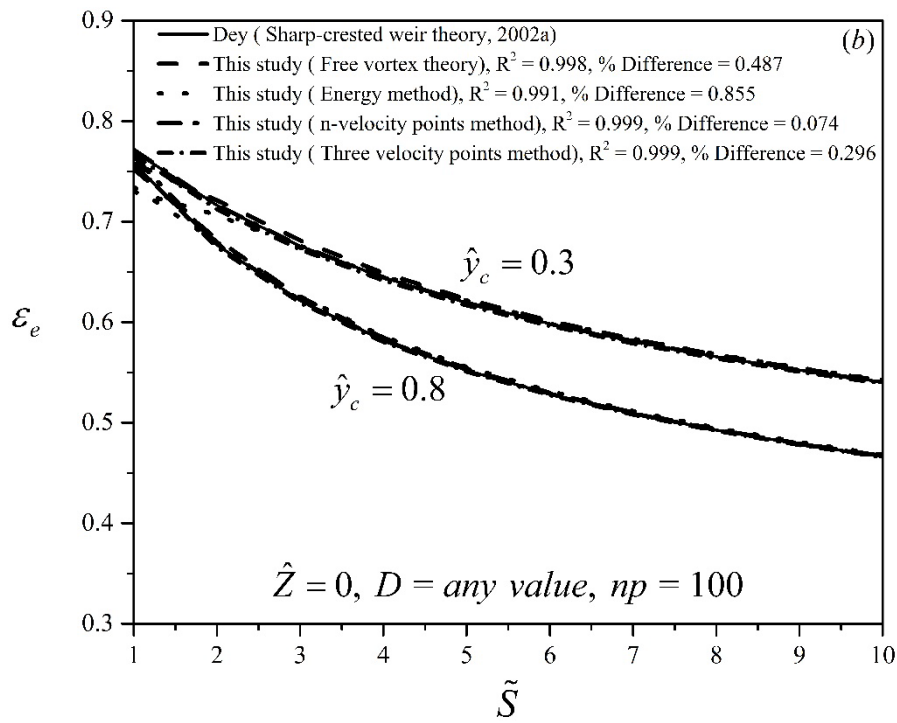
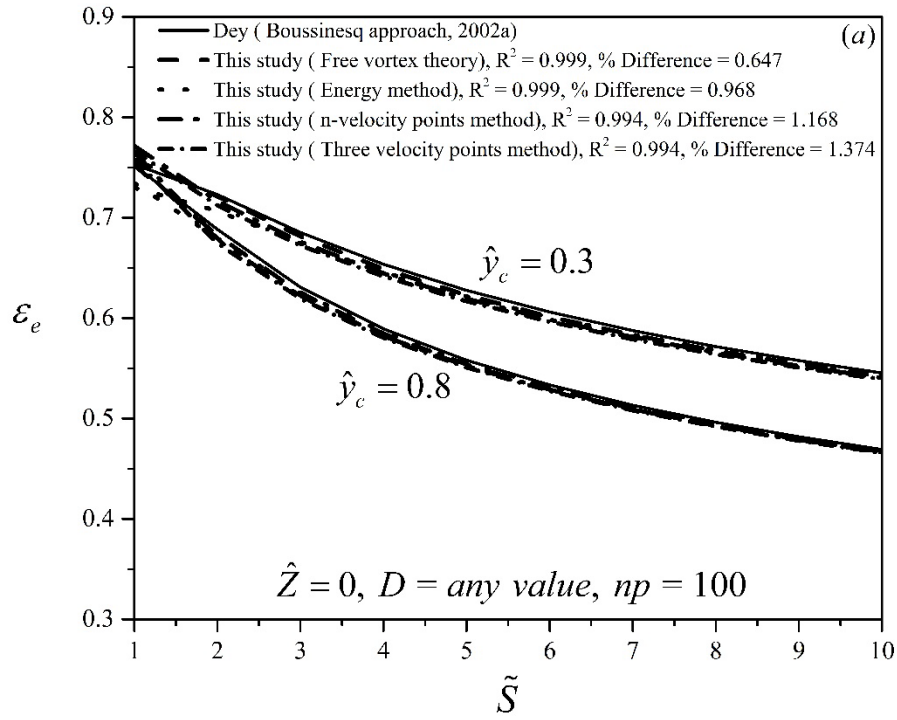


Figure 5.20: Comparison between ε_e versus \tilde{S} values based on the proposed four methods and (a) Dey (2002) by the Boussinesq approach; and (b) Dey (2002) by the sharp-crested weir theory of the circular channel cross-section for $\hat{Z} = 0$, $D = \text{any value}$, and $0.3 \leq \hat{y}_c \leq 0.8$

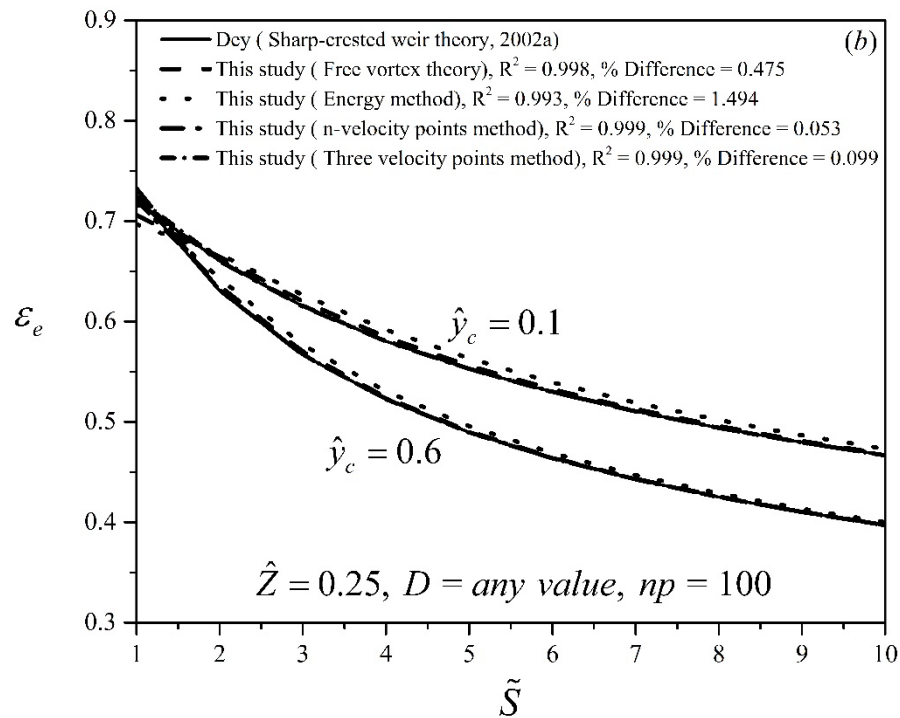
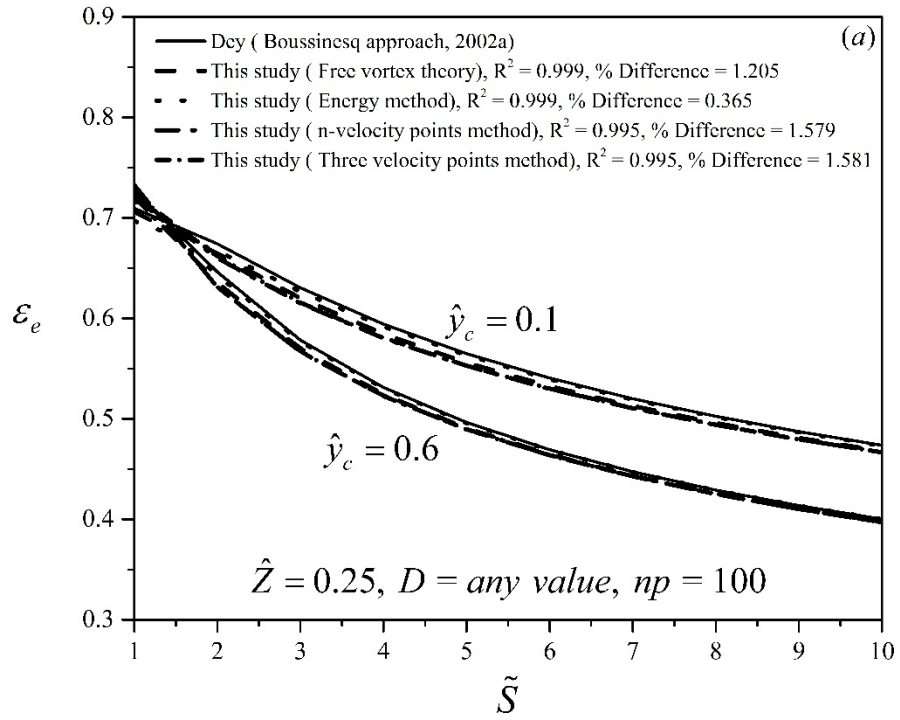


Figure 5.21: Comparison between ε_e versus \tilde{S} values based on the proposed four methods and (a) Dey (2002) by the Boussinesq approach; (b) Dey (2002) by the sharp-crested weir approach of the circular channel cross-section for $\hat{Z} = 0.25$, $D =$ any value, and $0.1 \leq \hat{y}_c \leq 0.6$

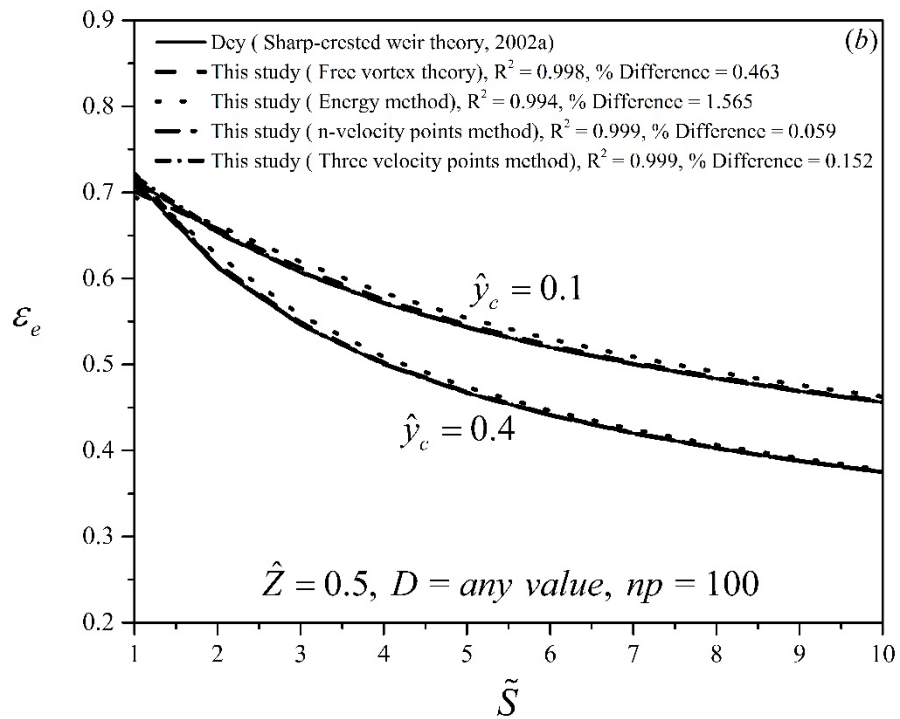
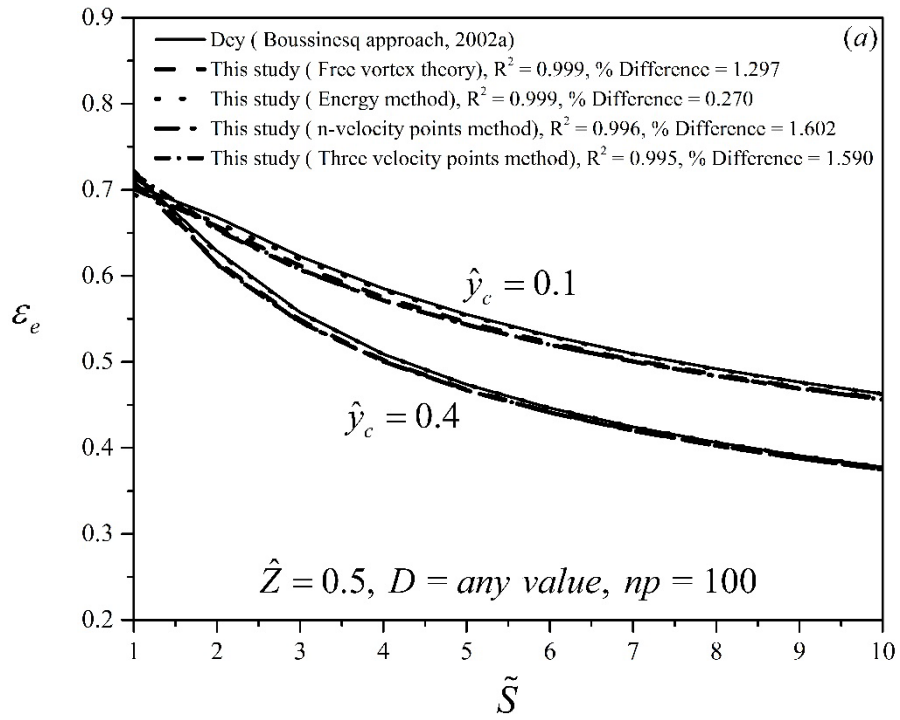


Figure 5.22: Comparison between ε_e versus \tilde{S} values based on the proposed four methods and (a) Dey (2002) by the Boussinesq approach; (b) Dey (2002) by the sharp-crested weir approach of the circular channel cross-section for $\hat{Z} = 0.5$, $D = \text{any value}$, and $0.1 \leq \hat{y}_c \leq 0.4$

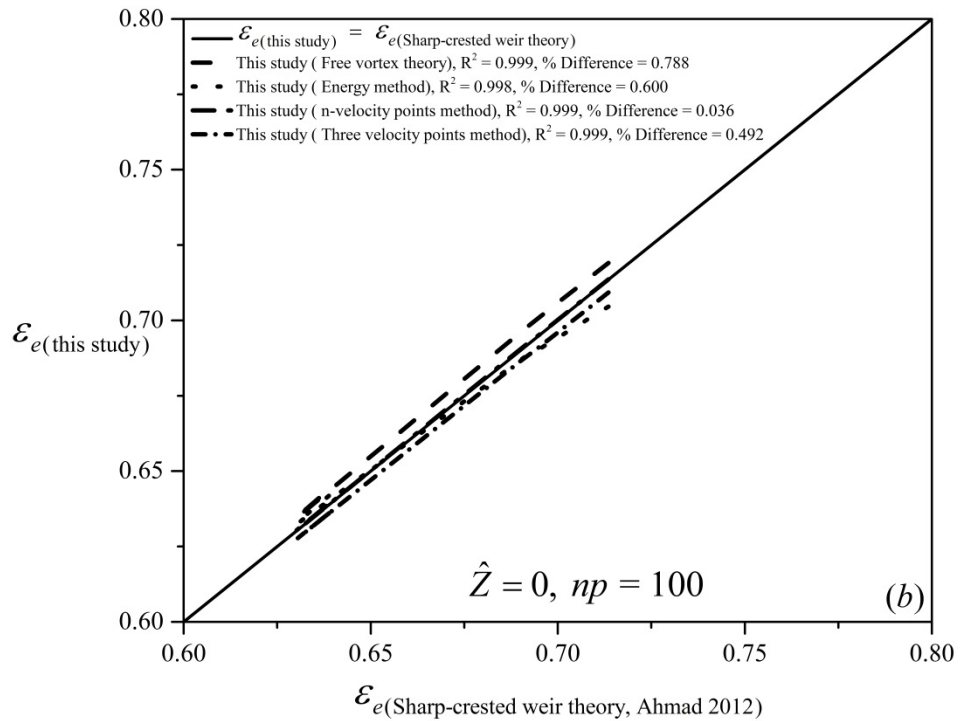
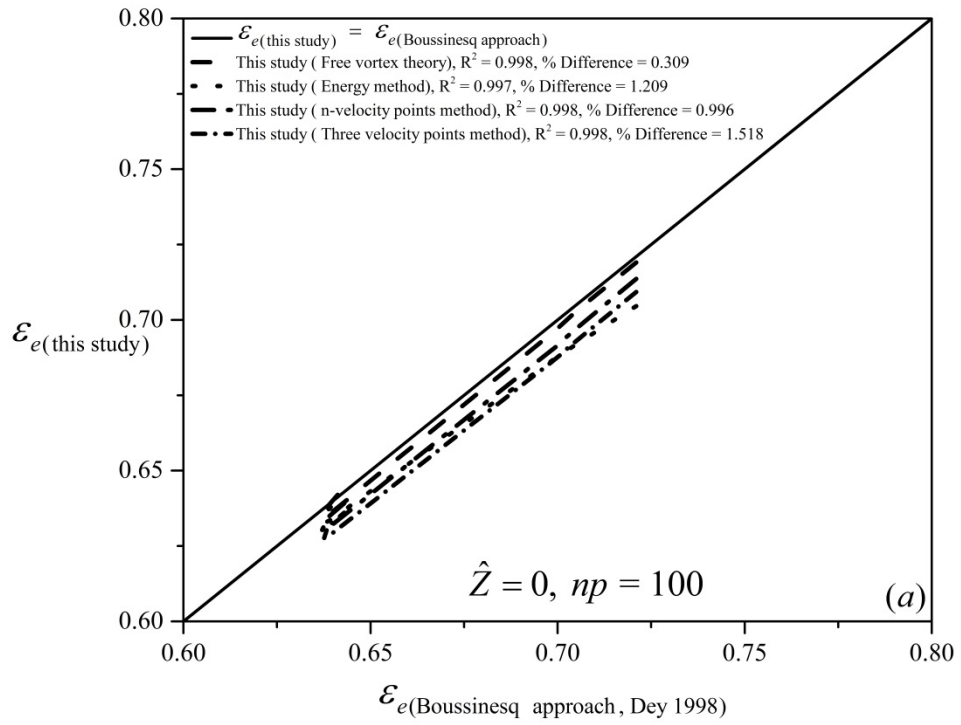


Figure 5.23: \mathcal{E}_e values based on the suggested methods of this study versus (a) \mathcal{E}_e values based on the theoretical study of Dey (1998) using Boussinesq approach; and (b) \mathcal{E}_e values based on the theoretical study of Ahmad (2012) using sharp-crested weir theory in circular channel with $\hat{Z} = 0$

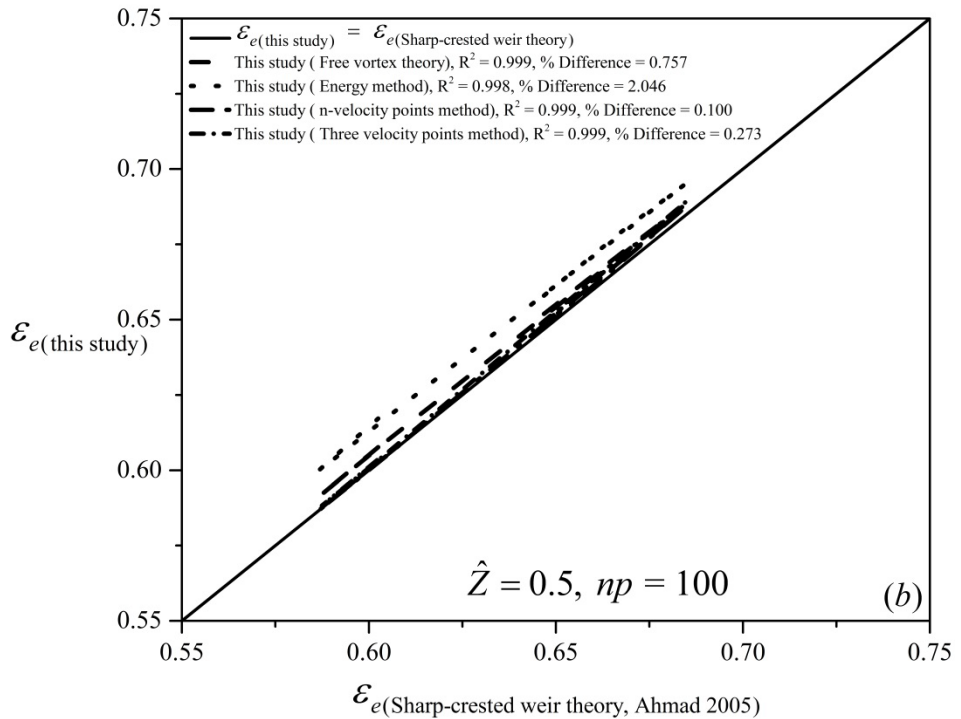
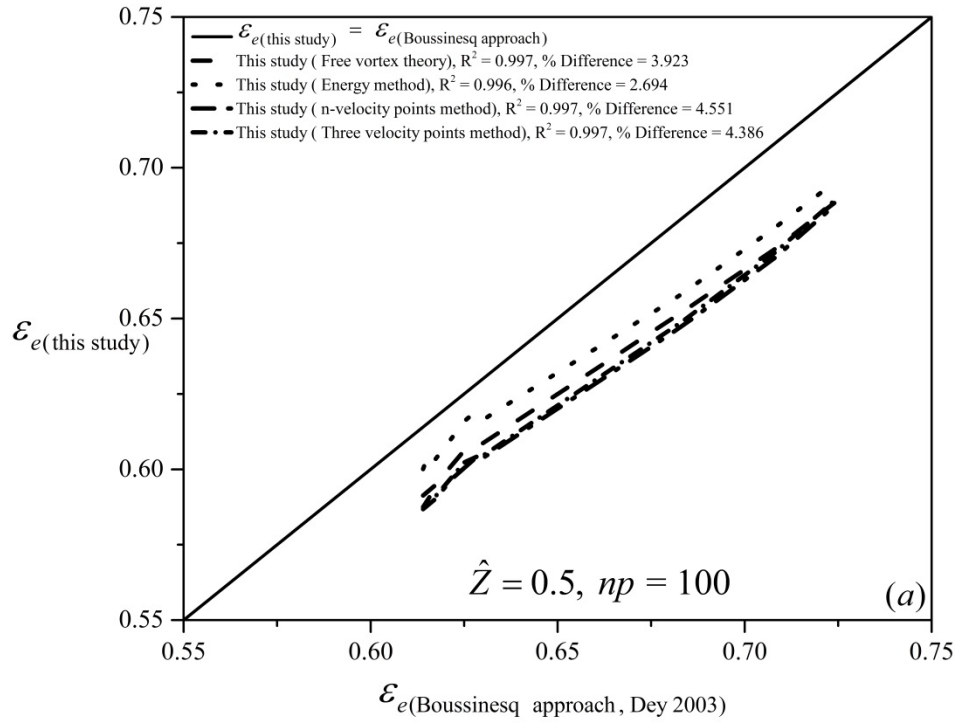


Figure 5.24: ε_e values based on the suggested methods of this study versus (a) ε_e values based on the theoretical study of Dey (2003) using Boussinesq approach; and (b) ε_e values based on the theoretical study of Ahmed (2005) using sharp-crested weir theory in circular channel with $\hat{Z} = 0.5$

5.4.4 EDD for Super Critical Flow Regimes

In super critical flow regimes, since the discharge is dependent on \hat{y}_n and Fr_n , so it is not explicitly possible to estimate the discharge from the given value of the end depth measurement only (Eq. (5.36)). On the other hand, it is difficult to determine the location of the normal section properly, hence, the known values of the relative channel bed slope (\tilde{S}) using Eq. (5.41) in the semi-empirical Manning-Strickler equation is coupled with the end depth measurements. To overcome this difficulty Eqs. (5.28), (5.37), (5.38), and (5.41) for the energy method, Eqs. (5.29), (5.37), (5.38), and (5.41) for the free vortex theory, Eqs. (5.32), (5.37), (5.38), and (5.41) for the three velocity points method, and Eqs. (5.34), (5.37), (5.38), and (5.41) for the infinite number velocity points method were solved, separately. Therefore \hat{y}_n , \hat{y}_c , and Fr_n were calculated for the given values of \hat{y}_e , \tilde{S} , and \hat{Z} . Then, Eq. (5.35) is used to compute the non-dimensional discharge (\hat{Q}) values for each method, separately. In order to show the accuracy of the suggested methods, a comparison between the computed values of \hat{Q} of the proposed approached and the experimental observations of Sterling and Knight (2001) is listed in Table 5.3 for the energy method, Table 5.4 for the free vortex theory, Table 5.5 for the three velocity points method, and Table 5.6 for the infinite number velocity points method. As can be seen, the computed values of \hat{Q} have a slight deviation from the observed data sets of Sterling and Knight (2001) for the different derivations of the generalized circular channel cross-sections.

To evaluate the better performance of the proposed approaches of this study graphically for the circular channel cross-sections ($\hat{Z} = 0$), a comparison between

the computed values of \hat{Q} for this study and the theoretical study of Dey (1998) and Ahmad (2012) is presented in Figs. 5.25(a) and (b). Also for the inverted semi-circular channel cases ($\hat{Z} = 0.25$), a comparison between the computed values of \hat{Q} for this study using different proposed methods and the theoretical study of Dey (2003) and Ahmad (2005) is shown in Figs. 5.25(a) and (b). As depicted in these figures, the two statistical measuring indices (R^2 and MARE) revealed that, the suggested approaches are in well agreement with the other theoretical studies.

Table 5.3: Comparison of observed data of \hat{Q} by Sterling and Knight (2001) with the computed data of \hat{Q} of the energy method

\hat{Z}	\hat{y}_e	\hat{y}_c	\tilde{S}	\hat{Q}_{obs}	\hat{Q}_{Energy}
0	0.124	0.081	2.242	0.0163	0.014057
0	0.233	0.155	2.487	0.0565	0.05194
0	0.332	0.215	2.509	0.1118	0.09932
0	0.474	0.321	2.347	0.2226	0.215693
0	0.386	0.236	4.279	0.1501	0.140086
0	0.495	0.299	4.002	0.2412	0.221051
0	0.608	0.36	3.548	0.3571	0.310441
0	0.666	0.397	3.253	0.4264	0.369513
0.25	0.206	0.149	1.575	0.0865	0.094081
0.25	0.246	0.175	1.214	0.1138	0.117668
0.25	0.45	0.325	1.958	0.2984	0.348093
0.25	0.478	0.345	1.775	0.3296	0.375136
0.25	0.529	0.38	1.47	0.3911	0.422099
0.25	0.497	0.357	1.657	0.3477	0.390464
0.25	0.323	0.232	3.167	0.1753	0.230128
0.25	0.361	0.261	2.713	0.2092	0.265802
0.33	0.169	0.124	1.824	0.0673	0.077209
0.33	0.193	0.144	1.484	0.0825	0.094052
0.33	0.228	0.172	1.162	0.1064	0.120844
0.33	0.281	0.213	1.849	0.1477	0.179972
0.33	0.307	0.227	1.638	0.1694	0.193977
0.33	0.312	0.234	1.602	0.1737	0.20267
0.33	0.241	0.175	2.294	0.1162	0.139184
0.33	0.303	0.22	1.667	0.1661	0.185234
0.5	0.193	0.143	1.939	0.0847	0.101608
0.5	0.318	0.24	1.451	0.1824	0.215976
0.5	0.354	0.269	1.264	0.2171	0.25328
0.5	0.067	0.041	3.162	0.0172	0.017155
0.5	0.206	0.121	3.086	0.0934	0.089916
0.5	0.287	0.164	2.59	0.1553	0.137946
0.66	0.082	0.049	3.283	0.0236	0.021576
0.66	0.101	0.065	3.34	0.0321	0.033514
0.66	0.12	0.069	3.356	0.042	0.036837
0.66	0.137	0.084	3.343	0.0507	0.050152
0.66	0.146	0.09	3.326	0.056	0.055921
0.66	0.154	0.095	3.309	0.0606	0.060938
0.66	0.168	0.105	3.27	0.0687	0.071611

Table 5.4: Comparison of observed data of \hat{Q} by Sterling and Knight (2001) with the computed data of \hat{Q} of the free vortex theory

\hat{Z}	\hat{y}_e	\hat{y}_c	\tilde{S}	\hat{Q}_{obs}	$\hat{Q}_{\text{Free vortex}}$
0	0.124	0.081	2.242	0.0163	0.013503
0	0.233	0.155	2.487	0.0565	0.050322
0	0.332	0.215	2.509	0.1118	0.096541
0	0.474	0.321	2.347	0.2226	0.210217
0	0.386	0.236	4.279	0.1501	0.139142
0	0.495	0.299	4.002	0.2412	0.219784
0	0.608	0.36	3.548	0.3571	0.308632
0	0.666	0.397	3.253	0.4264	0.367273
0.25	0.206	0.149	1.575	0.0865	0.093653
0.25	0.246	0.175	1.214	0.1138	0.11587
0.25	0.45	0.325	1.958	0.2984	0.3529
0.25	0.478	0.345	1.775	0.3296	0.37967
0.25	0.529	0.38	1.47	0.3911	0.42524
0.25	0.497	0.357	1.657	0.3477	0.394524
0.25	0.323	0.232	3.167	0.1753	0.234551
0.25	0.361	0.261	2.713	0.2092	0.270594
0.33	0.169	0.124	1.824	0.0673	0.077543
0.33	0.193	0.144	1.484	0.0825	0.093729
0.33	0.228	0.172	1.162	0.1064	0.119299
0.33	0.281	0.213	1.849	0.1477	0.181498
0.33	0.307	0.227	1.638	0.1694	0.194838
0.33	0.312	0.234	1.602	0.1737	0.203473
0.33	0.241	0.175	2.294	0.1162	0.141081
0.33	0.303	0.22	1.667	0.1661	0.186108
0.5	0.193	0.143	1.939	0.0847	0.103039
0.5	0.318	0.24	1.451	0.1824	0.219794
0.5	0.354	0.269	1.264	0.2171	0.257895
0.5	0.067	0.041	3.162	0.0172	0.017486
0.5	0.206	0.121	3.086	0.0934	0.091966
0.5	0.287	0.164	2.59	0.1553	0.141276
0.66	0.082	0.049	3.283	0.0236	0.022051
0.66	0.101	0.065	3.34	0.0321	0.034305
0.66	0.12	0.069	3.356	0.042	0.037722
0.66	0.137	0.084	3.343	0.0507	0.051437
0.66	0.146	0.09	3.326	0.056	0.057394
0.66	0.154	0.095	3.309	0.0606	0.062584
0.66	0.168	0.105	3.27	0.0687	0.073657

Table 5.5: Comparison of observed data of \hat{Q} by Sterling and Knight (2001) with the computed data of \hat{Q} of the three velocity points method

\hat{Z}	\hat{y}_e	\hat{y}_c	\tilde{S}	\hat{Q}_{obs}	$\hat{Q}_{\text{Three velocity points}}$
0	0.124	0.081	2.242	0.0163	0.013874
0	0.233	0.155	2.487	0.0565	0.051717
0	0.332	0.215	2.509	0.1118	0.099184
0	0.474	0.321	2.347	0.2226	0.215855
0	0.386	0.236	4.279	0.1501	0.142169
0	0.495	0.299	4.002	0.2412	0.224604
0	0.608	0.36	3.548	0.3571	0.315741
0	0.666	0.397	3.253	0.4264	0.376087
0.25	0.206	0.149	1.575	0.0865	0.093788
0.25	0.246	0.175	1.214	0.1138	0.114154
0.25	0.45	0.325	1.958	0.2984	0.357336
0.25	0.478	0.345	1.775	0.3296	0.384097
0.25	0.529	0.38	1.47	0.3911	0.428393
0.25	0.497	0.357	1.657	0.3477	0.398662
0.25	0.323	0.232	3.167	0.1753	0.237318
0.25	0.361	0.261	2.713	0.2092	0.274016
0.33	0.169	0.124	1.824	0.0673	0.077996
0.33	0.193	0.144	1.484	0.0825	0.093547
0.33	0.228	0.172	1.162	0.1064	0.117023
0.33	0.281	0.213	1.849	0.1477	0.182963
0.33	0.307	0.227	1.638	0.1694	0.195772
0.33	0.312	0.234	1.602	0.1737	0.204321
0.33	0.241	0.175	2.294	0.1162	0.14259
0.33	0.303	0.22	1.667	0.1661	0.187079
0.5	0.193	0.143	1.939	0.0847	0.103804
0.5	0.318	0.24	1.451	0.1824	0.220449
0.5	0.354	0.269	1.264	0.2171	0.257377
0.5	0.067	0.041	3.162	0.0172	0.017663
0.5	0.206	0.121	3.086	0.0934	0.09288
0.5	0.287	0.164	2.59	0.1553	0.142721
0.66	0.082	0.049	3.283	0.0236	0.022263
0.66	0.101	0.065	3.34	0.0321	0.034624
0.66	0.12	0.069	3.356	0.042	0.03807
0.66	0.137	0.084	3.343	0.0507	0.0519
0.66	0.146	0.09	3.326	0.056	0.057905
0.66	0.154	0.095	3.309	0.0606	0.063138
0.66	0.168	0.105	3.27	0.0687	0.0743

Table 5.6: Comparison of observed data of \hat{Q} by Sterling and Knight (2001) with the computed data of \hat{Q} ofr the infinite number velocity points method

\hat{Z}	\hat{y}_e	\hat{y}_c	\tilde{S}	\hat{Q}_{obs}	$\hat{Q}_{\text{Infinite number velocity points}}$
0	0.124	0.081	2.242	0.0163	0.013706
0	0.233	0.155	2.487	0.0565	0.051124
0	0.332	0.215	2.509	0.1118	0.098075
0	0.474	0.321	2.347	0.2226	0.213468
0	0.386	0.236	4.279	0.1501	0.140944
0	0.495	0.299	4.002	0.2412	0.222662
0	0.608	0.36	3.548	0.3571	0.312898
0	0.666	0.397	3.253	0.4264	0.37257
0.25	0.206	0.149	1.575	0.0865	0.094189
0.25	0.246	0.175	1.214	0.1138	0.114838
0.25	0.45	0.325	1.958	0.2984	0.357845
0.25	0.478	0.345	1.775	0.3296	0.384705
0.25	0.529	0.38	1.47	0.3911	0.429186
0.25	0.497	0.357	1.657	0.3477	0.399343
0.25	0.323	0.232	3.167	0.1753	0.237482
0.25	0.361	0.261	2.713	0.2092	0.27426
0.33	0.169	0.124	1.824	0.0673	0.078295
0.33	0.193	0.144	1.484	0.0825	0.094015
0.33	0.228	0.172	1.162	0.1064	0.117805
0.33	0.281	0.213	1.849	0.1477	0.183526
0.33	0.307	0.227	1.638	0.1694	0.196477
0.33	0.312	0.234	1.602	0.1737	0.205068
0.33	0.241	0.175	2.294	0.1162	0.142928
0.33	0.303	0.22	1.667	0.1661	0.187747
0.5	0.193	0.143	1.939	0.0847	0.104179
0.5	0.318	0.24	1.451	0.1824	0.221378
0.5	0.354	0.269	1.264	0.2171	0.258492
0.5	0.067	0.041	3.162	0.0172	0.0177
0.5	0.206	0.121	3.086	0.0934	0.093058
0.5	0.287	0.164	2.59	0.1553	0.143051
0.66	0.082	0.049	3.283	0.0236	0.022308
0.66	0.101	0.065	3.34	0.0321	0.034692
0.66	0.12	0.069	3.356	0.042	0.038144
0.66	0.137	0.084	3.343	0.0507	0.051999
0.66	0.146	0.09	3.326	0.056	0.058017
0.66	0.154	0.095	3.309	0.0606	0.063259
0.66	0.168	0.105	3.27	0.0687	0.074444

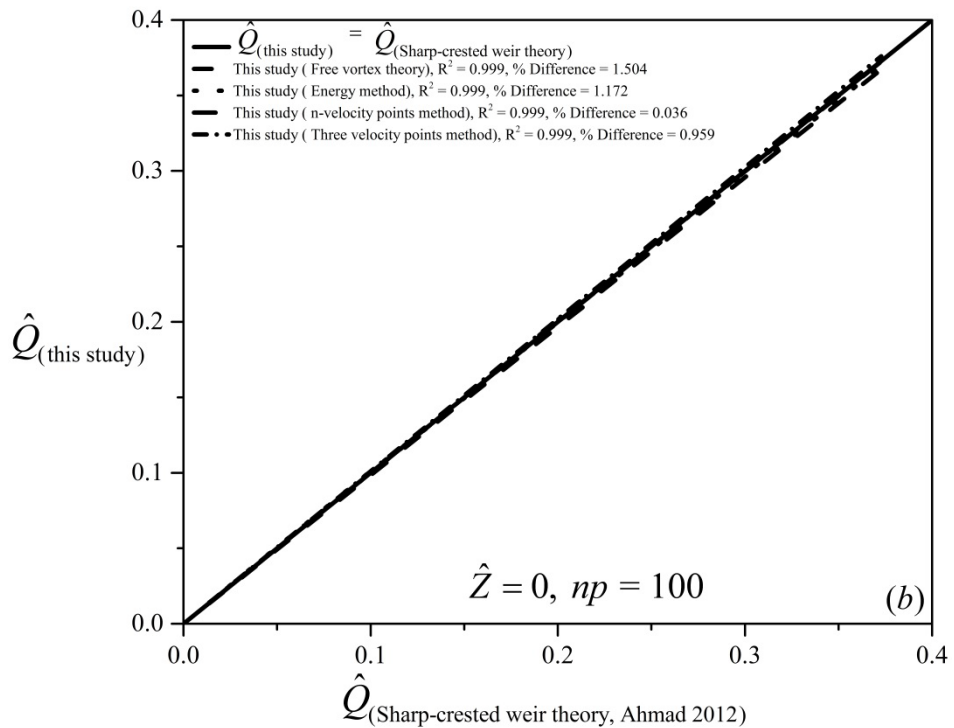
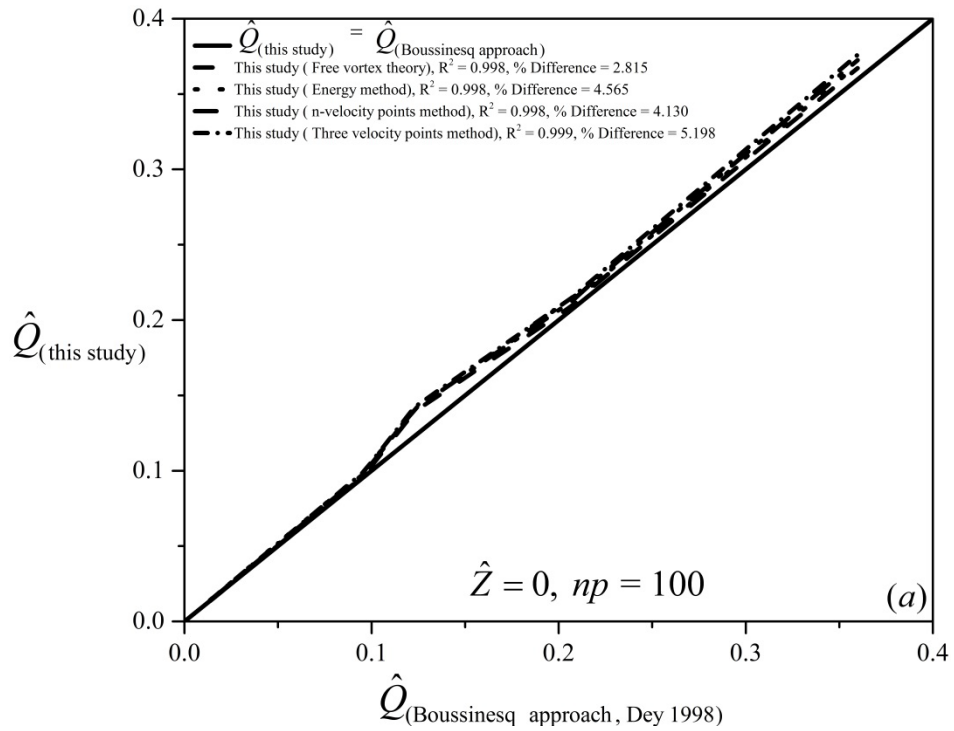


Figure 5.25: Comparison between the computed non-dimensional discharges (\hat{Q}) of the suggested methods of this study with (a) the theoretical \hat{Q} results of Dey (1998); and (b) the theoretical \hat{Q} results of Ahmad (2012) for the circular channel cross-section at super critical flow regime with $\hat{Z} = 0$

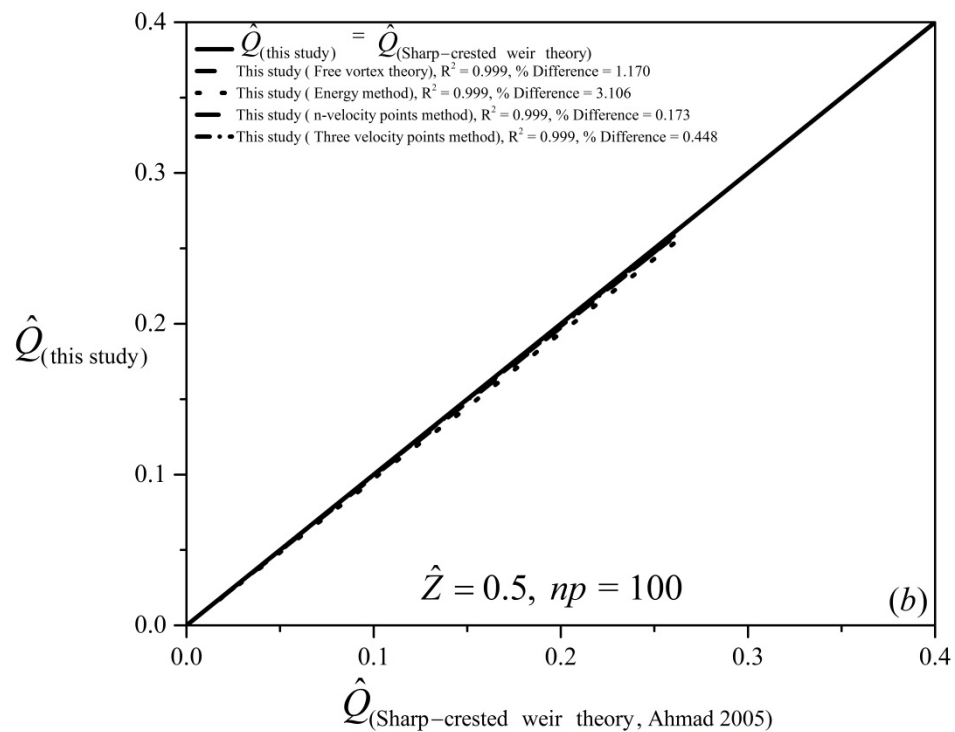
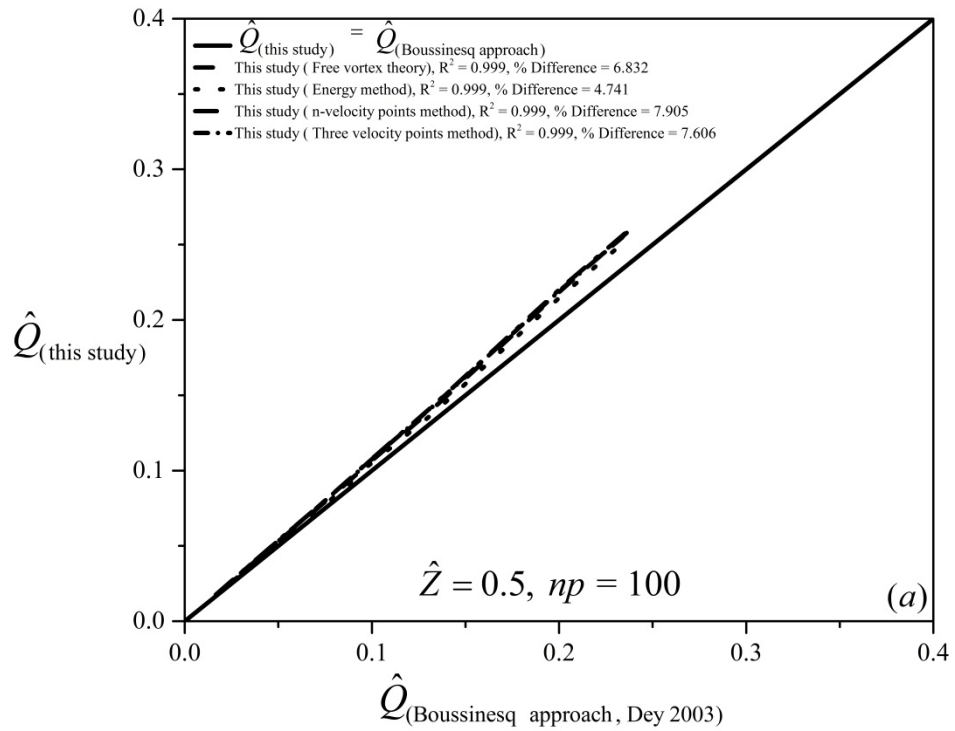


Figure 5.26: Comparison between the computed non-dimensional discharges (\hat{Q}) of the suggested methods of this study with (a) the theoretical \hat{Q} results of Dey (2003); and (b) the theoretical \hat{Q} results of Ahmad (2005) for the circular channel cross-section at super critical flow regime with $\hat{Z} = 0.5$

5.5 Direct Discharge Prediction

As discussed earlier, the free over-fall can be used as a flow measuring hydraulic structure in open channels. Hence, in this study, direct equations of the discharge for the different channel cross-sections in both sub- and super critical flow regimes were computed and presented mathematically based on the end depth and the channel geometric characteristics.

5.5.1 Sub-critical Flow Regimes

Since one of the main aims of this study is to estimate the discharge from the known end depth, the direct discharge equations in terms of the end depth values were proposed for flows at sub-critical regimes.

5.5.1.1 Generalized Trapezoidal Channel Cross-sections

Inserting the calculated EDR of Eq. (5.13) for the energy method, Eq. (4.17) where $Fr_n = 1$ for the free vortex theory, Eq. (5.15) for three velocity points method, and Eq. (5.18) for the infinite number velocity points method into Eq. (5.22) and incorporating the corrected values of η_3 , η_4 and $\eta_5=0$ for each cross-section, EDD values were computed for the different channel cross-sections at sub-critical regimes. Using the curve-fitting technique, non-linear equations were established for the engineers in practice for the trapezoidal, the semi-trapezoidal, the inverted triangular, and the semi-inverted triangular channel cross-sections and tabulated in Table 5.7 based on the different theoretical methods of this study. To evaluate their accuracies, based on the exact values of Q^* , the correlation coefficient (R^2) and the root mean square errors (RMSE) measures were determined as detailed. Both indices are indicating small deviation for the proposed dimensionless discharge (Q^*) equation, implying highly acceptable level.

5.5.1.2 Generalized Circular Channel Cross-sections

Inserting the calculated EDR of Eq. (5.28) for the energy method, Eq. (5.29) for the free vortex theory, Eq. (5.32) for three velocity points method, and Eq. (5.34) for the infinite number velocity points method into Eq. (5.36) for the different values of $\hat{Z} = 0, 0.25, 0.5, \text{ and } 0.66$, EDD values were computed for the different channel cross-sections at sub-critical regime. Using the curve-fitting technique, a non-linear equation was established for the engineers in practice in generalized circular channel cross-sections as listed in Table 5.7 for different theoretical methods of this study. To evaluate their accuracies, based on the exact values of \hat{Q} , R^2 and RMSE measures were determined as detailed. Both indices are indicating small deviation for the proposed dimensionless discharge (\hat{Q}) equation, implying highly acceptable level.

Table 5.7: Equation of discharge (Q) based on the end depth (y_e) at sub-critical flow regime for different channel cross-sections using different theoretical methods

Cross-section	Energy	Free vortex	Three velocity points	n-velocity points
Trapezoidal	$Q = \frac{g^{0.5} B^{2.5}}{m^{1.5}} \frac{\left[1.427 \left(\frac{my_e}{B} \right) + 1.518 \left(\frac{my_e}{B} \right)^2 \right]^{1.5}}{\left[1 + 1.819 \left(\frac{my_e}{B} \right) \right]^{0.5}}$ $R^2 = 1, RMSE = 3.42 * 10^{-4}$	$Q = \frac{g^{0.5} B^{2.5}}{m^{1.5}} \frac{\left[1.437 \left(\frac{my_e}{B} \right) + 1.522 \left(\frac{my_e}{B} \right)^2 \right]^{1.5}}{\left[1 + 2.32 \left(\frac{my_e}{B} \right) \right]^{0.5}}$ $R^2 = 1, RMSE = 9.16 * 10^{-4}$	$Q = \frac{g^{0.5} B^{2.5}}{m^{1.5}} \frac{\left[1.39 \left(\frac{my_e}{B} \right) + 1.515 \left(\frac{my_e}{B} \right)^2 \right]^{1.5}}{\left[1 + 2.317 \left(\frac{my_e}{B} \right) \right]^{0.5}}$ $R^2 = 1, RMSE = 4.97 * 10^{-4}$	$Q = \frac{g^{0.5} B^{2.5}}{m^{1.5}} \frac{\left[1.412 \left(\frac{my_e}{B} \right) + 1.52 \left(\frac{my_e}{B} \right)^2 \right]^{1.5}}{\left[1 + 2.417 \left(\frac{my_e}{B} \right) \right]^{0.5}}$ $R^2 = 1, RMSE = 5.66 * 10^{-4}$
Semi-trapezoidal	$Q = \frac{g^{0.5} B^{2.5}}{\left(\frac{m}{2} \right)^{1.5}} \frac{\left[1.427 \left(\frac{my_e}{2B} \right) + 1.518 \left(\frac{my_e}{2B} \right)^2 \right]^{1.5}}{\left[1 + 1.819 \left(\frac{my_e}{2B} \right) \right]^{0.5}}$ $R^2 = 1, RMSE = 3.42 * 10^{-4}$	$Q = \frac{g^{0.5} B^{2.5}}{\left(\frac{m}{2} \right)^{1.5}} \frac{\left[1.437 \left(\frac{my_e}{2B} \right) + 1.522 \left(\frac{my_e}{2B} \right)^2 \right]^{1.5}}{\left[1 + 2.32 \left(\frac{my_e}{2B} \right) \right]^{0.5}}$ $R^2 = 1, RMSE = 9.16 * 10^{-4}$	$Q = \frac{g^{0.5} B^{2.5}}{\left(\frac{m}{2} \right)^{1.5}} \frac{\left[1.39 \left(\frac{my_e}{2B} \right) + 1.515 \left(\frac{my_e}{2B} \right)^2 \right]^{1.5}}{\left[1 + 2.317 \left(\frac{my_e}{2B} \right) \right]^{0.5}}$ $R^2 = 1, RMSE = 4.97 * 10^{-4}$	$Q = \frac{g^{0.5} B^{2.5}}{\left(\frac{m}{2} \right)^{1.5}} \frac{\left[1.412 \left(\frac{my_e}{2B} \right) + 1.52 \left(\frac{my_e}{2B} \right)^2 \right]^{1.5}}{\left[1 + 2.417 \left(\frac{my_e}{2B} \right) \right]^{0.5}}$ $R^2 = 1, RMSE = 5.66 * 10^{-4}$
Inverted triangular	$Q = \frac{g^{0.5} B^{2.5}}{m^{1.5}} \frac{\left[1.437 \left(\frac{my_e}{B} \right) - 1.67 \left(\frac{my_e}{B} \right)^2 \right]^{1.5}}{\left[1 - 2.351 \left(\frac{my_e}{B} \right) \right]^{0.5}}$ $R^2 = 1, RMSE = 1.95 * 10^{-5}$	$Q = \frac{g^{0.5} B^{2.5}}{m^{1.5}} \frac{\left[1.4 \left(\frac{my_e}{B} \right) - 1.482 \left(\frac{my_e}{B} \right)^2 \right]^{1.5}}{\left[1 - 2.441 \left(\frac{my_e}{B} \right) \right]^{0.5}}$ $R^2 = 1, RMSE = 9.38 * 10^{-4}$	$Q = \frac{g^{0.5} B^{2.5}}{m^{1.5}} \frac{\left[1.382 \left(\frac{my_e}{B} \right) - 1.507 \left(\frac{my_e}{B} \right)^2 \right]^{1.5}}{\left[1 - 2.449 \left(\frac{my_e}{B} \right) \right]^{0.5}}$ $R^2 = 1, RMSE = 1.88 * 10^{-5}$	$Q = \frac{g^{0.5} B^{2.5}}{m^{1.5}} \frac{\left[1.38 \left(\frac{my_e}{B} \right) - 1.49 \left(\frac{my_e}{B} \right)^2 \right]^{1.5}}{\left[1 - 2.446 \left(\frac{my_e}{B} \right) \right]^{0.5}}$ $R^2 = 1, RMSE = 5.87 * 10^{-4}$
Semi-inverted triangular	$Q = \frac{g^{0.5} B^{2.5}}{\left(\frac{m}{2} \right)^{1.5}} \frac{\left[1.437 \left(\frac{my_e}{2B} \right) - 1.67 \left(\frac{my_e}{2B} \right)^2 \right]^{1.5}}{\left[1 - 2.351 \left(\frac{my_e}{2B} \right) \right]^{0.5}}$ $R^2 = 1, RMSE = 1.95 * 10^{-5}$	$Q = \frac{g^{0.5} B^{2.5}}{\left(\frac{m}{2} \right)^{1.5}} \frac{\left[1.4 \left(\frac{my_e}{2B} \right) - 1.482 \left(\frac{my_e}{2B} \right)^2 \right]^{1.5}}{\left[1 - 2.441 \left(\frac{my_e}{2B} \right) \right]^{0.5}}$ $R^2 = 1, RMSE = 9.38 * 10^{-4}$	$Q = \frac{g^{0.5} B^{2.5}}{\left(\frac{m}{2} \right)^{1.5}} \frac{\left[1.382 \left(\frac{my_e}{2B} \right) - 1.507 \left(\frac{my_e}{2B} \right)^2 \right]^{1.5}}{\left[1 - 2.449 \left(\frac{my_e}{2B} \right) \right]^{0.5}}$ $R^2 = 1, RMSE = 1.88 * 10^{-5}$	$Q = \frac{g^{0.5} B^{2.5}}{\left(\frac{m}{2} \right)^{1.5}} \frac{\left[1.38 \left(\frac{my_e}{2B} \right) - 1.49 \left(\frac{my_e}{2B} \right)^2 \right]^{1.5}}{\left[1 - 2.446 \left(\frac{my_e}{2B} \right) \right]^{0.5}}$ $R^2 = 1, RMSE = 5.87 * 10^{-4}$
Circular ($\hat{Z} = 0$)	$Q = g^{0.5} D^{2.5} (3.42 \sin^{-1} \hat{y}_e - 2.407 \hat{y}_e^{0.9105})^{1.206}$ $R^2 = 0.999, RMSE = 7.29 * 10^{-3}$	$Q = g^{0.5} D^{2.5} (3.599 \sin^{-1} \hat{y}_e - 2.625 \hat{y}_e^{0.9105})^{1.205}$ $R^2 = 0.999, RMSE = 8.31 * 10^{-3}$	$Q = g^{0.5} D^{2.5} (3.645 \sin^{-1} \hat{y}_e - 2.681 \hat{y}_e^{0.9104})^{1.205}$ $R^2 = 0.999, RMSE = 6.91 * 10^{-3}$	$Q = g^{0.5} D^{2.5} (3.517 \sin^{-1} \hat{y}_e - 2.571 \hat{y}_e^{0.910})^{1.205}$ $R^2 = 0.999, RMSE = 4.35 * 10^{-3}$
Circular ($\hat{Z} = 0.25$)	$Q = g^{0.5} D^{2.5} (4.275 \sin^{-1} \hat{y}_e - 2.923 \hat{y}_e^{0.95})^{1.31}$ $R^2 = 0.999, RMSE = 4.81 * 10^{-3}$	$Q = g^{0.5} D^{2.5} (4.673 \sin^{-1} \hat{y}_e - 3.292 \hat{y}_e^{0.945})^{1.32}$ $R^2 = 0.999, RMSE = 5.23 * 10^{-3}$	$Q = g^{0.5} D^{2.5} (4.519 \sin^{-1} \hat{y}_e - 3.13 \hat{y}_e^{0.94})^{1.35}$ $R^2 = 0.999, RMSE = 5.80 * 10^{-3}$	$Q = g^{0.5} D^{2.5} (4.575 \sin^{-1} \hat{y}_e - 3.197 \hat{y}_e^{0.94})^{1.34}$ $R^2 = 0.999, RMSE = 5.45 * 10^{-3}$
Circular ($\hat{Z} = 0.5$)	$Q = g^{0.5} D^{2.5} (1.012 \sin^{-1} \hat{y}_e + 1.365 \hat{y}_e^{2.3})^{1.3}$ $R^2 = 0.999, RMSE = 9.90 * 10^{-4}$	$Q = g^{0.5} D^{2.5} (0.9479 \sin^{-1} \hat{y}_e + 1.817 \hat{y}_e^{2.34})^{1.29}$ $R^2 = 0.999, RMSE = 1.55 * 10^{-3}$	$Q = g^{0.5} D^{2.5} (0.987 \sin^{-1} \hat{y}_e + 1.684 \hat{y}_e^{2.34})^{1.329}$ $R^2 = 0.999, RMSE = 3.18 * 10^{-3}$	$Q = g^{0.5} D^{2.5} (1.01 \sin^{-1} \hat{y}_e + 1.603 \hat{y}_e^{2.34})^{1.336}$ $R^2 = 0.999, RMSE = 1.77 * 10^{-3}$
Circular ($\hat{Z} = 0.66$)	$Q = g^{0.5} D^{2.5} (0.98 \sin^{-1} \hat{y}_e + 1.678 \hat{y}_e^{2.35})^{1.327}$ $R^2 = 0.999, RMSE = 6.50 * 10^{-4}$	$Q = g^{0.5} D^{2.5} (0.98 \sin^{-1} \hat{y}_e + 2.417 \hat{y}_e^{2.526})^{1.33}$ $R^2 = 0.999, RMSE = 3.30 * 10^{-4}$	$Q = g^{0.5} D^{2.5} (0.98 \sin^{-1} \hat{y}_e + 2.417 \hat{y}_e^{2.526})^{1.33}$ $R^2 = 0.999, RMSE = 3.85 * 10^{-4}$	$Q = g^{0.5} D^{2.5} (0.977 \sin^{-1} \hat{y}_e + 2.396 \hat{y}_e^{2.547})^{1.34}$ $R^2 = 0.999, RMSE = 3.50 * 10^{-4}$

5.5.2 Super Critical Flow Regimes

Since part of the outcomes of this study is to obtain a direct discharge solution for the different channel cross-sections as detailed earlier, other than the flow depth at the end section (y_e), the upstream Froude number (Fr_n) is also an effective parameter for the discharge calculations in super critical flow regime. Since Fr_n can be determined with the help of the longitudinal channel bed slope S , the Mannings-Strickler channels bed friction coefficient (n), and one of the parameters among the side channels vertical to horizontal ratio (m), the channel bed width (B), the channels top width at the end depth (T_e), (whichever is appropriate for parabolic cross-section), and the channel diameter (D) is as well introduced as an influencing parameter for generating the empirical discharge relationships.

To consider the roughness effect along the channel wetted perimeter, Manning's roughness coefficient (n) was selected. Hence, application of Manning's equation for the upstream normal section in exponential, generalized trapezoidal, and the generalized circular channel cross-sections gives the non-dimensional discharge (Q^*) relationships (rectangular (Eq. (5.42)), parabolic (Eq. (5.43)), triangular (Eq. (5.44)), trapezoidal and inverted triangular (Eq. (5.45)), semi-trapezoidal and semi-inverted triangular (Eq. (5.46)) and generalized circular (Eq. (5.47)) channel cross-sections) as follows:

$$Q_{rect}^* = \left(\frac{S}{n^2 g} \right)^{1/2} \frac{y_n^{5/3}}{\left(1 + \frac{2y_n}{\eta_1} \right)^{2/3}} \quad (5.42)$$

$$Q_{par}^* = \left(\frac{S}{n^2 g} \right)^{1/2} \frac{y_n^{13/6}}{\left[\frac{3}{4} \sqrt{1 + \left(\frac{4y_n}{T_n} \right)^2} + \frac{3T_n}{16y_n} \text{Ln} \left(\frac{4y_n}{T_n} + \sqrt{1 + \left(\frac{4y_n}{T_n} \right)^2} \right) \right]^{2/3}} \quad (5.43)$$

$$Q_{tri}^* = \left(\frac{S}{n^2 g} \right)^{1/2} \frac{y_n^{8/3}}{(4 + 4\eta_1^{-2})^{1/3}} \quad (5.44)$$

$$Q_{trap,inv tri}^* = \left(\frac{S\eta_3^{1/3}}{n^2 g\eta_4^{1/3}} \right)^{1/2} \frac{(N_n + (-1)^{\eta_5} N_n^2)^{5/3}}{\left[1 + N_n \sqrt{\eta_4^{-2} + 1} \right]^{2/3}} \quad (5.45)$$

$$Q_{semi-trap,semi-inv tri}^* = \left(\frac{S\eta_3^{1/3}}{n^2 g\eta_4^{1/3}} \right)^{1/2} \frac{(N_n + (-1)^{\eta_5} N_n^2)^{5/3}}{\left[1 + N_n (\eta_4^{-1} + \sqrt{\eta_4^{-2} + 4}) \right]^{2/3}} \quad (5.46)$$

$$Q_{gen cir}^* = \frac{1}{4\sqrt[3]{16}} \left(\frac{SD^{1/3}}{n^2 g} \right)^{1/2} \frac{(\varphi(\hat{I}_n) - \varphi(\hat{Z}))^{5/3}}{\left[2\sqrt{\hat{Z} - \hat{Z}^2} + \cos^{-1}(1 - 2\hat{I}_n) - \cos^{-1}(1 - \hat{Z}) \right]^{2/3}} \quad (5.47)$$

Note that, for empirical similarity with Mannings-Strickler equation, the root squared of this longitudinal channel bed slope (\sqrt{S}) is selected.

$$Q = Q(y_e, \sqrt{S}, n, m, B, T_e, D) \quad (5.48)$$

For the exponential and the generalized trapezoidal channel cross-sections, one of the empirical equations suggested by Sharifi et al. (2009) was selected and modified due to above mentioned reasons so as to obtain these empirically expressed direct discharge relationships:

$$Q = C_1 \frac{BT_e m}{n} e^{c_2 \sqrt{S}} y_e^{c_3} \quad (5.49)$$

However, for the generalized circular channel cross-sections, the suggested equation suggested by Dey (2003) was selected in order to generate the direct discharge relationships:

$$Q = C_4 \hat{y}_e^{c_5} z^{c_6}, \quad z = \frac{SD^{1/3}}{n^2 g} \quad (5.50)$$

5.5.2.1 Exponential Channel Cross-section

5.5.2.1.1 Rectangular Channel Cross-sections

Eqs. (4.16), (5.1), and (5.42) for the free vortex theory, Eqs. (4.36), (5.1), and (5.42) for the three velocity points method, and Eqs. (4.42), (5.1), and (5.42) for the infinite number velocity points method, are solved simultaneously to obtain the direct discharge estimation for rectangular channel cross-sections in super critical flow regime by inserting $\eta_2 = 1$. The suggested equations for the direct discharge prediction based on the different theoretical methods of this study are tabulated in Table 5.8 with the statistical measuring indices (R^2 and RMSE). To be able to obtain empirical direct solutions of discharge in the suggested form of Eq. (5.49), a total of 1260 relevant data sets, all satisfying $Fr_n > 1$, were mathematically generated separately. The range of applicability of the channel parameters (S , y_e , n , B) and the discharge (Q) are also detailed in Table 5.8.

5.5.2.1.2 Parabolic Channel Cross-sections

In a similar way, Eqs. (4.16), (5.1), and (5.43) for the free vortex theory, Eqs. (4.36), (5.1), and (5.43) for the three velocity points method, and Eqs. (4.42), (5.1), and (5.43) for the infinite number velocity points method, are solved simultaneously to

obtain the direct discharge estimation for parabolic channel cross-sections in super critical flow regimes by inserting $\eta_2 = 1.5$. The suggested equations for the direct discharge prediction based on the different theoretical methods of this study are tabulated in Table 5.8 with the statistical measuring indices (R^2 and RMSE). To be able to obtain empirical direct solutions of discharge in the suggested form of Eq. (5.49), a total of 2064 relevant data sets, all satisfying $Fr_n > 1$, were mathematically generated separately. The range of applicability of the channel parameters (S , y_e , n , T_e) and the discharge (Q) are also detailed in Table 5.8.

5.5.2.1.3 Triangular Channel Cross-sections

Similarly, Eqs. (4.16), (5.1), and (5.44) for the free vortex theory, Eqs. (4.36), (5.1), and (5.44) for the three velocity points method, and Eqs. (4.42), (5.1), and (5.44) for the infinite number velocity points method, are solved simultaneously to obtain the direct discharge estimation for triangular channel cross-sections in super critical flow regimes by inserting $\eta_2 = 2$. The suggested equations for the direct discharge prediction based on the different theoretical methods of this study are tabulated in Table 5.8 with the statistical measuring indices (R^2 and RMSE). To be able to create empirical direct solutions of discharge in the suggested form of Eq. (5.49), a total of 1596 relevant data sets, all satisfying $Fr_n > 1$, were created separately. The range of applicability of the channel parameters (S , y_e , n , m) and the discharge (Q) are also detailed in Table 5.8.

5.5.2.2 Generalized Trapezoidal Channel Cross-section

5.5.2.2.1 Trapezoidal and Inverted Triangular Channel Cross-sections

Eqs. (4.9), (5.27), and (5.45) for the energy method, Eqs. (4.17), (5.27), and (5.45) for the free vortex theory, Eqs. (4.37), (5.27), and (5.45) for the three velocity points method, and Eqs. (4.49), (5.27), and (5.45) for the infinite number velocity points

method, are solved simultaneously to obtain the direct discharge estimation in a supercritical flow regime by inserting $\eta_3 = B$, $\eta_4 = m$, and $\eta_5 = 0$ for the trapezoidal and $\eta_3 = B$, $\eta_4 = m$, and $\eta_5 = 1$ for the inverted-triangular channel cross-sections. The suggested equations for the direct discharge prediction based on the different theoretical methods of this study are tabulated in Table 5.8 for the trapezoidal and inverted-triangular channel cross-sections, with the statistical measuring indices (R^2 and RMSE). To be able to obtain empirical direct solutions of discharge in the suggested form of Eq. (5.49), a total of 864 relevant data sets for the trapezoidal and 852 relevant data sets for the inverted-triangular channel cross-sections, all satisfying $Fr_n > 1$, were mathematically generated separately. The range of applicability of the channel parameters (S , y_e , n , m , B) and the discharge (Q) are also detailed in Table 5.8.

5.5.2.2.2 Semi-trapezoidal and Semi-inverted Triangular Channel Cross-sections

Eqs. (4.9), (5.27), and (5.46) for the energy method, Eqs. (4.17), (5.27), and (5.46) for the free vortex theory, Eqs. (4.37), (5.27), and (5.46) for the three velocity points method, and Eqs. (4.49), (5.27), and (5.46) for the infinite number velocity points method, are solved simultaneously to obtain the direct discharge estimation in supercritical flow regimes by inserting $\eta_3 = B$, $\eta_4 = m/2$, and $\eta_5 = 0$ for the semi-trapezoidal and $\eta_3 = B$, $\eta_4 = m/2$, and $\eta_5 = 1$ for the semi-inverted-triangular channel cross-sections. The suggested equations for the direct discharge prediction based on the different theoretical methods of this study are tabulated in Table 5.8 for the semi trapezoidal and semi inverted-triangular channel cross-sections, with the statistical measuring indices (R^2 and RMSE). To be able to obtain empirical direct solutions of discharge in the suggested form of Eq. (5.49), a total of 840 relevant data sets for the

semi-trapezoidal and 852 relevant data sets for the semi-inverted triangular channel cross-sections, all satisfying $Fr_n > 1$, were mathematically generated separately. The range of applicability of the channel parameters (S, y_e, n, m, B) and the discharge (Q) are also detailed in Table 5.8.

5.5.2.3 Generalized Circular Channel Cross-section

Eqs. (4.12), (5.35), and (5.47) for the energy method, Eqs. (4.18), (5.35), and (5.47) for the free vortex theory, Eqs. (4.40), (5.35), and (5.47) for the three velocity points method, and Eqs. (4.44), (5.35), and (5.47) for the infinite number velocity points method, are solved simultaneously to obtain the direct discharge estimation in super critical flow regimes by inserting $\hat{Z} = 0, 0.25, 0.5,$ and 0.66 for the generalized circular channel cross-sections. The suggested equations for the direct discharge prediction based on the different theoretical methods of this study are tabulated in Table 5.8 with the statistical measuring indices (R^2 and RMSE). To be able to obtain empirical direct solutions of discharge in the suggested form of Eq. (5.50), a total of 233 relevant data sets for the circular channel ($\hat{Z} = 0$), a total of 203 relevant data sets for the generalized circular channel where $\hat{Z} = 0.25$, a total of 156 relevant data sets for the inverted semi-circular channel ($\hat{Z} = 0.5$), and a total of 93 relevant data sets for the generalized circular channel where $\hat{Z} = 0.66$, all satisfying $Fr_n > 1$, were mathematically generated separately. The range of applicability of the channel parameters (\hat{y}_e and $\zeta_{cir} = \frac{SD^{1/3}}{n^2 g}$) and the non-dimensional discharge (\hat{Q}) are also detailed in Table 5.8.

Table 5.8: Equation of discharge (Q) based on the end depth (y_e) at super critical flow regime for different channel cross-sections using different theoretical methods with the range of applicability of the effective parameters

Cross-section	Energy	Free vortex	Three velocity points	n-velocity points
Rectangular	-	$Q = 0.02874 \frac{B}{n} e^{2.504\sqrt{y_e}} y_e^{1.25}$ R ² = 0.998, RMSE = 5.64*10 ⁻⁵	$Q = 0.0288 \frac{B}{n} e^{2.498\sqrt{y_e}} y_e^{1.249}$ R ² = 0.998, RMSE = 5.63*10 ⁻⁵	$Q = 0.02887 \frac{B}{n} e^{2.495\sqrt{y_e}} y_e^{1.249}$ R ² = 0.998, RMSE = 5.62*10 ⁻²
		B (m) y_e (m) n 0.1 - 0.2 0.055 - 0.195 0.010 - 0.013	S 0.00779 - 0.16046 0.01566 - 0.09396	Q (m ³ /s)
Parabolic	-	$Q = 0.04211 \frac{T_e}{n} e^{3.858\sqrt{y_e}} y_e^{1.616}$ R ² = 0.999, RMSE = 1.24*10 ⁻⁵	$Q = 0.04276 \frac{T_e}{n} e^{3.82\sqrt{y_e}} y_e^{1.616}$ R ² = 0.999, RMSE = 1.19*10 ⁻⁵	$Q = 0.04253 \frac{T_e}{n} e^{3.833\sqrt{y_e}} y_e^{1.616}$ R ² = 0.999, RMSE = 1.77*10 ⁻⁵
		T_e (m) y_e (m) n 0.237 - 1.039 0.028 - 0.135 0.010 - 0.013	S 0.007164 - 0.169736 0.008859 - 0.236237	Q (m ³ /s)
Triangular	-	$Q = 0.04679 \frac{m}{n} e^{4.055\sqrt{y_e}} y_e^{2.622}$ R ² = 0.999, RMSE = 4.49*10 ⁻⁶	$Q = 0.04847 \frac{m}{n} e^{3.985\sqrt{y_e}} y_e^{2.623}$ R ² = 0.9989, RMSE = 7.81*10 ⁻⁶	$Q = 0.04747 \frac{m}{n} e^{4.021\sqrt{y_e}} y_e^{2.622}$ R ² = 0.999, RMSE = 5.52*10 ⁻⁶
		m y_e (m) n 1 - 2 0.0525 - 0.1500 0.010 - 0.013	S 0.003941 - 0.161915 0.006264 - 0.093963	Q (m ³ /s)
Trapezoidal	$Q = 0.1627 \frac{Bm}{n} e^{4.161\sqrt{y_e}} y_e^{1.96}$ R ² = 0.999, RMSE = 8.41*10 ⁻⁴	$Q = 0.1559 \frac{Bm}{n} e^{4.255\sqrt{y_e}} y_e^{1.959}$ R ² = 0.999, RMSE = 8.70*10 ⁻⁴	$Q = 0.1591 \frac{Bm}{n} e^{4.213\sqrt{y_e}} y_e^{1.96}$ R ² = 0.999, RMSE = 8.68*10 ⁻⁴	$Q = 0.1582 \frac{Bm}{n} e^{4.231\sqrt{y_e}} y_e^{1.961}$ R ² = 0.999, RMSE = 1.00*10 ⁻³
		B (m) m y_e (m) n 0.1 - 0.2 1 - 2 0.0195 - 0.4230 0.010 - 0.013	S 0.00371 - 0.34607 0.0070 - 0.0926	Q (m ³ /s)
Semi-trapezoidal	$Q = 0.1095 \frac{Bm}{n} e^{3.848\sqrt{y_e}} y_e^{1.93}$ R ² = 0.999, RMSE = 4.91*10 ⁻⁴	$Q = 0.1053 \frac{Bm}{n} e^{3.99\sqrt{y_e}} y_e^{1.93}$ R ² = 0.999, RMSE = 5.03*10 ⁻⁴	$Q = 0.1053 \frac{Bm}{n} e^{3.99\sqrt{y_e}} y_e^{1.93}$ R ² = 0.999, RMSE = 8.03*10 ⁻⁴	$Q = 0.1073 \frac{Bm}{n} e^{3.945\sqrt{y_e}} y_e^{1.933}$ R ² = 0.999, RMSE = 8.04*10 ⁻⁴
		B (m) m y_e (m) n 0.1 - 0.3 1 - 2 0.039 - 0.846 0.010 - 0.013	S 0.0044 - 0.3446 0.00198 - 2.62020	Q (m ³ /s)
Inverted triangular	$Q = 0.1504 \frac{Bm}{n} e^{2.072\sqrt{y_e}} y_e^{1.782}$ R ² = 0.999, RMSE = 5.94*10 ⁻⁵	$Q = 0.1547 \frac{Bm}{n} e^{2.054\sqrt{y_e}} y_e^{1.784}$ R ² = 0.999, RMSE = 6.18*10 ⁻⁵	$Q = 0.1546 \frac{Bm}{n} e^{2.054\sqrt{y_e}} y_e^{1.784}$ R ² = 0.999, RMSE = 5.95*10 ⁻⁵	$Q = 0.1549 \frac{Bm}{n} e^{2.053\sqrt{y_e}} y_e^{1.784}$ R ² = 0.999, RMSE = 6.19*10 ⁻⁵
		B (m) m y_e (m) n 0.1 - 0.2 0.5 - 1.0 0.0125 - 0.1360 0.010 - 0.013	S 0.026 - 0.350 0.00198 - 0.06339	Q (m ³ /s)
Semi-inverted triangular	$Q = 0.1029 \frac{Bm}{n} e^{1.906\sqrt{y_e}} y_e^{1.71}$ R ² = 0.998, RMSE = 2.46*10 ⁻⁴	$Q = 0.1048 \frac{Bm}{n} e^{1.88\sqrt{y_e}} y_e^{1.707}$ R ² = 0.998, RMSE = 2.46*10 ⁻⁴	$Q = 0.1046 \frac{Bm}{n} e^{1.881\sqrt{y_e}} y_e^{1.706}$ R ² = 0.999, RMSE = 1.69*10 ⁻⁴	$Q = 0.1062 \frac{Bm}{n} e^{1.863\sqrt{y_e}} y_e^{1.71}$ R ² = 0.999, RMSE = 1.94*10 ⁻⁴
		B (m) m y_e (m) n 0.1 - 0.2 0.5 - 1.0 0.025 - 0.272 0.010 - 0.013	S 0.030416 - 0.370399 0.0056 - 0.1793	Q (m ³ /s)
Circular ($\hat{Z} = 0$)	$\hat{Q} = 0.6358 \hat{y}_e^{1.832} \zeta_{cir}^{0.4748}$ R ² = 0.999, RMSE = 2.37*10 ⁻³	$\hat{Q} = 0.6413 \hat{y}_e^{1.83} \zeta_{cir}^{0.4732}$ R ² = 0.999, RMSE = 2.19*10 ⁻³	$\hat{Q} = 0.657 \hat{y}_e^{1.83} \zeta_{cir}^{0.4684}$ R ² = 0.999, RMSE = 2.34*10 ⁻³	$\hat{Q} = 0.6482 \hat{y}_e^{1.83} \zeta_{cir}^{0.4712}$ R ² = 0.999, RMSE = 2.18*10 ⁻³
		\hat{y}_e 0.082 - 0.740	ζ_{cir} 2.47389 - 544.85230	\hat{Q} 0.1 - 1.0
Circular ($\hat{Z} = 0.25$)	$\hat{Q} = 0.6169 \hat{y}_e^{1.408} \zeta_{cir}^{0.466}$ R ² = 1, RMSE = 1.93*10 ⁻³	$\hat{Q} = 0.6336 \hat{y}_e^{1.407} \zeta_{cir}^{0.4614}$ R ² = 0.999, RMSE = 2.36*10 ⁻³	$\hat{Q} = 0.6377 \hat{y}_e^{1.405} \zeta_{cir}^{0.4596}$ R ² = 0.999, RMSE = 2.43*10 ⁻³	$\hat{Q} = 0.6377 \hat{y}_e^{1.405} \zeta_{cir}^{0.4595}$ R ² = 0.999, RMSE = 2.43*10 ⁻³
		\hat{y}_e 0.043 - 0.580	ζ_{cir} 2.70507 - 594.90100	\hat{Q} 0.1 - 1.0
Circular ($\hat{Z} = 0.5$)	$\hat{Q} = 0.4145 \hat{y}_e^{1.229} \zeta_{cir}^{0.4811}$ R ² = 0.999, RMSE = 2.67*10 ⁻³	$\hat{Q} = 0.4284 \hat{y}_e^{1.234} \zeta_{cir}^{0.4774}$ R ² = 0.999, RMSE = 3.09*10 ⁻³	$\hat{Q} = 0.4294 \hat{y}_e^{1.221} \zeta_{cir}^{0.4733}$ R ² = 0.999, RMSE = 2.77*10 ⁻³	$\hat{Q} = 0.43 \hat{y}_e^{1.221} \zeta_{cir}^{0.4731}$ R ² = 0.999, RMSE = 3.12*10 ⁻³
		\hat{y}_e 0.040 - 0.430	ζ_{cir} 3.32946 - 579.72720	\hat{Q} 0.1 - 1.0
Circular ($\hat{Z} = 0.66$)	$\hat{Q} = 0.4264 \hat{y}_e^{1.281} \zeta_{cir}^{0.4396}$ R ² = 0.986, RMSE = 0.015	$\hat{Q} = 0.4424 \hat{y}_e^{1.264} \zeta_{cir}^{0.4226}$ R ² = 0.986, RMSE = 0.015	$\hat{Q} = 0.4425 \hat{y}_e^{1.254} \zeta_{cir}^{0.418}$ R ² = 0.986, RMSE = 0.015	$\hat{Q} = 0.4461 \hat{y}_e^{1.264} \zeta_{cir}^{0.4212}$ R ² = 0.986, RMSE = 0.015
		\hat{y}_e 0.030 - 0.240	ζ_{cir} 4.92487 - 581.20970	\hat{Q} 0.06 - 0.21

Chapter 6

CONCLUSION AND RECOMMENDATIONS

6.1 Conclusion

The flow upstream of a free over-fall has been theoretically investigated to compute the end depth ratio (EDR) and the end depth discharge (EDD) relationships of the exponential channel cross-sections (rectangular, parabolic, and triangular), the generalized trapezoidal channel cross-sections (rectangular, triangular, trapezoidal, inverted triangular, semi-trapezoidal, and semi-inverted triangular), and the generalized circular channel cross-sections (with and without horizontal flat base with different elevations) in both sub- and super critical flow regimes.

Four different theoretical methods were used to compute the EDR relationships for the above-mentioned channel cross-sections including two new suggested approaches as:

1. Energy method
2. Free vortex theory
3. Three velocity points method (suggested)
4. Infinite velocity points method (suggested).

The first method was based on Anderson's (1967) work, where the energy equation has been used to obtain the EDR and the EDD relationships of the different channel cross-sections for both sub- and super critical flow regimes. This approach eliminates

the need of an experimental determination of the pressure coefficient at the end section (brink), since the pressure effect at the end section was considered based on the assumption of the formulation of this method.

In the second method, the momentum equation has been coupled with the free vortex theory to compute the EDR relationships from which the EDD values were determined. This approach also eliminates the need of the pressure coefficient at the end section (brink) that should be determined experimentally, since the pressure coefficient at the end section was incorporated into the momentum equation based on the suggested theory.

In the third method, the energy equation over the control volume between the upstream and the downstream sections has been utilized in order to obtain the velocity values for three different depths at the end section (at the top, at the geometric center and at the bottom). Subsequently, the continuity equation and the definition of the upstream Froude number were used to compute the EDR relationships for the different channel cross-section in both flow regimes. Finally the EDD relationships were calculated based on the relevant EDR values for each cross-section in both flow regimes. This approach eliminates the need of an empirical pressure coefficient at the brink, since the continuity equation was used to compute the EDR and the EDD relationships.

In the fourth method, by expanding the three velocity points method, the velocities were computed for infinite depths at the end section. Afterward, using the continuity equation and the upstream Froude number, the EDR relationships were obtained for the above-mentioned channel cross-sections. This approach also eliminates the need

of an empirical pressure coefficient at the brink, since the continuity equation was used to compute the EDR and the EDD relationships.

In this chapter, the obtained relationships by different methods in both sub- and super critical flow regimes are yielding:

1. the EDR values of the exponential channel cross-sections are constant for sub-critical flow regimes.
2. for generalized trapezoidal channel cross-sections, even when the flow is in sub-critical regime, the EDR value cannot be expressed as a constant value due to the channel characteristics and in fact, varies within the range of lower limit (implying rectangular channel cross-sections) and the upper limit (implying triangular channel cross-sections).
3. for the generalized circular channel cross-sections, as the height of the flat base increases, the EDR value decreases in sub-critical flow regimes (Figs. 5.18 (a), (b), (c), (d), and (e)).
4. the EDR value for super critical flow regimes is a function of the relative slope (S/S_c) and the channel characteristics parameters. In super critical flow regimes, for any channel cross-section, there is no single (constant) value, since the EDR value changes with the increase in the longitudinal channel bed slope (S).
5. in super critical flow regimes, due to the lack of the critical depth occurrence within the studied control volume of the approaching flow, the water depth at the brink has been correlated to the longitudinal channel bed slope and the channel bed roughness through the semi-empirical Manning's equation.

Hence, an explicit equation for discharge cannot be defined for super critical flow regimes.

Furthermore, as one of the outcome of this study, empirical equations were generated mathematically for the prediction of discharges from the known values of the end depth and the geometric characteristics of the channel cross-sections for different channel cross-sections in both flow regimes. In addition to the benefit of accurately predicting the flow discharge directly from a known value of the water depth at the brink, the suggested empirical equations of the discharges (Q) are also simple.

The results of this study were verified by comparing the well-known, the widely used and the relevant experimental and theoretical studies. The comparisons of the analytical approaches with the experimental data and the other relevant theoretical studies were examined through widely used statistical measuring indices (R^2 and RMSE). The verifications of solutions of all suggested approaches have presented highly satisfactory results with the relevant theoretical studies and a range of acceptable level with the available experimental data set in both flow regimes. The agreement between the suggested methods and the observed values of different researchers enhances the utility and the validity of the suggested approaches.

6.2 Recommendations for Future Studies

Although large number of studies theoretically and experimentally have been done on free over-fall with different channel cross-sections, and all the obtained results improve the misunderstandings characteristics of the flow on the free over-fall, there are some researches remain untouched. Hence, I am suggesting additional works that can be done to enlighten untouched topics:

1. measuring the appropriate pressure coefficients experimentally for a wide variety of cross sectional shapes.
2. analyzing the free over-fall in compound channel in both sub- and super critical flow regimes.
3. analyzing the free over-fall in composite channel beds for the rectangular and the triangular cross-sectional shapes in order to investigate the effect of Manning's roughness coefficient.
4. establishing the EDR and EDD relationships for the rounded bottom triangular, rounded corner rectangular, oval, and horseshoe channel cross-sections in both sub- and super critical flow regimes.
5. investigating the inclination of the water surface profile at the vicinity of the brink for different channel cross-sections in both sub- and super critical flow regimes.

REFERENCES

- Abrari, E., Ergil, M., & Beirami, M. K. (2016). Free over-fall in exponential channel cross-sections based on free vortex theory in supercritical flow regimes. *Flow Measurement and Instrumentation*, 50, 269-279.
- Abrari, E., Beirami, M. K., & Ergil, M. (2017a). Prediction of the discharges within exponential and generalized trapezoidal channel cross-sections using three velocity points. *Flow Measurement and Instrumentation*, 54, 27-38.
- Abrari, E., Ergil, M., & Beirami, M. K. (2017b). Direct Prediction of Discharge at Supercritical Flow Regime Based on Brink Depth for Inverted Semicircular Channels. *Journal of Irrigation and Drainage Engineering*, ASCE, 143(9):06017010 (available online, in press).
- Abrari, E., Ergil, M., & Beirami, M. K. (2018). Solving Trapezoidal Free Over-fall by Inserting a Brink Pressure Effect into Sharp-Crested Weir Theory. *Journal of Irrigation and Drainage Engineering*, ASCE, (accepted for publication with decision of Manuscript MS IRENG-8210R2).
- Ahmad, Z. (2001). Flow measurement with trapezoidal free overfall. *Journal of Hydraulic Engineering*, ISH, 7(2), 32-44.
- Ahmad, Z. (2002). Free overfall as measuring device in triangular channels. *Hydraulic Conference, Water Resources Ocean Engineering*, 115-119.

- Ahmad, Z. (2003). Quasi-Theoretical End-Depth-Discharge Relationship for Rectangular Channels. *Journal of Irrigation and Drainage Engineering*, ASCE, 129(2), 138-141.
- Ahmad, Z. (2005). Flow measurement using free overfall in inverted semi-circular channel. *Flow Measurement and Instrumentation*, 16, 21-26.
- Ahmad, Z., & Azamathulla, H. Md. (2012). Quasi-theoretical end-depth-discharge relationship for trapezoidal channels. *Journal of Hydrology*, 456-457, 151-155.
- Ahmad, Z. & Azamathulla H. MD. (2012). Direct solution for discharge in circular free overfall. *Journal of Hydrology*, 446-447, 116-120.
- Ali, K. M. H., & Sykes, A. (1972). Free-vortex theory applied to free overfall. *Journal of Hydraulic Division*, ASCE, 98(5), 973-979.
- Ali, K. H. M., & Ridgway, A. (1977). The circular free overfall. *Water Power and Dam Construction*, 29 (5), 42-45.
- Anastasiadou-Partheniou, L., & Hatziagiannakis, E. (1995). General end-depth-discharge relationship at free overfall in trapezoidal channel. *Journal of Irrigation and Drainage Engineering*, ASCE, 121(2), 143-151.
- Anderson, M. V. (1967). Non-uniform flow in front of a free overfall. *Acta Polytechnic Scandinavia*, 42, 1-24.

- Beirami, M. K., Nabavi, S. V., & Chamani, M. R. (2006). Free overfall in channels with different cross sections and sub-critical flow. *Iranian Journal of Science & Technology*, 30 (B1), 97-105.
- Chow, V. T. (1959). *Open channel hydraulics*. McGraw Hill Publishing Company, New York.
- Clausnitzer, B., & Hager, W. H. (1997). Outflow characteristics from circular pipe. *Journal of Hydraulic Engineering*, ASCE, 123 (10), 914–917.
- Davis, A.C., Ellet, B.G.S., & Jacob, R.P. (1998). Flow measurement in sloping channels with rectangular free overfall. *Journal of Hydraulic Engineering*, ASCE, 124 (7), 760–763.
- Delleur, J. W., Dooge, J. C., & Gent, K.W. (1956). “Influence of the slopes and roughness on the free overfall. *Journal of Hydraulic Division*, ASCE, 82(4), 30-35.
- Dey, S. (2000). End depth in steeply sloping rough rectangular channels. *Sadhana*, 25(1), 1-10.
- Dey, S. (2001). EDR in circular channels. *Journal of Irrigation and Drainage Engineering*, ASCE, 127 (2), 110–112.
- Dey, S. (2002a). Free overall in circular channels with flat base: a method of open flow measurement. *Flow Measurement and Instrumentation*, 13, 209-221.

- Dey, S. (2002b). Free overfall in open channels: state-of-the-art review. *Flow Measurement and Instrumentation*, 13(5-6), 247-264.
- Dey, S. (1998). End depth in circular channels. *Journal of Hydraulic Engineering*, ASCE, 124 (8), 856-863.
- Dey, S. (2003). Free overfall in inverted semicircular channels. *Journal of Hydraulic Engineering*, ASCE, 129 (6), 438-447.
- Dey, S. & Ravi Kumar, B. (2002). Hydraulic of free overfall in Δ -shaped channels. *Sadhana Proceedings of Indian Academy Science*. 27(June), 353-363.
- Dey, S., Kumar, D. N., and Singh, D. R. (2003). End-depth in inverted semicircular channels: experimental and theoretical studies. *Nordic Hydrology*, 35(1), 73-79.
- Diskin, M. H. (1961). The end depth at a drop in trapezoidal channels. *Journal of Hydraulic Division*, ASCE, 87(4), 11-32.
- Fathy, A., & Shaarawi, M. A. (1954). Hydraulics of free overfall. Proceedings of ASCE, 80 1-12.
- Ferro, V. (1992). Flow measurement with rectangular free overfall. *Journal of Irrigation and Drainage Engineering*, ASCE, 118 (6), 956-970.
- Ferro, V. (1999). Theoretical end-depth-discharge relationships for free overfall. *Journal of Irrigation and Drainage Engineering*, ASCE, 125(1), 40-44.

- Hager, W. H. (1983). Hydraulics of plane free overfall. *Journal of Hydraulic Engineering*, ASCE, 109(2), 1683-1697.
- Henderson, F. M. (1966). *Open Channels*. Tata MacMillan, New York.
- Jaeger, C. (1948). Hauteur d'eau a l'extremite d'un long deversoir, *La Houille Blanche*, French, 3(6), 518-523.
- Jaeger, C. (1957). *Engineering fluid mechanics*. St. Martin's Press, New York.
- Jagannadha Rao, M. V., & Lakshmana Rao, N. S. (1971). Discussion of Free overfall as flow measuring device. *Journal of Irrigation and Drainage Engineering*, ASCE, 97(4), 656-657.
- Keller, R. J., & Fong, S. S. (1989). Flow measurement with trapezoidal free overfall. *Journal of Irrigation and Drainage Engineering*, ASCE, 115(1), 125-136.
- Kraijenhoff, D. A., & Dommerholt, A. (1977). Brink depth method in rectangular channel. *Journal of Irrigation and Drainage Division*, ASCE, 103 (2), 171-177.
- Montes, J. S. (1992). A potential flow solution for the free overfall. *Water, Maritime and Energy Proceedings of Institution of Civil Engineers*, London (December), 259-266.
- Murty Bhallamudi, S. (1994). End depth in trapezoidal and exponential channels. *Journal of Hydraulic Research*, 32 (2), 219-232.

- Nabavi, S. V., Beirami, M. K., Chamani, M. R., & Sterling, M. (2011). Free over falls in flat-based circular and U-shaped channels. *Flow Measurement and Instrumentation*, 22, 17-24.
- Pagliara, S. & Viti, C. (1995). Discussion of 'Discharge prediction in smooth trapezoidal free overfall (positive, zero and negative slopes)' by R.D. Gupta, M. Jamil, & M. Mohsin. *Journal of Irrigation and Drainage Engineering*, ASCE, 121(1), 128-130.
- Pal, M. & Goel, A. (2006). Prediction of the end-depth ratio and discharge in semi-circular and circular channels using support vector machines. *Flow Measurement and Instrumentation*, 17, 49-57.
- Rajaratnam, N. & Muralidhar, D. (1964a). End depth for exponential channels. *Journal of Irrigation and Drainage Division*, ASCE, 90(1), 17-39.
- Rajaratnam N., & Muralidhar, D. (1964b). End depth for circular channels. *Journal of Hydraulic Division*, ASCE 90 (2), 99–119.
- Rajaratnam, N., & Muralidhar, D. (1968). The rectangular free over-fall. *Journal of Hydraulic Division*, ASCE, 94(3), 849-850.
- Rajaratnam, N., & Muralidhar, D. (1970). The trapezoidal free overfall. *Journal of Hydraulic Research*, 8(4), 419-447.

- Rajaratnam, N., Muralidhar, D., & Beltaos, S. (1976). Roughness effects on rectangular overfall. *Journal of Hydraulic Division*, ASCE, 102 (5), 599–614.
- Ramamurthy, A. S., Zhai, C., & Qu, J. (2004). End Depth-Discharge Relation at Free Overfall of Trapezoidal Channels. *Journal of Irrigation and Drainage Engineering*, ASCE, 130, 432-436.
- Ramamurthy, A. S., Qu, J., & Vo, D. (2006). VOF Model for Simulation of a Free overfall in Trapezoidal Channels. *Journal of Irrigation and Drainage Engineering*, ASCE, 132, 425-428.
- Replogle, J. A. (1962). Discussion on ‘End depth at a drop in trapezoidal channels’ by M.H. Diskin. *Journal of Hydraulic Division*, ASCE, 88 (2), 161–165.
- Rikar, R. V., Kumar, D. N., & Dey, S. (2004). End depth computation in inverted semicircular channels using ANNs. *Flow Measurement and Instrumentation*, 15, 285-293.
- Rohwer, C. (1943). Discharge of pipes flowing partly full, *Civil Engineering*, ASCE, 13 (10), 488–490.
- Rouse, H. (1932). Verteilung der hydraulischen energie bei einem lotrechten absturz, Dissertation, TU Karlsruhe, Germany.
- Rouse, H. (1936). Discharge characteristics of the free overfall. *Civil Engineering*, ASCE, 6(4), 257-260.

- Sharifi, S., Sterling, M., & Knight, D. W. (2009). End-Depth Ratio Prediction in Rectangular and Trapezoidal channels Using Genetic Programming. *Proceeding, 17th. UK Conference, Computational Mechanics (ACME)*, 105-108.
- Smith, C. D. (1962). Brink depth for a circular channel, *Journal of Hydraulic Division, ASCE*, 88 (6), 125–134.
- Sterling M., & Knight, D. W. (2001). The free overfall as a flow measuring device in a circular channel. *Water and Maritime Engineering Proceedings of Institution of Civil Engineers*, London, 148 (December), 235–243.
- Subramanya, K., & Kumar, N. (1993). End depth in a horizontal circular free overfall. *Journal of Institution of Engineers, India*, 73 (CI3), 185–187.
- Subramanya, K. (1998). *Flow in Open Channels*. Tata McGraw-Hill Publishing Company Limited, New Delhi, India.
- Tigrek, S., Firat, C. E., & Ger, A. M. (2008). Use of Brink Depth in Discharge Measurement. *Journal of Irrigation and Drainage Engineering, ASCE*, 134 (2), 89–95.
- Vatankhah, A. R. (2013). Direct solution for discharge in generalized trapezoidal free overfall. *Flow Measurement and Instrumentation*, 29, 61-64.
- Vatankhah, A. R. (2015). ‘‘Power-law free overfall in subcritical flow regime. *Ain Shams Engineering Journal*, 6, 399-402.

Veronese, A. (1948). Rilievi sperimentali sugli sbocchi liberi, *L'Energia Elettrica*, Italian, December, 441-638.

APPENDICES

Appendix A: The velocity head correction coefficient (C_v)

Applying the energy equation by considering the local energy loss due to the streamline curvature at the vicinity of the brink, over the control volume between the upstream (critical or normal) section and the downstream (brink) section, gives:

$$H_n = C_p(y_e - y) + \frac{v_e^2}{2g} + \frac{kv_e^2}{2g} \quad (\text{A-1})$$

$$v_e = \frac{1}{\sqrt{1+k}} \sqrt{2g(H_n - C_p(y_e - y))} \quad (\text{A-2})$$

$$C_v = \frac{1}{\sqrt{1+k}} \quad (\text{A-3})$$

where

y = vertical coordinate measured from the channel bottom.

Appendix B: Solution of three velocity points method for the exponential channel cross-sections

Applying the continuity equation for three different locations at the end section gives:

$$Q = \frac{v_{et} + v_{ec}}{2} A_{et-ec} + \frac{v_{ec} + v_{eb}}{2} A_{ec-eb} \quad (\text{B-1})$$

By substituting the velocity values at these three different locations, one obtains:

$$Q = \frac{\sqrt{2g(H_n - y_n)} + \sqrt{2g(H_n - y_n + \bar{y}_n)}}{2} A_{et-ec} + \frac{\sqrt{2g(H_n - y_n + \bar{y}_n)} + \sqrt{2gH_n}}{2} A_{ec-eb} \quad (\text{B-2})$$

Based on the characteristics of the exponential channel cross-section the following equations can be generated as:

$$A_{ec-eb} = \eta_1 \left(\frac{\eta_2}{\eta_2 + 1} y_e \right)^{\eta_2} \quad (\text{B-3})$$

$$A_{et-ec} = \eta_1 \left[(y_e)^{\eta_2} - \left(\frac{\eta_2}{\eta_2 + 1} y_e \right)^{\eta_2} \right] \quad (\text{B-4})$$

$$H_n = y_n + \frac{v_n^2}{2g} = y_n + \frac{A_n Fr_n^2}{2T_n} \quad (\text{B-5})$$

$$\bar{y}_n = \frac{y_n}{\eta_2 + 1} \quad (\text{B-6})$$

So, by substituting Eqs. (B-3), (B-4), (B-5), and (B-6) into Eq. (B-2), one can get:

$$Q = \frac{\sqrt{2g \left(\frac{y_n Fr_n^2}{2\eta_2} \right)} + \sqrt{2g \left(\frac{y_n Fr_n^2}{2\eta_2} + \frac{y_n}{\eta_2 + 1} \right)}}{2} \cdot A_{et-ec} + \frac{\sqrt{2g \left(\frac{y_n Fr_n^2}{2\eta_2} + \frac{y_n}{\eta_2 + 1} \right)} + \sqrt{2g \left(y_n + \frac{y_n Fr_n^2}{2\eta_2} \right)}}{2} \cdot A_{ec-eb} \quad (\text{B-7})$$

By the definition of the upstream Froude number at the upstream normal section for the exponential channel cross-sections, the following equation for the discharge is obtained:

$$Q = \frac{g^{0.5} \eta_1 y_n^{\eta_2 + 0.5}}{\eta_2^{0.5}} Fr_n \quad (\text{B-8})$$

By equating Eqs. (B-7) and (B-8), the following equation for the EDR of the exponential channel cross-section is computed as:

$$\text{EDR} = \left[\frac{2Fr_n}{Fr_n + \sqrt{Fr_n^2 + \frac{2\eta_2}{\eta_2 + 1}} + \left(\sqrt{Fr_n^2 + 2\eta_2} - Fr_n \right) \left(\frac{\eta_2}{\eta_2 + 1} \right)^{\eta_2}} \right]^{\frac{1}{\eta_2}} \quad (\text{B-9})$$

Appendix C: Solution of three velocity points method for the generalized trapezoidal channel cross-sections

Applying the continuity equation for three different locations at the end section gives:

$$Q = \frac{v_{et}+v_{ec}}{2} A_{et-ec} + \frac{v_{ec}+v_{eb}}{2} A_{ec-eb} \quad (C-1)$$

By substituting the velocity values at these three different locations, one obtains:

$$Q = \frac{\sqrt{2g(H_n - y_n)} + \sqrt{2g(H_n - y_n + \bar{y}_n)}}{2} A_{et-ec} + \frac{\sqrt{2g(H_n - y_n + \bar{y}_n)} + \sqrt{2gH_n}}{2} A_{ec-eb} \quad (C-2)$$

Based on the characteristics of the generalized trapezoidal channel cross-section the following equations can be generated as:

$$A_{ec-eb} = \left(\eta_3 + (-1)^{\eta_5} \frac{3\eta_3\eta_4 y_e + 4(-1)^{\eta_5} \eta_4^2 y_e^2}{6(\eta_3 + (-1)^{\eta_5} \eta_4 y_e)} \right) \cdot \left(\frac{3\eta_3 y_e + 4(-1)^{\eta_5} \eta_4 y_e^2}{6(\eta_3 + (-1)^{\eta_5} \eta_4 y_e)} \right) \quad (C-3)$$

$$A_{et-ec} = \left(\eta_3 y_e + (-1)^{\eta_5} \eta_4 y_e^2 \right) - \left(\eta_3 + (-1)^{\eta_5} \frac{3\eta_3\eta_4 y_e + 4(-1)^{\eta_5} \eta_4^2 y_e^2}{6(\eta_3 + (-1)^{\eta_5} \eta_4 y_e)} \right) \cdot \left(\frac{3\eta_3 y_e + 4(-1)^{\eta_5} \eta_4 y_e^2}{6(\eta_3 + (-1)^{\eta_5} \eta_4 y_e)} \right) \quad (C-4)$$

$$H_n = y_n + \frac{v_n^2}{2g} = y_n + \frac{A_n Fr_n^2}{2T_n} = y_n + \frac{\eta_3 y_n + (-1)^{\eta_5} \eta_4 y_n^2}{2\eta_3 + 4(-1)^{\eta_5} \eta_4 y_n} Fr_n^2 \quad (C-5)$$

$$\bar{y}_n = \frac{3\eta_3 y_n + 2(-1)^{\eta_5} \eta_4 y_n^2}{6(\eta_3 + (-1)^{\eta_5} \eta_4 y_n)} \quad (C-6)$$

So, by substituting Eqs. (C-3), (C-4), (C-5), and (C-6) into Eq. (C-2), one can get:

$$Q = \frac{\sqrt{2g \left\{ \left[\frac{\eta_3 y_n + (-1)^{\eta_5} \eta_4 y_n^2}{2\eta_3 + 4(-1)^{\eta_5} \eta_4 y_n} Fr_n^2 \right] + \left[\frac{3\eta_3 y_n + 2(-1)^{\eta_5} \eta_4 y_n^2}{6(\eta_3 + (-1)^{\eta_5} \eta_4 y_n)} \right] \right\} + \sqrt{2g \left\{ \left[\frac{\eta_3 y_n + (-1)^{\eta_5} \eta_4 y_n^2}{2\eta_3 + 4(-1)^{\eta_5} \eta_4 y_n} Fr_n^2 \right] + \left[\frac{3\eta_3 y_n + 2(-1)^{\eta_5} \eta_4 y_n^2}{6(\eta_3 + (-1)^{\eta_5} \eta_4 y_n)} \right] \right\}}}{2} \cdot A_{et-ec} + \frac{\sqrt{2g \left\{ \left[\frac{\eta_3 y_n + (-1)^{\eta_5} \eta_4 y_n^2}{2\eta_3 + 4(-1)^{\eta_5} \eta_4 y_n} Fr_n^2 \right] + \left[\frac{3\eta_3 y_n + 2(-1)^{\eta_5} \eta_4 y_n^2}{6(\eta_3 + (-1)^{\eta_5} \eta_4 y_n)} \right] \right\} + \sqrt{2g \left[y_n + \left\{ \left[\frac{\eta_3 y_n + (-1)^{\eta_5} \eta_4 y_n^2}{2\eta_3 + 4(-1)^{\eta_5} \eta_4 y_n} Fr_n^2 \right] + \left[\frac{3\eta_3 y_n + 2(-1)^{\eta_5} \eta_4 y_n^2}{6(\eta_3 + (-1)^{\eta_5} \eta_4 y_n)} \right] \right\} \right]}}{2} \cdot A_{ec-eb} \quad (C-7)$$

By the definition of the upstream Froude number at the upstream normal section for the generalized trapezoidal channel cross-sections, the following equation for the discharge is obtained:

$$Q = \frac{g^{0.5} \left[\eta_3 y_n + (-1)^{\eta_5} \eta_4 y_n^2 \right]^{1.5}}{\left[\eta_3 + 2(-1)^{\eta_5} \eta_4 y_n \right]^{0.5}} Fr_n \quad (C-8)$$

By equating Eqs. (C-7) and (C-8), the following equation for the EDR of the generalized trapezoidal channel cross-section is computed as:

$$f_1(N_n) + f_2(N_n) - 36 \left[N_n^2 \text{EDR}^2 + 2(-1)^{n_s} N_n \text{EDR} + 1 \right] * \frac{\left[1 + (-1)^{n_s} N_n \right]^{1.5} Fr_n}{\left[0.5 + (-1)^{n_s} N_n \right]^{0.5}} = 0 \quad (\text{C-9})$$

where:

$$f_1(N_n) + f_2(N_n) - 36 \left[N_n^2 \text{EDR}^2 + 2(-1)^{n_s} N_n \text{EDR} + 1 \right] * \frac{\left[1 + (-1)^{n_s} N_n \right]^{1.5} Fr_n}{\left[0.5 + (-1)^{n_s} N_n \right]^{0.5}} = 0 \quad (\text{C-10})$$

$$f_2(N_n) = \left[16(-1)^{n_s} N_n^3 \text{EDR}^4 + 48N_n^2 \text{EDR}^3 + 51(-1)^{n_s} N_n \text{EDR}^2 + 18\text{EDR} \right] \cdot \left[\sqrt{1 + \frac{(1 + (-1)^{n_s} N_n) Fr_n^2}{2 + 4(-1)^{n_s} N_n}} + \sqrt{\frac{(1 + (-1)^{n_s} N_n) Fr_n^2}{2 + 4(-1)^{n_s} N_n} + \frac{3 + 2(-1)^{n_s} N_n}{6 + 6(-1)^{n_s} N_n}} \right] \quad (\text{C-11})$$

Appendix D: Solution of three velocity points method for the generalized circular channel cross-sections

Applying the continuity equation for three different locations at the end section gives:

$$Q = \frac{v_{et}+v_{ec}}{2} A_{et-ec} + \frac{v_{ec}+v_{eb}}{2} A_{ec-eb} \quad (D-1)$$

By substituting the velocity values at these three different locations, one obtains:

$$Q = \frac{\sqrt{2g(H_n - y_n)} + \sqrt{2g(H_n - y_n + \bar{y}_n)}}{2} A_{et-ec} + \frac{\sqrt{2g(H_n - y_n + \bar{y}_n)} + \sqrt{2gH_n}}{2} A_{ec-eb} \quad (D-2)$$

Based on the characteristics of the generalized trapezoidal channel cross-section the following equations can be generated as:

$$A_{ec-eb} = \frac{D^2}{4} \left(\varphi(\hat{I}_e - \hat{y}_e) - \varphi(\hat{Z}) \right) \quad (D-3)$$

$$A_{et-ec} = \frac{D^2}{4} \left(\varphi(\hat{I}_e) - \varphi(\hat{Z}) \right) - \frac{D^2}{4} \left(\varphi(\hat{I}_e - \hat{y}_e) - \varphi(\hat{Z}) \right) \quad (D-4)$$

$$H_n = y_n + \frac{v_n^2}{2g} = y_n + \frac{A_n Fr_n^2}{2T_n} = y_n + y_n + \frac{D \left(\varphi(\hat{I}_n) - \varphi(\hat{Z}) \right) Fr_n^2}{16 \left(\hat{I}_n - \hat{I}_n^2 \right)^{0.5}} \quad (D-5)$$

$$\bar{y}_n = \left[\hat{I}_n - \frac{1}{2} - \frac{8 \left((\hat{Z} - \hat{Z}^2)^{1.5} - (\hat{I}_n - \hat{I}_n^2)^{1.5} \right)}{3 \varphi(\hat{I}_n) - \varphi(\hat{Z})} \right] D \quad (D-6)$$

So, by substituting Eqs. (D-3), (D-4), (D-5), and (D-6) into Eq. (D-2), one can get:

$$\begin{aligned}
 Q = & \frac{\sqrt{2g \left[\frac{D (\varphi(\hat{I}_n) - \varphi(\hat{Z})) Fr_n^2}{16 (\hat{I}_n - \hat{I}_n^2)^{0.5}} \right] + \sqrt{2g \left\{ \left[\frac{D (\varphi(\hat{I}_n) - \varphi(\hat{Z})) Fr_n^2}{16 (\hat{I}_n - \hat{I}_n^2)^{0.5}} \right] + \left[\hat{I}_n - \frac{1}{2} - \frac{8 \left((\hat{Z} - \hat{Z}^2)^{1.5} - (\hat{I}_n - \hat{I}_n^2)^{1.5} \right)}{\varphi(\hat{I}_n) - \varphi(\hat{Z})} \right] D \right\}}}{2} \\
 & \cdot A_{et-ec} + \\
 & \frac{\sqrt{2g \left\{ \left[\frac{D (\varphi(\hat{I}_n) - \varphi(\hat{Z})) Fr_n^2}{16 (\hat{I}_n - \hat{I}_n^2)^{0.5}} \right] + \left[\hat{I}_n - \frac{1}{2} - \frac{8 \left((\hat{Z} - \hat{Z}^2)^{1.5} - (\hat{I}_n - \hat{I}_n^2)^{1.5} \right)}{\varphi(\hat{I}_n) - \varphi(\hat{Z})} \right] D \right\} + \sqrt{2g \left[y_n + \frac{D (\varphi(\hat{I}_n) - \varphi(\hat{Z})) Fr_n^2}{16 (\hat{I}_n - \hat{I}_n^2)^{0.5}} \right]}}{2} A_{ec-eb} \\
 & (3.33)
 \end{aligned}$$

$$\cdot A_{ec-eb} \tag{D-7}$$

By the definition of the upstream Froude number at the upstream normal section for the generalized circular channel cross-sections, the following equation for the discharge is obtained:

$$Q = \frac{g^{0.5} \left[\frac{D^2}{4} (\varphi(\hat{I}_n) - \varphi(\hat{Z})) \right]^{1.5}}{\left[2D (\hat{I}_n - \hat{I}_n^2)^{0.5} \right]^{0.5}} Fr_n \tag{D-8}$$

By equating Eqs. (D-7) and (D-8), the following equation for the EDR of the generalized circular channel cross-section is computed as:

$$\begin{aligned}
& \left[\sqrt{\frac{(\varphi(\hat{I}_n) - \varphi(\hat{Z})) Fr_n^2}{16(\hat{I}_n - \hat{I}_n^2)^{0.5}}} + \sqrt{\frac{(\varphi(\hat{I}_n) - \varphi(\hat{Z})) Fr_n^2}{16(\hat{I}_n - \hat{I}_n^2)^{0.5}}} + \left(\hat{I}_n - \frac{1}{2} - \frac{8}{3} \frac{((\hat{Z}_{fb} - \hat{Z}^2)^{1.5} - (\hat{I}_n - \hat{I}_n^2)^{1.5})}{\varphi(\hat{I}_n) - \varphi(\hat{Z})} \right) \right] \\
& \cdot (\varphi(\hat{I}_e) - \varphi(\hat{I}_e - \hat{y}_e)) + \\
& \left[\sqrt{\hat{y}_n + \frac{(\varphi(\hat{I}_n) - \varphi(\hat{Z})) Fr_n^2}{16(\hat{I}_n - \hat{I}_n^2)^{0.5}}} + \sqrt{\frac{(\varphi(\hat{I}_n) - \varphi(\hat{Z})) Fr_n^2}{16(\hat{I}_n - \hat{I}_n^2)^{0.5}}} + \left(\hat{I}_n - \frac{1}{2} - \frac{8}{3} \frac{((\hat{Z} - \hat{Z}^2)^{1.5} - (\hat{I}_n - \hat{I}_n^2)^{1.5})}{\varphi(\hat{I}_n) - \varphi(\hat{Z})} \right) \right] \\
& \cdot (\varphi(\hat{I}_e - \hat{y}_e) - \varphi(\hat{Z})) - \frac{(\varphi(\hat{I}_n) - \varphi(\hat{Z}))^{1.5} Fr_n}{2(\hat{I}_n - \hat{I}_n^2)^{0.25}} = 0 \tag{D-9}
\end{aligned}$$

Appendix E: Solution of infinite number velocity points method for the exponential channel cross-sections

Applying the continuity equation for three different locations at the end section gives:

$$Q = \frac{v_1+v_2}{2} A_{(1)to(2)} + \frac{v_2+v_3}{2} A_{(2)to(3)} + \dots + \frac{v_i+v_{i+1}}{2} A_{(i)to(i+1)} + \dots + \frac{v_{np-1}+v_{np}}{2} A_{(np-1)to(n)} = \sum_{i=1}^{np-1} \frac{v_i+v_{i+1}}{2} A_{(i)to(i+1)} \quad (E-1)$$

Based on the characteristics of the exponential channel cross-section the following equations can be generated as:

$$A_{(1)to(2)} = \eta_l \left(\frac{y_e}{np-1} \right)^{\eta_2} \left((np-1)^{\eta_2} - (np-2)^{\eta_2} \right) \quad (E-2)$$

$$A_{(2)to(3)} = \eta_l \left(\frac{y_e}{np-1} \right)^{\eta_2} \left((np-2)^{\eta_2} - (np-3)^{\eta_2} \right) \quad (E-3)$$

$$v_1 = \sqrt{2g(H_n - y_n)} = \sqrt{2g \left(\frac{v_n^2}{2g} \right)}, \quad v_2 = \sqrt{2g \left[\frac{v_n^2}{2g} + \frac{1}{np-1} y_n \right]}, \quad \dots \quad (E-4)$$

$$v_{np} = \sqrt{2g \left[\frac{v_n^2}{2g} + \frac{np-1}{np-1} y_n \right]}, \quad v_i = \sqrt{2g \left[\frac{v_n^2}{2g} + \frac{i-1}{np-1} y_n \right]} \quad (E-5)$$

So, by substituting Eqs. (E-2), (E-3), (E-4), and (E-5) into Eq. (E-1), one can get:

$$Q = \frac{g^{0.5}}{\sqrt{2}} \sum_{i=1}^{np-1} \left\{ \left[\sqrt{\frac{v_n^2}{2g} + \frac{i-1}{np-1} y_n} + \sqrt{\frac{v_n^2}{2g} + \frac{i}{np-1} y_n} \right] \cdot \left[\eta_1 \left(\frac{y_e}{np-1} \right)^{\eta_2} \cdot \left((np-i)^{\eta_2} - (np-(i+1))^{\eta_2} \right) \right] \right\} \quad (E-6)$$

By the definition of the upstream Froude number at the upstream normal section for the exponential channel cross-sections, the following equation for the discharge is obtained:

$$Q = \frac{g^{0.5} \eta_1 y_n^{\eta_2+0.5}}{\eta_2^{0.5}} Fr_n \quad (E-7)$$

By equating Eqs. (E-6) and (E-7), the following equation for the EDR of the exponential channel cross-section is computed as:

$$EDR = \left\{ \frac{\sqrt{2} (np-1)^{\eta_2} Fr_n}{\eta_2^{\frac{1}{2}} \sum_{i=1}^{np-1} \left[\left(\sqrt{\frac{Fr_n^2}{2\eta_2} + \frac{i-1}{np-1}} + \sqrt{\frac{Fr_n^2}{2\eta_2} + \frac{i}{np-1}} \right) \left((np-i)^{\eta_2} - (np-i-1)^{\eta_2} \right) \right]} \right\}^{\frac{1}{\eta_2}} \quad (E-8)$$

Appendix F: Solution of infinite number velocity points method for the generalized trapezoidal channel cross-sections

Applying the continuity equation for three different locations at the end section gives:

$$Q = \frac{v_1+v_2}{2} A_{(1)to(2)} + \frac{v_2+v_3}{2} A_{(2)to(3)} + \dots + \frac{v_i+v_{i+1}}{2} A_{(i)to(i+1)} + \dots + \frac{v_{np-1}+v_{np}}{2} A_{(np-1)to(n)} = \sum_{i=1}^{np-1} \frac{v_i+v_{i+1}}{2} A_{(i)to(i+1)} \quad (F-1)$$

Based on the characteristics of the generalized trapezoidal channel cross-section the following equations can be generated as:

$$A_{(1)to(2)} = \frac{\eta_3}{np-1} y_e + \frac{(-1)^{\eta_5} \eta_4 \left(\frac{np-1}{np-1} + \frac{np-2}{np-1} \right)}{np-1} y_e^2 \quad (F-2)$$

$$A_{(2)to(3)} = \frac{\eta_3}{np-1} y_e + \frac{(-1)^{\eta_5} \eta_4 \left(\frac{np-2}{np-1} + \frac{np-3}{np-1} \right)}{np-1} y_e^2 \quad (F-3)$$

$$v_1 = \sqrt{2g(H_n - y_n)} = \sqrt{2g \left(\frac{v_n^2}{2g} \right)}, v_2 = \sqrt{2g \left[\frac{v_n^2}{2g} + \frac{1}{np-1} y_n \right]}, \dots \quad (F-4)$$

$$v_{np} = \sqrt{2g \left[\frac{v_n^2}{2g} + \frac{np-1}{np-1} y_n \right]}, v_i = \sqrt{2g \left[\frac{v_n^2}{2g} + \frac{i-1}{np-1} y_n \right]} \quad (F-5)$$

So, by substituting Eqs. (F-2), (F-3), (F-4), and (F-5) into Eq. (F-1), one can get:

$$Q = \frac{g^{0.5}}{\sqrt{2}} \sum_{i=1}^{np-1} \left\{ \left[\sqrt{\frac{v_n^2}{2g} + \frac{i-1}{np-1} y_n} + \sqrt{\frac{v_n^2}{2g} + \frac{i}{np-1} y_n} \right] \cdot \left[\frac{\eta_3}{np-1} y_e + \frac{(-1)^{\eta_5} \eta_4 y_e^2}{(np-1)^2} (np-i+np-(i+1)) \right] \right\} \quad (F-6)$$

By the definition of the upstream Froude number at the upstream normal section for the generalized trapezoidal channel cross-sections, the following equation for the discharge is obtained:

$$Q = \frac{g^{0.5} \left[\eta_3 y_n + (-1)^{\eta_5} \eta_4 y_n^2 \right]^{1.5}}{\left[\eta_3 + 2(-1)^{\eta_5} \eta_4 y_n \right]^{0.5}} Fr_n \quad (F-7)$$

By equating Eqs. (F-6) and (F-7), the following equation for the EDR of the generalized trapezoidal channel cross-section is computed as:

$$\sum_{i=1}^{np-1} \left[\left(\sqrt{\frac{(1+(-1)^{\eta_5} N_n) Fr_n^2}{(2+4(-1)^{\eta_5} N_n)} + \frac{i-1}{np-1}} + \sqrt{\frac{(1+(-1)^{\eta_5} N_n) Fr_n^2}{(2+4(-1)^{\eta_5} N_n)} + \frac{i}{np-1}} \right) \cdot \left(\frac{EDR}{np-1} + (-1)^{\eta_5} \frac{N_n EDR^2 (2np-2i-1)}{(np-1)^2} \right) \right] - \frac{\sqrt{2} (1+(-1)^{\eta_5} N_n)^{1.5} Fr_n}{(1+2(-1)^{\eta_5} N_n)^{\frac{1}{2}}} = 0 \quad (F-8)$$

Appendix G: Solution of infinite number velocity points method for the generalized circular channel cross-sections

Applying the continuity equation for three different locations at the end section gives:

$$Q = \frac{v_1+v_2}{2} A_{(1)to(2)} + \frac{v_2+v_3}{2} A_{(2)to(3)} + \dots + \frac{v_i+v_{i+1}}{2} A_{(i)to(i+1)} + \dots + \frac{v_{np-1}+v_{np}}{2} A_{(np-1)to(n)} = \sum_{i=1}^{np-1} \frac{v_i+v_{i+1}}{2} A_{(i)to(i+1)} \quad (G-1)$$

Based on the characteristics of the generalized circular channel cross-section the following equations can be generated as:

$$A_{(1)to(2)} = \frac{D^2}{4} \left(\varphi(\hat{y}_e + \hat{Z}) - \varphi\left(\frac{np-2}{np-1} \hat{y}_e + \hat{Z}\right) \right) \quad (G-2)$$

$$A_{(2)to(3)} = \frac{D^2}{4} \left(\varphi\left(\frac{np-2}{np-1} \hat{y}_e + \hat{Z}\right) - \varphi\left(\frac{np-3}{np-1} \hat{y}_e + \hat{Z}\right) \right) \quad (G-3)$$

$$v_1 = \sqrt{2g(H_n - y_n)} = \sqrt{2g \left(\frac{v_n^2}{2g} \right)}, \quad v_2 = \sqrt{2g \left[\frac{v_n^2}{2g} + \frac{1}{np-1} y_n \right]}, \quad \dots \quad (G-4)$$

$$v_{np} = \sqrt{2g \left[\frac{v_n^2}{2g} + \frac{np-1}{np-1} y_n \right]}, \quad v_i = \sqrt{2g \left[\frac{v_n^2}{2g} + \frac{i-1}{np-1} y_n \right]} \quad (G-5)$$

So, by substituting Eqs. (G-2), (G-3), (G-4), and (G-5) into Eq. (G-1), one can get:

$$Q = \frac{g^{0.5}}{\sqrt{2}} \sum_{i=1}^{np-1} \left\{ \left[\sqrt{\frac{v_n^2}{2g} + \frac{i-1}{np-1} y_n} + \sqrt{\frac{v_n^2}{2g} + \frac{i}{np-1} y_n} \right] \cdot \frac{D^2}{4} \left(\varphi\left(\frac{np-i}{np-1} \hat{y}_e + \hat{Z}\right) - \varphi\left(\frac{np-(i+1)}{np-1} \hat{y}_e + \hat{Z}\right) \right) \right\} \quad (G-6)$$

By the definition of the upstream Froude number at the upstream normal section for the generalized circular channel cross-sections, the following equation for the discharge is obtained:

$$Q = \frac{g^{0.5} \left[\frac{D^2}{4} (\varphi(\hat{I}_n) - \varphi(\hat{Z})) \right]^{1.5}}{\left[2D(\hat{I}_n - \hat{I}_n^2)^{0.5} \right]^{0.5}} Fr_n \quad (G-7)$$

By equating Eqs. (G-6) and (G-7), the following equation for the EDR of the generalized trapezoidal channel cross-section is computed as:

$$\sum_{i=1}^{np-1} \left[\left(\sqrt{\frac{(\varphi(\hat{I}_n) - \varphi(\hat{Z})) Fr_n^2}{4(\hat{I}_n - \hat{I}_n^2)^{0.5}} + \frac{i-1}{np-1}} + \sqrt{\frac{(\varphi(\hat{I}_n) - \varphi(\hat{Z})) Fr_n^2}{4(\hat{I}_n - \hat{I}_n^2)^{0.5}} + \frac{i}{np-1}} \right) \cdot \left(\varphi\left(\frac{np-i}{np-1} \hat{y}_e + \hat{Z}\right) - \varphi\left(\frac{np-i-1}{np-1} \hat{y}_e + \hat{Z}\right) \right) \right] - \frac{(\varphi(\hat{I}_n) - \varphi(\hat{Z}))^{1.5} Fr_n}{(\hat{I}_n - \hat{I}_n^2)^{0.25}} = 0 \quad (G-8)$$